COMPOUND DROPLETS FOR LAB-ON-A-CHIP

A Dissertation
Presented to
The Academic Faculty

by

James A. Black

In Partial Fulfillment
of the Requirements for the Degree
Doctor of Philosophy in the
School of Mechanical Engineering

Georgia Institute of Technology
May 2016

COMPOUND DROPLETS FOR LAB-ON-A-CHIP

Approved by:

Dr. G. Paul Neitzel, Advisor
School of Mechanical Engineering
Georgia Institute of Technology

Dr. Michael Schatz
School of Physics
Georgia Institute of Technology

Dr. G. P. "Bud" Peterson, President
School of Mechanical Engineering
Georgia Institute of Technology

Dr. David Quéré
Departments of Physics and Mechanics
ESPCI ParisTech

Dr. Marc K. Smith
School of Mechanical Engineering
Georgia Institute of Technology

Date Approved: January 13, 2016

“Do. Or do not. There is no try.”

— Master Yoda

ACKNOWLEDGMENTS

This dissertation is the culmination and tangible representation of my journey through graduate school at Georgia Tech. It's fitting for me to begin this document with a few words of thanks to all the people who have advised, shaped, and otherwise affected the path I have taken to this point. To my graduate school and Graduate Student Government Association colleagues, whether you've "gotten out" or not, accept my gratitude for your words of wisdom, encouragement, and support. To the Woodruff School faculty and staff, thank you for your financial, professional, and academic support. To the funding agencies including the National Aeronautics and Space Administration and National Science Foundation, thank you for funding much of the work that comprises this dissertation. To my advisor, who asked me to call him Paul the very first day I met him, your command of both fluid mechanics and the written word is something I will always strive towards. Thank you for your guidance. To Theta Chi Fraternity and the Foundation Chapter, thank you for your financial support throughout my education. To my family, including those whose own journeys through life have ended, thank you for the stable foundation on which I might build a successful future. You'll never know the extent of my appreciation.

TABLE OF CONTENTS

LIST OF TABLES

LIST OF FIGURES

LIST OF SYMBOLS AND ABBREVIATIONS

A	amplitude of sinusoidal deflection OR length of major axis of ellipse
A_{lub}	lubricating region area
B	length of minor axis of ellipse
C	constant (set experimentally) for mirror actuation
C_k, C_d, C_t	coefficients of second order analogy terms for bouncing droplet
D_m	molecular diffusion coefficient
D_w	diameter of inner, water droplet
E	electric field magnitude
f	mirror actuation frequency
F_{lub}	force exerted by pressure acting over the lubricating area
F_w	water volume fraction
g	gravitational acceleration
h	length of vertical laser path from mirror to substrate
H	average thickness of lubricating region
λ	lubricating region radius
l_c	capillary length
LOC	Lab on a Chip
m_{EO}	electro-osmotic flow local mobility parameter
μ_g	gas viscosity
μ_l	liquid viscosity
n	number of periods of oscillation
ν	kinematic viscosity
ΔP	pressure gradient

P_{lub}	lubricating region pressure
q	any calculated quantity for error analysis
R	droplet radius
R_l	channel cross-sectional length scale
R_m	radius of merged droplet
ρ	density
s	particle path
σ	surface tension
σ_0	surface tension at reference temperature
$\sigma_T = -d\sigma/dT$	surface-tension/temperature coefficient
T	period of oscillation
ΔT	temperature difference across heated drop
T_0	reference temperature
T_{tr}	period of droplet translation path
t_c	contact time (for bouncing droplets) OR scaled film thickness for compound droplets
t_d	diffusion timescale
TAB	Taylor Analogy Breakup
τ_p	pulse duration for compound-droplet generation
τ_R	Rayleigh time
θ	mirror angular deflection angle
u_z	average axial flow velocity
V	droplet volume
V_c	compound-droplet volume
V_e	volume of (elliptical) spheroid

V_{EOF}	electro-osmotic flow slip speed
V_f	final velocity
V_i	initial velocity
V_m	volume of merged droplet
V_M	Marangoni velocity
V_{SO}	thermocapillary pumping speed for silicone oil
V_{Tol}	thermocapillary pumping speed for toluene
W	droplet weight
We	Weber number (ratio of inertial to surface tension forces)
ω_n	natural (angular) frequency
ω_r	resonant frequency
ζ	damping ratio

SUMMARY

The development of a novel method of droplet levitation to be employed in lab-on-a-chip (LOC) applications relies upon the mechanism of thermocapillary convection (due to the temperature dependence of surface tension) to drive a layer of lubricating gas between droplet and substrate. The fact that most droplets of interest in LOC applications are aqueous in nature, coupled with the fact that success in effecting thermocapillary transport in aqueous solutions has been limited, has led to the development of a technique for the controlled encapsulation of water droplets within a shell of inert silicone oil. These droplets can then be transported, virtually frictionlessly, resulting in ease of transport due to the lack of friction as well as improvements in sample cross-contamination prevention for multiple-use chips. Previous reports suggest that levitation of spherical *O*(nL)-volume droplets requires squeezing to increase the apparent contact area over which the pressure in the lubricating layer can act allowing sufficient opposition to gravity. This research explores thermocapillary levitation and translation of *O*(nL)-volume single-phase oil droplets; generation, capture, levitation, and translation of *O*(nL)-volume oil-encapsulated water droplets to demonstrate the benefits and applicability to LOC operations.

1. INTRODUCTION

The field of microfluidics has undergone rapid development due to innovations in micro-electro-mechanical systems (MEMS) fabrication techniques leading to a desire to perform facility-intensive fluid testing on chip-level architectures (Whitesides 2006). The successive processes involved in these so called "labs on a chip" (LOCs) have a plethora of uses including biological assaying processes such as DNA testing (Burns *et al.* 1998), which require batch processing of aqueous samples. Due to small cross-sectional length scales of only tens to hundreds of microns, microfluidic transport through channels requires large pressure gradients or some other method to overcome large, retarding viscous and capillary forces.

The simplest technique for accomplishing microfluidic transport is to force liquids through microchannels under high pressure gradients. Such flows are characterized by the Hagen–Poiseuille equation which requires a pressure gradient ΔP that scales as R_l^{-4} where R_l is the cross-sectional length scale of the channel. For a microchannel with a cross-sectional lengthscale of O(100μm), these pressure forces become undesirably large. Other methods use thermocapillarity, the variation of a liquid's surface tension with temperature, to drive surface motion that can lead to bulk liquid motion. Smith (1995) has demonstrated the ability of thermocapillarity to move a two-dimensional droplet along a surface and Darhuber *et al.* (2003) have exploited this practically.

Thermocapillary pumping utilizes heating and cooling elements along a microchannel to induce temperature gradients and impose a difference in surface tension between the leading and trailing ends of a droplet fully enclosed in a tube. The driving

speed of a droplet is limited by a balance between the capillary pressure drop and viscosity. An order-of-magnitude analysis presented in Chapter 3 estimates that pumping speeds on the order of 10μm/s are possible for silicone oil, but these slow speeds would require inordinately large times for LOC applications.

Electro-osmotic flows are another means by which fluids can be moved on the micro-scale. An order of magnitude estimate suggests large electric field strengths on the order of kV/cm to achieve mm/s-speed flows would be required.

Examination of the Reynolds Number ($u_z R_l/\nu$), where u_z is the average axial flow velocity and ν is the kinematic viscosity of the fluid, for a typical flow in LOC applications shows the lack of importance of inertial effects and usual laminar flow ($Re \sim 10^{-1}$) associated with LOC flows. In these applications, orders of magnitude of variables are: u_z ~ mm/s, R_l ~ 10^{-1}mm, and ν ~ mm^2/s. Thus, diffusion dominates mixing processes. The diffusion time scale t_d is given as $t_d = {R_l}^2/D_m$ where D_m is the molecular diffusion coefficient (D_m ~ 10^{-5}cm/s for most liquid mixtures) is on the order of 10s. The mixing timescale, here the diffusion timescale due to the dominance of diffusion, while not terribly long, could be improved significantly by introducing additional means of mixing through the stretching and folding of phase fields.

Cross-contamination is also a concern when considering multiple-use chips. A liquid droplet moving along a surface in contact with it leaves behind a part (perhaps only a monolayer) of itself, which then contaminates the next droplet to take the same path. Preventing contact between a sample and substrate would therefore eliminate these concerns. The overall goal of this research is to demonstrate improvements to LOC

processes by applying recent advances in permanent nonwetting achieved through the use of thermocapillarity.

1.1 Nanoliter-Volume Droplet Levitation

Research on permanent noncoalescence and nonwetting via thermocapillarity shows promise in its application to LOCs. It has been shown (e.g. in Figure 1) by Nagy and Neitzel (2008) that microliter-volume droplets can be levitated above a cold solid surface by heating radiatively from above (see Figure 2). The normal wetting action is permanently inhibited by the constant replenishment of an interstitial lubrication layer between the liquid sample and solid substrate via thermocapillary convection. These levitated droplets can also be transported along arbitrary paths by moving the heat source, inducing a propelling asymmetry in the surrounding flow field, causing the droplet to track the heater motion.

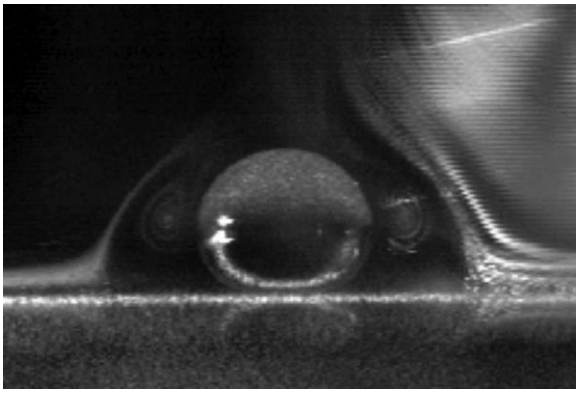

Figure 1 – A levitating microliter-volume silicone oil droplet. The droplet is levitated by inducing thermocapillary convection between the top (heated by a CO2 laser) and the bottom (over a cooled glass plate) (Nagy and Neitzel 2008).

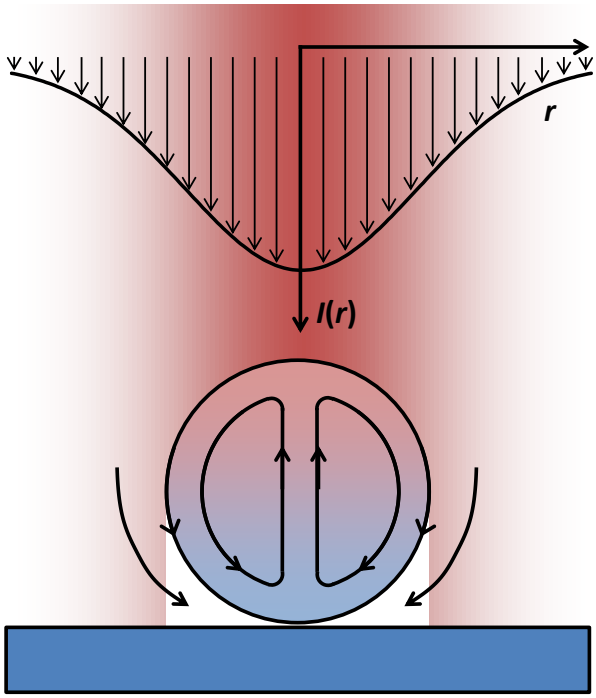

Figure 2 – An illustration of the levitated droplet of Nagy and Neitzel (2008) heated from above by an infrared heat source with a Gaussian intensity profile *I*(*r*) and cooled via the substrate. A surface flow and internal convective currents are induced by the imposed temperature gradient which drives air between the droplet and substrate preventing wetting and sustaining levitation.

The first part of this research aims to demonstrate the ability of the previously mentioned levitation technique to levitate *O*(μL)-volume droplets on a scale more applicable to microfluidics, namely *O*(nL)-volume droplets. As a droplet's diameter decreases to a value less than the capillary length ($l_c = \sqrt{\sigma/\rho g}$, where σ and ρ are, respectively, surface tension and density and g is the gravitational acceleration), a near-spherical geometry can be safely assumed and the area of apparent contact between a droplet and substrate decreases. Initial hypotheses predicted *O*(nL)-volume droplets might need to be squeezed in order to increase the apparent contact area over which the lubricating pressure acts to support the droplet's weight, but the following analysis suggests otherwise.

A fundamental assumption of this analysis is that the shape of the droplet outside the lubricating region is spherical. In droplet levitation, wetting is suppressed by a lubricating layer of gas thick enough to prevent the van der Waals forces from bridging the gap and inducing wetting. The pressure within the layer must be able to balance the droplet's weight as shown in Figure 3.

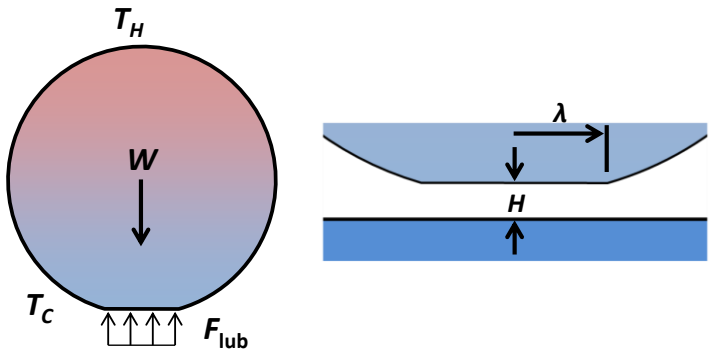

Figure 3 – Force balance for a stationary, levitated droplet (left) and a detailed view of the lubricating region (right), over which the lubricating pressure supports the droplet's weight.

For levitation in equilibrium, a droplet's weight W and the lubricating force F_{lub} must balance, yielding $F_{lub} = W \sim \rho g R^3$ where ρ is the liquid density, g is the gravitational acceleration, and R is the drop radius. The lubricating force is simply the lubricating pressure field integrated over the lubricating region area or, more simply, $F_{lub} \sim P_{lub} A_{lub}$ where P_{lub} is the average lubrication pressure and A_{lub} is the area of the lubricating region. From Dell'Aversana and Neitzel (2004), we have $P_{lub} \sim \mu_g V_M \lambda / H^2$ and $A_{lub} \sim \lambda^2$ where μ_g is the lubricating gas viscosity, V_M is the characteristic Marangoni velocity, λ is the lubricating region radius, and H is the average thickness of the lubricating layer. The Marangoni velocity is defined for this system as $V_M \sim \sigma_T \Delta T / \mu_l$ where $\sigma_T = -d\sigma/dT$ is the surface-tension/temperature coefficient, ΔT is the

temperature difference between the hot and cold sides of the drop, and μ_l is the viscosity of the drop liquid. An analysis by Quéré and Aussillous (2002) on their droplets covered in a hydrophobic powder is analogous to the levitated drop system, and it gives an approximation for the radius of the contact (lubricating) region as $\lambda \sim R^2/l_c$ where l_c is the capillary length. Combining the relations above we obtain the following estimate for the magnitude of the lubricating force:

$$F_{lub} \sim \frac{\mu_g \sigma_T \Delta T \lambda^3}{\mu_l H^2} \sim \frac{\mu_g \sigma_T \Delta T R^6}{\mu_l H^2 l_c^3} \sim \frac{\mu_g \sigma_T \Delta T R^6}{\mu_l H^2 (\sigma/\rho g)^{3/2}} \tag{1}$$

As mentioned previously, the lubricating force and droplet's weight must balance yielding.

$$\frac{\mu_g \sigma_T \Delta T R^6}{\mu_l H^2 (\sigma/\rho g)^{3/2}} \sim \rho g R^3. \tag{2}$$

Therefore, an approximate order of magnitude of the thickness of the lubricating region is given as

$$H \sim \left[\frac{\mu_g}{\mu_l} \frac{\sigma_T \Delta T}{\sigma} \frac{R^3}{(\sigma/\rho g)^{1/2}} \right]^{1/2}. \tag{3}$$

Based on the approximation given in (3), $H \sim O(10\mu m)$ for a single-phase silicone oil droplet with O(nL) volume (O(100μm) radius). This is consistent with previous work on levitating droplets and actual measurements of the lubrication layer thickness (Dell'Aversana, Tontodonato and Carotenuto 1997) shown in Figure 4 leading one to

believe that the levitation of such droplets would indeed be possible without squeezing to increase the apparent contact area.

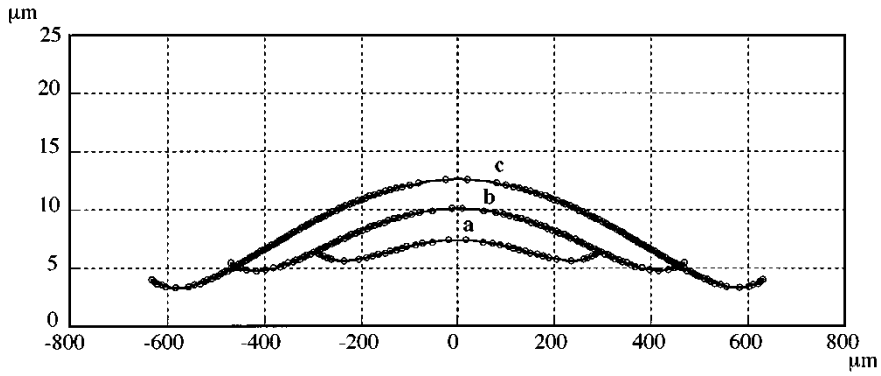

Figure 4 – Shape of the lubricating region for heated droplets pressed against a cooled solid surface (Dell'Aversana *et al.* 1997).

Surfactants can have a significant retarding effect on thermocapillary surface flows as discussed by Chen and Stebe (1997). Due to the aqueous nature of biological samples, and water's high surface tension, such samples are not good candidates for this method of transport due to the likelihood of surface contamination and possible thermocapillary-surface-flow impedance. The contaminant buildup at the base of a levitated droplet as shown in Figure 5 would decrease the ability for the sample to be levitated. A possible solution to this would be to encapsulate an aqueous sample within an inert fluid, such as silicone oil, whose properties lower the likelihood of surface contamination and the lessen the possibility for a breakdown in thermocapillary flow and lubricating layer replenishment.

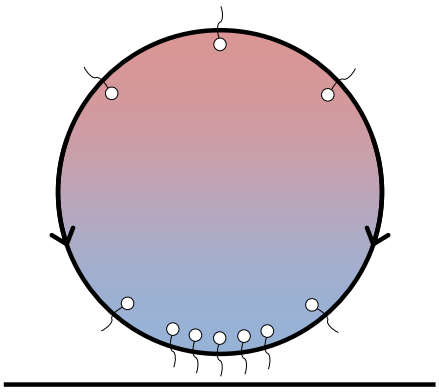

Figure 5 – Surfactant collection at the base of the droplet can retard surface flow, the direction of which is depicted by the arrows, and prevent it from driving gas into the lubricating region.

1.2 Compound-Droplet Generation

The second component of this research aims to provide a solution to the surface contamination issue presented previously. Utilization of this novel thermocapillary transport mechanism in biological assaying applications necessitates a method of controlled encapsulation of samples in an appropriate liquid–silicone oil for the purposes of this research. A system capable of producing samples in a "drop-on-demand" mode is a logical choice for delivery of these nanoliter-volume samples. A simple, single-phase drop-on-demand system devised by (Yang *et al.* 1997) serves as the basis for the design proposed, tested, and utilized here. This design uses a piezoelectric diaphragm in contact with a liquid-filled chamber to initiate droplet ejection.

The ability to generate compound-phase droplets results from the use of a specialized compound nozzle that allows for controlled variations in the encapsulant layer thickness; one would like to use the minimum amount of encapsulant necessary to permit levitation to facilitate subsequent manipulation/analysis of sample contents. Control over the encapsulant layer thickness is achieved by varying the droplet generator

system's pressure to control fluid levels at the tip of the nozzle. It's hypothesized that an encapsulant layer too thin will prevent levitation, and a layer too thick would prevent two merged samples from mixing efficiently. Reducing the encapsulant layer thickness below the threshold where sample mixing is prevented while still achieving levitation is the goal.

1.3 Compound-Droplet Levitation

The presence of the liquid-liquid interface in the interior of a compound droplet will alter the internal flow patterns from those normally seen in single-phase levitated droplets. Single-phase levitated droplets exhibit axisymmetric internal flow similar to that of Hill's spherical vortex, the streamlines of which are shown below in Figure 6a (Hill 1894). Two-phase levitated droplets exhibit asymmetric flow patterns shown in Figure 6b.

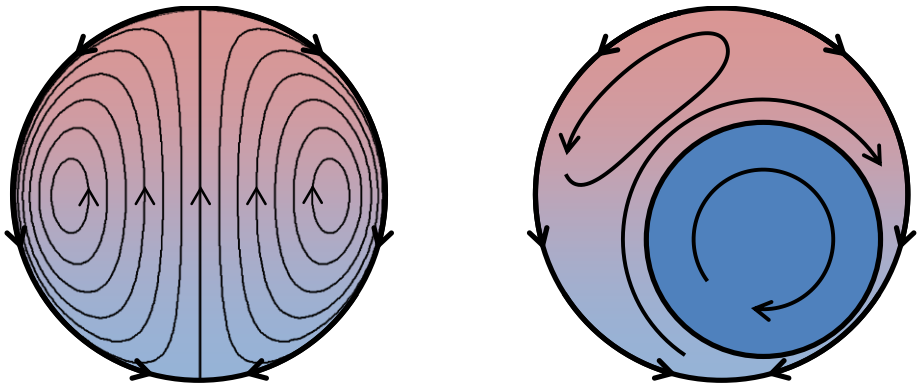

Figure 6 – (a) Streamlines for Hill's spherical vortex (Hill 1894) superimposed on a droplet representative of axisymmetric flow within a single-phase levitating droplet and (b) asymmetric flow pattern within a levitating compound droplet.

Studies investigating permanent nonwetting utilizing pendant droplets squeezed against a substrate were precursors to levitation studies (Dell'Aversana *et al.* 1997; Nagy and Neitzel 2008). Initial nonwetting explorations have been similarly conducted utilizing pendant compound droplets squeezed against a cooled substrate to investigate whether the presence of the liquid-liquid interface has a destructive effect on the surface flow that prevents wetting. Changes to the internal flow patterns from single to two-phase systems can also be seen as a result of this boundary.

Pendant droplet experiments have yielded insight into internal flow characteristics and the capability of the surfaces of thin oil-layers moving under thermocapillary action to replenish the lubricating air film, suppress wetting, and promote levitation. To date, no extensive studies have been performed to explore the internal flow patterns of two-phase droplets. Experimental and studies will clarify these flow structures and allow them to be utilized to enhance merging and mixing processes.

1.4 Droplet Translation, Merging, and Mixing

Asymmetric heating of levitated droplets provides a propelling force towards the highest intensity region of heating for the purposes of controlled translation. Unfortunately, droplets ejected from the generator designed for the present levitation have speeds of O(0.1-1 m/s) and are likely not easily captured by utilizing this propelling force alone. An order of magnitude estimate for the maximum droplet acceleration a (or in this case, deceleration) provided by asymmetric heating is devised by Nagy (2006) and is

$$a \sim \frac{3\rho_g \left(\frac{\sigma_T \Delta T}{\mu_l}\right)^2}{4\rho_l R}, \tag{4}$$

where g and l subscripts refer to gas and liquid, respectively. The stopping distance s, where the final velocity V_f is zero, of a particle traveling in a linear path with initial velocity V_i under constant deceleration a is derived from kinematics, assuming constant acceleration to be

$$s = \frac{V_f^2 - V_i^2}{2a} = \frac{-{V_i}^2}{2a}. \tag{5}$$

For a single-phase droplet of silicone oil with a radius of *O*(100μm) undergoing levitation in air, accelerations on the order of 0.1m/s^2 can be expected. At minimum droplet ejection speeds of *O*(0.1m/s) under constant deceleration, a stopping distance of *O*(50mm) and thus a laser beam of *O*(100mm) in diameter would be required to provide an adequate distance over which the droplet could be decelerated and captured. Laser beams have diameters in the millimeter range, so the stationary heat source alone cannot be used to passively capture a droplet. Active tracking of the droplet might accomplish this.

In addition to the propelling force due to laser beam intensity variations, additional forces can be imposed by system components designed to direct an ejected droplet towards the center of the laser beam for sustained levitation. Aerodynamic forces might be imposed by air streams directed vertically through the substrate to oppose the

vertical velocity component and reduce droplet bouncing or horizontally to decrease the speed at which the droplet is traveling across the laser beam. Gravitational forces can also be harnessed from bowl-shaped surfaces whereby droplets are accelerated towards the beam directed at the lowest point of the bowl. Once droplets are captured, they can be moved to a flat portion of the substrate for experimentation.

Finally, after demonstrating levitation and aqueous sample transport via compound droplets, the effect of thermocapillary convection on internal stirring and its impact on LOC processes when two encapsulated droplets are merged will be explored. Given the small sizes of LOC samples and the low Reynolds numbers typically involved, mixing is generally difficult to accomplish (Grigoriev, Schatz and Sharma 2006). For compound droplets, the water volume fraction is the ratio of water droplet volume to total compound-droplet volume. The internal flow currents could suppress inner droplet interactions and merging if two identical compound droplets with volume V_c and water volume fraction F_w are merged unless the radius of the merged compound droplet R_m is less than the diameters of the two inner droplets D_w (6) as shown in Figure 7 below. This would guarantee some physical interaction between the inner droplets and yields a prediction for the lower composition threshold for successful droplet merging shown below, where V_m is the resulting volume of two identical merged droplets of volume V_c (7).

$$R_m < D_w = 2R_w \tag{6}$$

$$V_m = 2V_c \tag{7}$$

Expressing (6) in terms of the volume of the constituent compound droplets V_c and the composition parameter F_w, we obtain the following:

$$\left[\frac{3(2V_c)}{4\pi}\right]^{1/3} < 2\left[\frac{3(F_w V_c)}{4\pi}\right]^{1/3} \tag{8}$$

$$\therefore\ F_w > 0.25 \tag{9}$$

Therefore, to guarantee that two identical compound droplets will fully merge, their individual water volume fractions must be above 0.25.

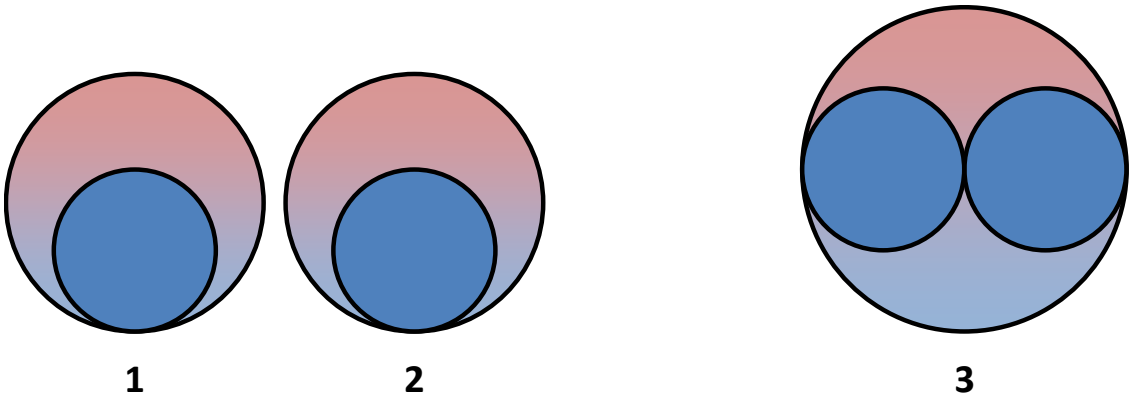

Figure 7 – Droplets 1 and 2 on the left are identical compound droplets with F_w = 0.25, the maximum oil layer thickness which will allow inner droplet interactions upon merging to form droplet 3 on the right.

1.5 Summary

This research aims to explore the application of thermocapillary levitation to lab-on-a-chip applications through the use of compound droplets. There are many studies relevant to this research which will be summarized in the following chapter to guide the development of tools and experiments to accomplish the previously outlined goals.

2. RELEVANT RESEARCH

2.1 Microfluidics and Lab-on-a-chip

Microfluidic studies evolved largely as an application of microfabrication techniques developed to create early silicon diaphragm pressure sensors as was demonstrated in the work of Pfann and Thurston (1961) and Tufte, Long and Chapman (1962). Terry (1975) is widely regarded as the first to develop a microfluidic device in his miniature gas chromatography system fabricated on a silicon wafer. These microfabrication techniques also yielded pumps, valves, motors and other components on the micro scale, and when combined with microfluidics, comprise the field of micro-total-analysis-systems (μTAS) also referred to as lab-on-a-chip (LOC) systems.

These systems have numerous benefits, including their ability to handle and test extremely small amounts of liquid (both reagents and sample carrier fluids), allowing for cost reductions associated with decreased waste of materials. The integration of multiple tasks onto a single chip can improve testing times and decrease facility costs. These integrated tasks allow for simple, inexpensive systems. A widely used example of such a system is a blood-glucose level testing device for diabetes patients in the home.

Scaling fluid transport down to this regime poses issues in the form of increased viscous and capillary effects. Mixing fluids is also time consuming due to the increased dependence on diffusion for such low-Reynolds-number flows. However, several methods for effecting liquid transport are in use as outlined by Stone, Stroock and Ajdari (2004) in their summary of microfluidics pertaining to LOC applications. Rice and Whitehead (1965) demonstrated the use of electroosmosis by applying an electric field to

a fluid to cause bulk fluid motion. Disadvantages of this method include necessary field strengths of *O*(kV/cm) magnitude, ohmic heating of the fluid, and impurity adsorption potentially clogging the channels (Whitesides and Stroock 2001). Electrophoresis is also used, but this method requires the presence of charged particles within the liquid to be transported since the force applied by the electric field is on the particles and not the bulk liquid. Magnetohydrodynamics can be employed, but similarly to electrophoresis, the magnetic field acts upon particles suspended in the liquid and not the bulk liquid itself (unless a ferrofluid is employed – not likely for LOC applications). In order to facilitate mixing, complicated geometries can be employed to induce secondary internal flows as shown by Song, Tice and Ismagilov (2003). Thermocapillary flows can aid mixing as demonstrated by Grigoriev, Schatz and Sharma (2006), and the internal flows driven by the method of Nagy and Neitzel (2008) would have an obvious benefit through the dramatic increase in internal mixing.

2.2 Nonwetting and Noncoalescence Phenomena

The first observations of noncoalescence phenomena were those by Lord Rayleigh (1879) dealing with the random scattering of droplets issuing from a vertical jet and by Reynolds (1881) who observed temporary noncoalescence between a droplet and liquid surface. Bradley and Stow (1978) were among the first to study how the impact parameter, defined as the distance between two colliding droplets normal to the relative velocity scaled by the droplet diameter, can affect the outcome of a droplet collision. The work of Qian and Law (1997) to map the collision regimes of colliding droplets builds on the work of Jiang, Umemura and Law (1992) on hydrocarbon droplet collisions and identified the importance of draining the interstitial film in affecting coalescence. The

temporary nature of the previously mentioned examples of noncoalescence is due to the finite amount of time it takes the fluid to drain from the lubricating layer.

It is the constant replenishment of this interstitial film (e.g. in Figure 8) that transforms the temporary nature of these phenomena into a permanent one. The noncoalescence and nonwetting behavior of liquids is summarized by Neitzel and Dell'Aversana (2002).

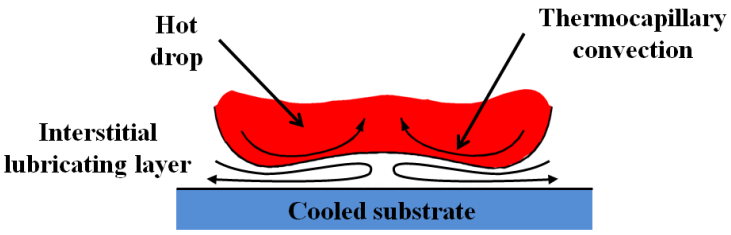

Figure 8 – Illustration showing interstitial lubricating layer.

Alternate mechanisms for replacing the interstitial fluid layer include evaporation and relative surface motion. An example of coalescence suppression by evaporation, in this case slow evaporation, is given in the work of Weilert *et al.* (1996) during their demonstrations of magnetic levitation of liquid Helium droplets which, when squeezed against each other by a magnetic field, deform but do not coalesce. Rapid evaporation, i.e. boiling, of droplet liquid in the vicinity of a superheated surface gives rise to a form of nonwetting called the Leidenfrost effect (Leidenfrost 1966). Surface temperatures must remain above the so-called Leidenfrost temperature to maintain a nonwetting state. It should be noted that if some manner of replacing the drop fluid is not provided, this noncoalescence will not truly be permanent due to the eventual complete evaporation of the liquid.

The relative surface motion needed to suppress coalescence or wetting can be achieved either through the bulk motion of a lower fluid (or surface, in the case of wetting) as in the work of DellAversana, Banavar and Koplik (1996) (Figure 9) to drive surrounding gas into the lubricating layer or via thermocapillary convection as demonstrated in the same work (Figure 10). The focus of this proposed research is in the latter of these two cases where variations in surface tension caused by temperature gradients drive the convective currents.

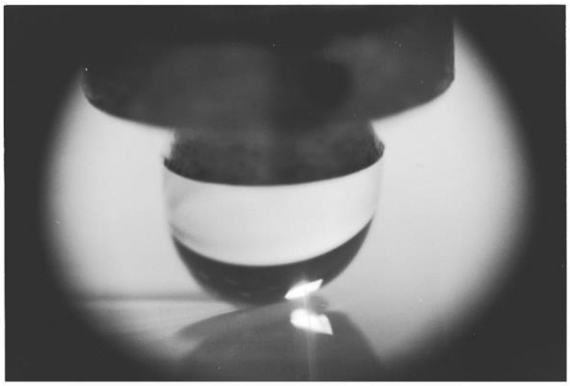

Figure 9 – An isothermal noncoalescing pendant drop displacing the fluid below in the vicinity of the contact region (DellAversana *et al.* 1996).

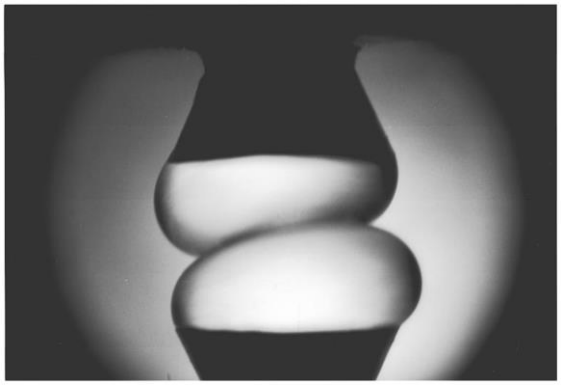

Figure 10 – Permanent noncoalescence via thermocapillary convection between two silicone oil drops pinned at the edges of pedestals (DellAversana *et al.* 1996).

Typically a fluid's surface tension is a function of temperature and is usually modeled to be linear and of the form $\sigma(T) = \sigma_0 - \sigma_T(T - T_0)$, where σ_0 is the surface temperature at the reference temperature T_0. For the majority of liquids and all of those of interest to this research, the surface tension gradient takes a negative value (also previously defined as the surface tension-temperature coefficient) $-d\sigma/dT = \sigma_T$, which yields surface flows in the direction of decreasing temperature (Neitzel and Dell'Aversana 2002). It is this surface flow, caused by the imbalance in tangential surface stresses, and the resulting bulk flow that is named thermocapillary convection. The first studies showing the use of thermocapillarity to drive fluid motion were those by Young, Goldstein and Block (1959), who used it to keep a bubble stationary in a buoyant situation. Such flows were also exhibited in zero gravity experiments performed by Thompson, DeWitt and Labus (1980). Work extending this phenomena to liquid-liquid systems was done by Barton and Subramanian (1989) who studied the migration of liquid droplets in a vertical temperature gradient. Studies by Darhuber *et al.* (2003) show that thermal modulation of surface stresses can be utilized to actuate fluids of microliter-volumes along chemically patterned substrates with a gas as the surrounding fluid.

The cases giving rise to permanent nonwetting are analogous to those for permanent noncoalescence. Again, evaporation can be employed to replenish the interstitial lubricating layer as in the case of the Leidenfrost effect, whereby droplets dance across a surface heated above the Leidenfrost point of the liquid; their weight is supported by the stable film boiling of the liquid in the drop closest to the heated surface which prevents fluid-substrate contact. Relative surface motion can also be employed in the form of a moving substrate as in the experiments of Neitzel *et al.* (2000) in which a

spinning glass disk is used to drive the surrounding gas into the lubricating layer similarly to the spinning fluid bath used by DellAversana *et al.* (1996). Thermocapillarity can also be employed to suppress wetting by the method of Dell'Aversana *et al.* (1997) preventing wetting by a pendant droplet heated through its pedestal and cooled by the substrate against which it is pressed.

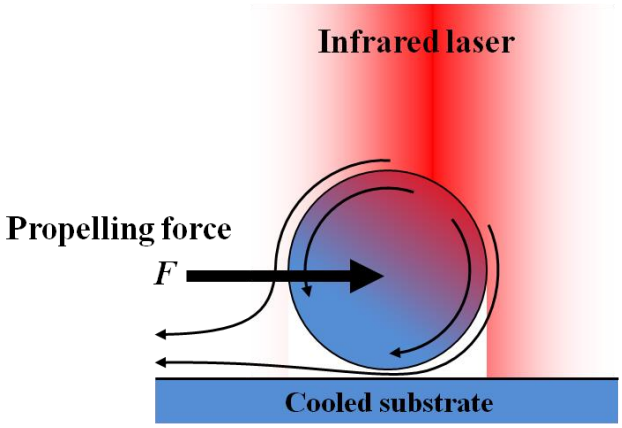

Figure 11 – Graphic showing asymmetric flow conditions surrounding an *O*(nL) spherical droplet due to off-center heating creating a propelling force towards the center of the infrared laser beam.

The foundation for this research is the proof-of-concept work of Nagy and Neitzel (2008) who described a new levitation and transport method utilizing the permanent nonwetting phenomenon via thermocapillary convection. A droplet is levitated by heating the top with an infrared (IR) laser and cooling the substrate using a Peltier module, inducing the surface tension gradients and surface flow. As shown by Nagy (2006), a levitated droplet prefers to remain in the center of intensity of the infrared beam to preserve the surrounding flow symmetry. When the heat source is moved and the droplet is off-center of the laser beam, a flow asymmetry develops causing a net momentum flux in the surrounding air currents that propels the droplet toward the

location of highest intensity within the beam. It is in this way that droplet transport achieved (Figure 11).

2.3 Compound-Droplet Generation

To apply the method of droplet levitation and transport developed by Nagy and Neitzel (2008) to LOC processes, two main complications must be overcome: surface contamination and liquid volatility. Biological samples of interest in an LOC used for bio-processing are aqueous-based. Water has a high surface tension, making these droplets especially susceptible to surface contamination that leads to inhibition of surface flow. An additional component of the aforementioned experimental study of thermocapillary-driven droplet transport by Barton and Subramanian (1989) were studies in the presence of a surfactant. In these experiments, and in subsequent models developed by Chen and Stebe (1997), it is shown that surfactant accumulation in a cap at the high-tension region of the drop can totally retard surface mobility. For the levitation application, this region must remain uncontaminated to allow the surface motion to replenish the lubricating gas layer, thus sustaining levitation. The use of an immiscible encapsulating liquid with a smaller surface tension will presumably allow for more reliable droplet levitation/translation. The second consideration is the volatility of the carrier liquid, given that the desired technique requires heating of the droplet. By choosing an encapsulating liquid such as low-viscosity (5cSt) silicone oil, which is both non-volatile in the temperature range needed for levitation and of a low enough surface tension such that surface contamination issues are mitigated, we minimize sample evaporation and expect surface motion vigorous enough to enable levitation.

Existing compound-droplet generation mechanisms, as well as the method presented in this work, are extensions of well-studied methods to generate single-phase droplets. Basaran (2002) surveys droplet generation methods (shown in Figure 12), whose suitability can be explored for the desired application.

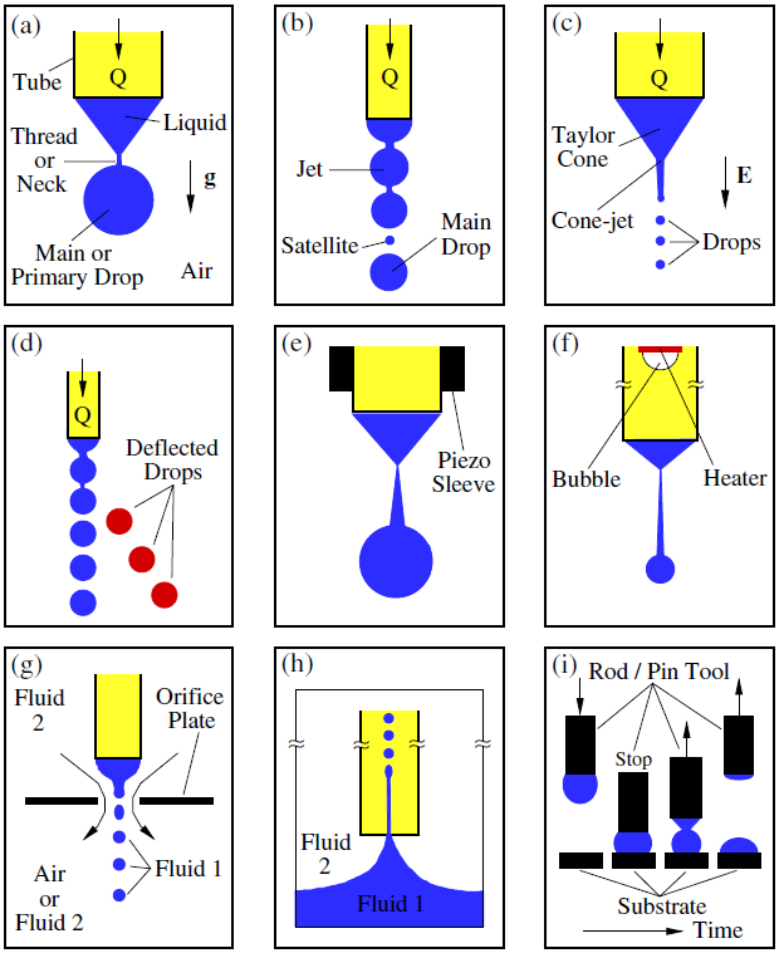

Figure 12 – Common droplet generation methods as outlined by Basaran (2002): a) dripping; b)jetting; c) electrohydrodynamic jetting; d) continuous ink-jet printing; e) piezoelectric droplet-on-demand; f) bubble jet droplet-on-demand; g) flow focusing; h) selective withdrawal; i) stretching liquid bridge

Gravitational stretching is the simplest and is employed by Planchette, Lorenceau and Brenn (2010) to create a pendant water droplet on a thin wire. This droplet is

encapsulated by oil and allowed to break away from the wire under its own weight, creating a compound droplet. A device created by Che *et al.* (2012) uses a small capillary tube with two alternating fluids flowing within to generate compound-phase droplets which drip from the nozzle orifice. For the present application, gravitational stretching is an undesirable method as surface deformation of the pendant droplet is necessary to induce separation and this would be difficult, if at all possible, to employ reliably for droplets of nanoliter volume.

As described by Christopher and Anna (2007), microfluidic devices have been designed to generate droplets in multi-phase systems through the use of co-flowing streams (Umbanhowar, Prasad and Weitz 2000), cross-flowing streams (Okushima *et al.* 2004) or flow-focusing geometries (Utada *et al.* (2005)). A method devised by Terwagne *et al.* (2010) utilizes impacting streams of droplets of immiscible liquids to also generate steady streams of droplets with varying composition. Although a similar apparatus could be developed using air as a tertiary fluid to drive droplet breakup, steady streams of droplets are less desirable to the present work than a system that will provide droplets on-demand. Electrospray techniques, when utilized with coaxial liquid jets, can produce compound droplets as shown by Loscertales *et al.* (2002). Electrical discharge from droplet to substrate of any residual charge from the electrospray process would cause failure of the lubricating film and wetting as discussed by Dell'Aversana and Neitzel (2004), an undesirable effect in the desired application.

2.4 Summary

The end goal of improving LOC processes through the use of thermocapillary levitation requires that nanoliter-volume droplets be able to undergo levitation by this means. Prior to this research, levitation experiments have been limited to microliter-volume droplets with droplet diameters an order of magnitude larger. Based on this previous research, it is not yet clear whether levitation on this scale is possible. Thus, it is natural that the levitation and translation of nanoliter-volume single-phase droplets be the first topic of exploration.

3. NANOLITER-VOLUME DROPLET LEVITATION

3.1 Introduction

As discussed in the Introduction, it was hypothesized that levitating droplets with diameters much lower than the capillary length of the liquid might be non-trivial due to the reduction of the area over which the pressure within the lubricating region acts to support the droplet's weight. Scaling arguments have been presented which suggest levitating such droplets is possible and consistent with previous research. Here, experiments are conducted which demonstrate both the levitation and translation of single-phase nanoliter-volume silicone-oil droplets. The "droplet capture" problem, elaborated on later in this work, for droplet-on-demand generation is first encountered here, but not addressed immediately. The following generation method for single-phase nanoliter droplets is chosen which naturally incorporates a capturing mechanism.

3.2 Generation Mechanism

For droplet-on-demand generation, a droplet's size is controlled primarily by nozzle size, i.e. a droplet generated will have roughly the same radius as the nozzle through which it is ejected (Le 1998). It follows that reducing the nozzle size to a radius of 50-100μm will produce droplets in the nanoliter range. Droplets of this size have been readily produced, but capturing a single droplet under a laser beam for levitation has yet to be achieved for drop-on-demand production.

A simple method of generating and capturing single-phase oil droplets is utilized for this investigation. Overheating and boiling of pendant silicone oil droplets at the end

of a syringe tip produces a cloud of droplets of *O*(μm) diameter. These droplets fall under the influence of gravity (see Figure 13) to the cooled substrate where impact is prevented by thermocapillary flows induced by the imposed temperature difference between the top and bottom of each droplet. These droplets naturally migrate to the region of highest laser intensity, due to the previously described gas flow asymmetry, coalescing to form a droplet whose size is roughly controlled by the duration that boiling of the pendant droplet is allowed to occur (i.e. the longer boiling is allowed to occur, the larger the resulting levitating droplet will be). There are often numerous residual droplets trapped within the air currents under the laser beam that are prevented from coalescing with the primary droplet of interest. Due to their small size, they are gently blown away from the test area while the primary droplet remains for study.

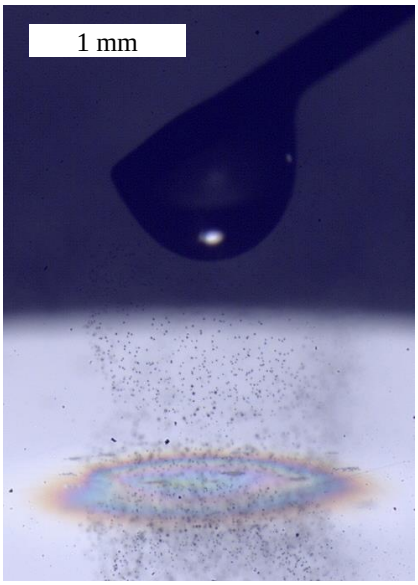

Figure 13 – This image depicts the method by which nanoliter-volume droplets are deposited. In this image, the infrared laser strikes the substrate from above under which a pendant droplet of silicone oil is held. Small droplets of silicone oil can be seen falling toward the cooled glass substrate.

Due to their small size, the droplets under study are quite susceptible to being blown out from under the laser beam by ambient air currents. Droplets are protected by a tall glass enclosure with planar sides open at the top for unimpeded laser beam entry. This glass enclosure blocks air currents while allowing optical access to the experimental area without adverse refractive effects.

3.3 Experimental Setup

In order for levitation and droplet translation to be achieved and sustained, a temperature gradient must be imposed on a droplet's surface via a heat source and sink and the heat source moved for translation. A CO_2 laser (Synrad 48-1KWM) is used as the heat source. The laser emits a 3mm wide beam of 10.6μm wavelength infrared radiation. The substrate (in this case glass) is cooled by a Peltier module (Laird Technologies - 63205-501) sandwiched between the substrate and a heat sink. The heat sink is composed of a copper plate cooled by water circulated in parallel with the laser cooling system allowing for steady-state operation. The laser beam is controlled using a fast-tracking mirror (Optics in Motion - OIM100 Series) whose striking position on the substrate and levitation plane is controlled by voltage inputs from a LabView program. The experimental setup is show in Figure 14 below.

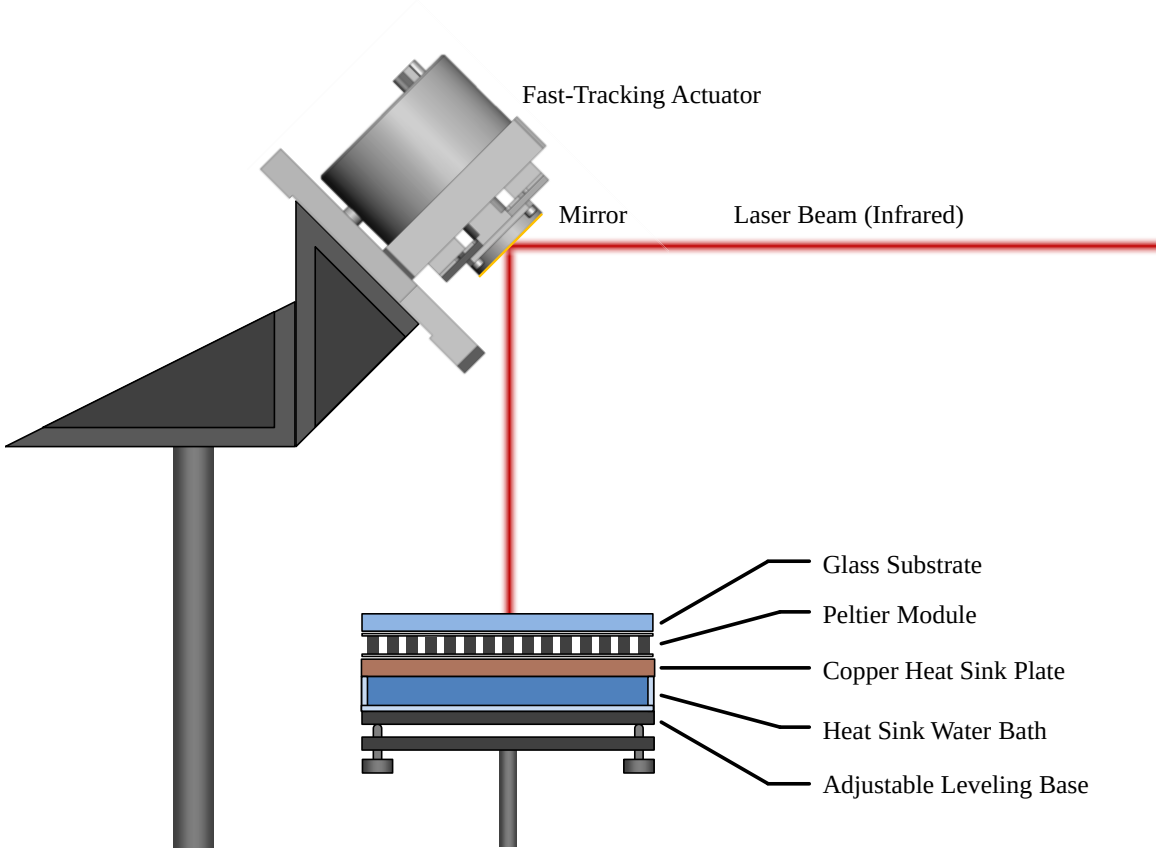

Figure 14 – The experimental apparatus for translation experiments consists of a laser beam generator (not shown), a fast-tracking mirror for control of beam direction and substrate striking location, a glass substrate, Peltier module for substrate cooling, heat sink (copper plate and water cooling bath), and an adjustable leveling base. Droplets are filmed by a high-speed camera (also not shown).

For the translation experiments conducted in this study, mirror actuation is utilized to alter the beam path to the test substrate. A simple, sinusoidal voltage input is used to alter the angle of incidence of the laser beam on the mirror surface yielding control over the x-position of the beam (as defined in Figure 16). The reflected angle from the mirror is equal to the incident angle as the infrared wavelength beam is specularly reflected off this surface. The imaging camera (Miro 4C) is attached to an Olympus SZX16 microscope whose orientation is such that the line the beam's point of

contact makes with the cooled substrate as it is swept along via mirror actuation lies within the camera's focal plane. A representative image from high-speed video acquired during these experiments is shown in Figure 15 below.

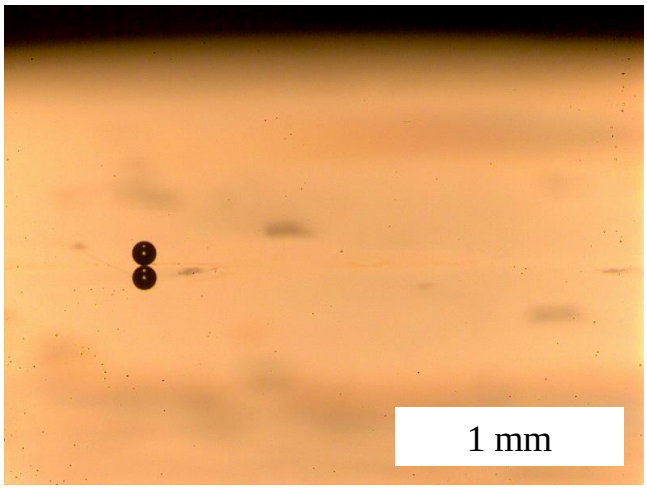

Figure 15 – This image is a single frame from high-speed video acquired during droplet levitation and translation.

Measurements along the x-axis can be made without correcting for the camera's viewing angle from horizontal as long as the beam-substrate contact line lies within the camera's thin focal plane. Figure 16 shows the geometric relationship between mirror actuation angle θ and the path (x-position) of the beam-substrate contact point. In this configuration, h is the vertical distance the laser travels to the substrate after its reflection from the mirror, A is the amplitude of the sinusoidal angular deflection, and f is the frequency of the mirror actuation in Hz.

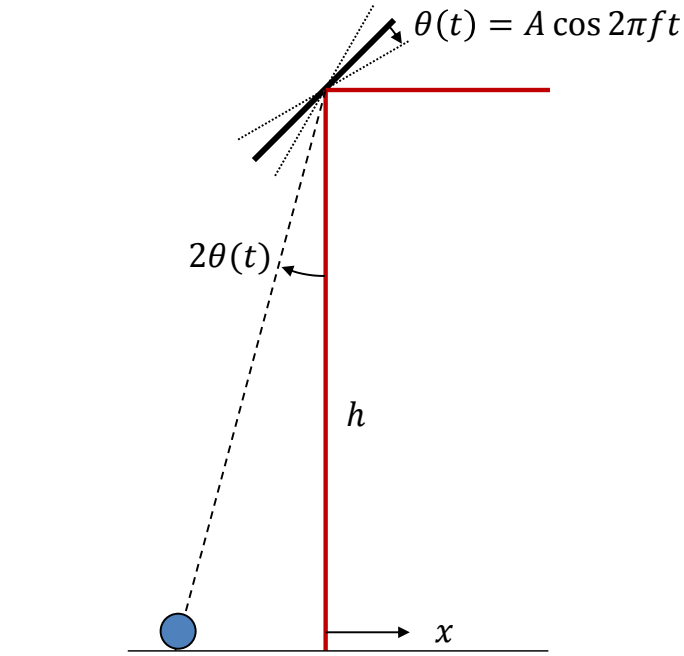

$$x(t) = -h\tan(\theta) = -h\tan(2A\cos(2\pi ft))$$

Figure 16 – The geometric relationship between droplet position, x and the angle of deflection of the mirror $\theta(t)$ is shown here.

3.4 Experimental Results

3.4.1 Levitation of Nanoliter-Volume Droplets

Using the previously described generation mechanism, nanoliter-volume silicone oil droplets were successfully levitated. One such droplet with a diameter (volume) of 232µm (2.09nl) is shown in Figure 17 below. The capillary length for 5cSt silicone oil is approximately 1.5mm. As a diameter-to-capillary-length comparison for a silicone-oil droplet of this size would suggest (i.e. a 1.5mm capillary length is roughly an order of magnitude larger than the droplet diameter of 232µm), the droplet takes a spherical shape which successfully tests and validates the hypothesis that levitation of nanoliter-volume droplets is indeed possible.

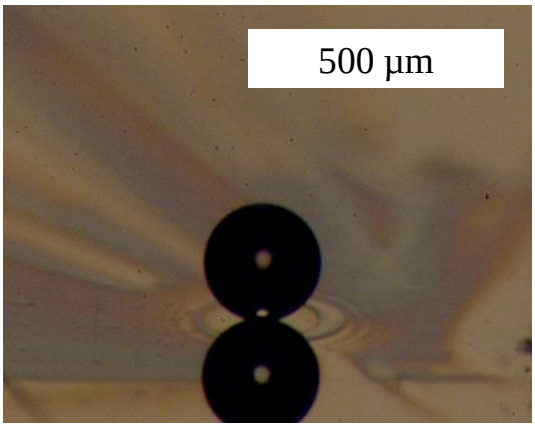

Figure 17 – A levitating single-phase silicone-oil droplet with a diameter of 232µm and volume of 2.09nl.

3.4.2 Translation of Nanoliter-Volume Droplets

The experiments presented here test various values of mirror actuation frequencies for identical angular amplitudes to explore the range of attainable droplet accelerations. The constants A and h, as defined in Figure 16, were set such that the distance traveled by the beam-substrate contact point was approximately 2mm, i.e. for x-positions as defined in Figure 16 in the range of -1mm to 1mm. Table 1 summarizes relevant parameters from each data set.

Table 1 – This table summarizes the relevant parameters in each translation experiment. Mirror actuation frequencies range from 0.1-0.4Hz, droplet diameters from 104-138µm, and droplet volumes from 0.586-1.38nl.

f (Hz)	D (µm)	V (nl)
0.1	112	0.735
0.2	138	1.38
0.3	122	0.939
0.4	104	0.586

High-speed video footage is analyzed using Tracker 4.80 software to obtain droplet positions along the x-axis over time. The images presented in Figure 18(a)-(d) were created from the same high-speed video footage used to measure position. Each image in Figure 18 is comprised of horizontally-stacked, single-pixel-wide slices centered on the droplet from every frame of the corresponding video to demonstrate the droplet's motion in time. The period of a droplet's translational oscillation in each case is roughly given by Equation 10 where T_{tr} is the translational period and f is the frequency of mirror actuation. Oscillation periods, as can be seen in Figure 18(a)-(d), are roughly 10, 5, 3.3, and 2.5 seconds, respectively.

$$T_{tr} = \frac{1}{f} \tag{10}$$

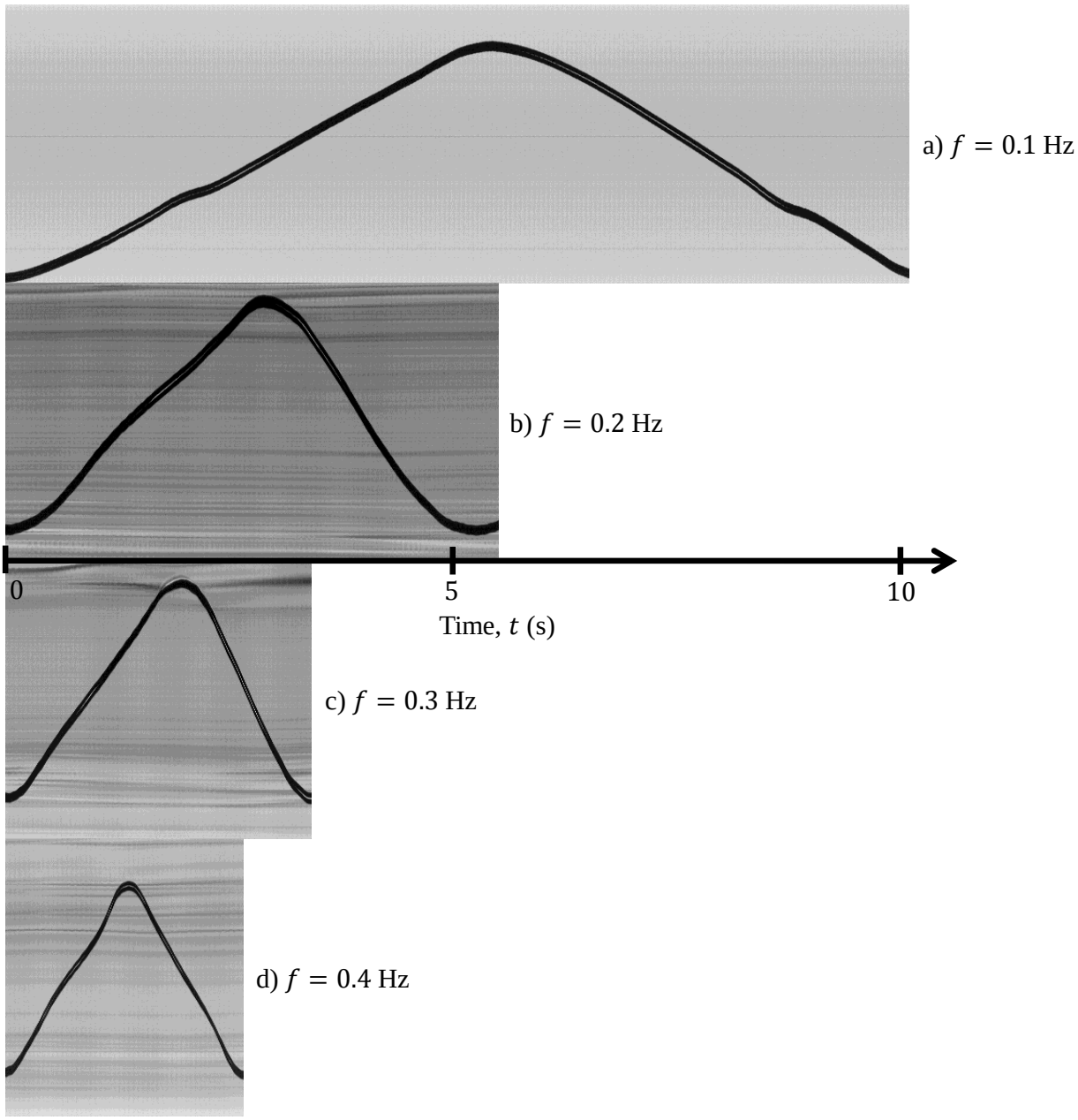

Figure 18 – Images created from high-speed video showing droplet translation in time. Mirror deflection frequencies are a) 0.1 Hz b) 0.2 Hz c) 0.3 Hz and d) 0.4 Hz.

The x-components of both droplet velocity and acceleration are calculated from position data using Equations 11 and 12.

$$V_{x,t1} = \frac{dx}{dt}\Big]_{t1} \sim \frac{x_{t2} - x_{t1}}{t_2 - t_1} \tag{11}$$

$$a_{x,t1} = \frac{dV_x}{dt}\Big]_{t1} \sim \frac{V_{x,t2} - V_{x,t1}}{t_2 - t_1} \tag{12}$$

Upon analyzing calculated velocity and acceleration values and close examination of the high speed video, it was realized that small but relatively steady vibrations of the camera-microscope assembly persisted throughout the video acquisition process. The magnitude of high-frequency changes in velocity are generally around an order of magnitude lower than those of bulk droplet motion, but due to their high frequency values add enormous error to values of acceleration obtained using Equation 12. High-frequency fluctuations in velocity make no physical sense in the system as they would require accelerations on the order of 1000 mm/s^2 to be achieved.

Vibrational distortion is confirmed by performing a Fourier Transform on the velocity data sets. The following plots in Figure 19(a)-(d) show the magnitude of periodic signals at frequencies up to the Nyquist frequency (defined as one half of the sampling rate of the data set, in this case the frame rate of video acquisition) that compose the velocity of the droplet as a function of time. In each plot, the "Raw" label corresponds to the unfiltered data obtained from the high-speed video and the "Filtered" data corresponds to the same Fourier analysis performed on data after a low-pass filter is

employed to smooth the data. It's clear from these comparisons that the smoothing process preserved data for frequencies less than a few Hz (much larger than the 0.1-0.4Hz frequencies of translation), and most importantly the fundamental frequency, while higher frequency fluctuations are removed.

a)

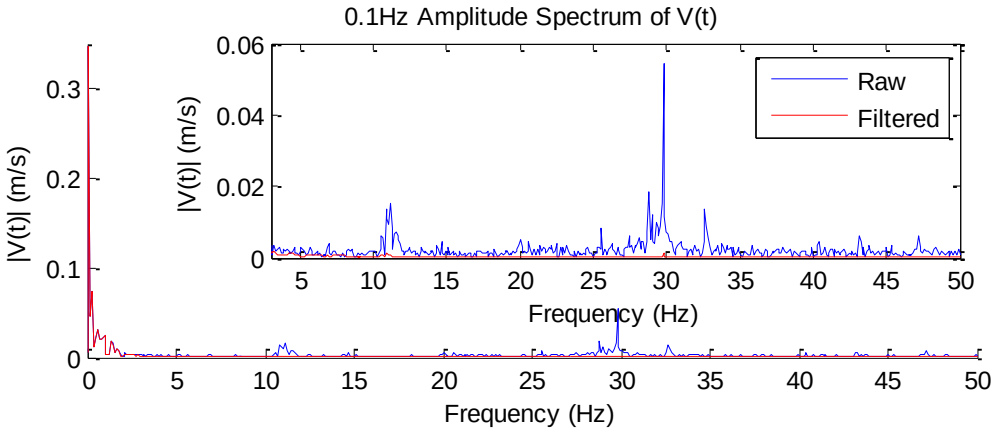

b)

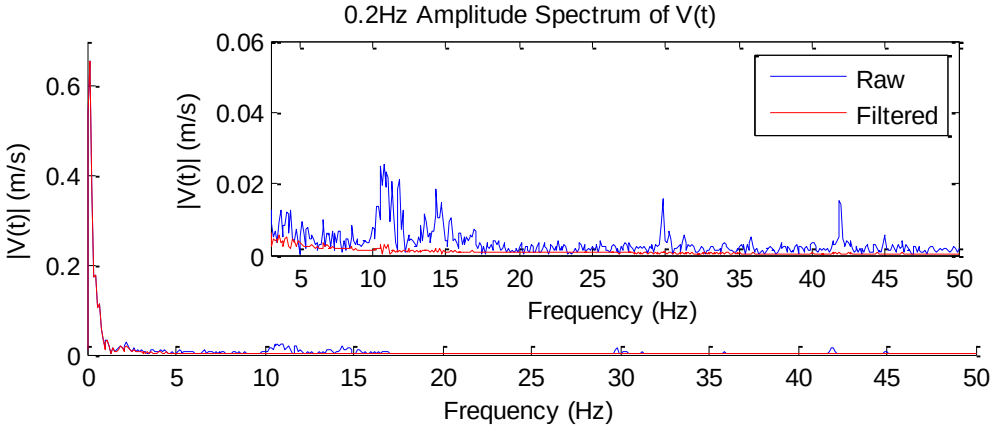

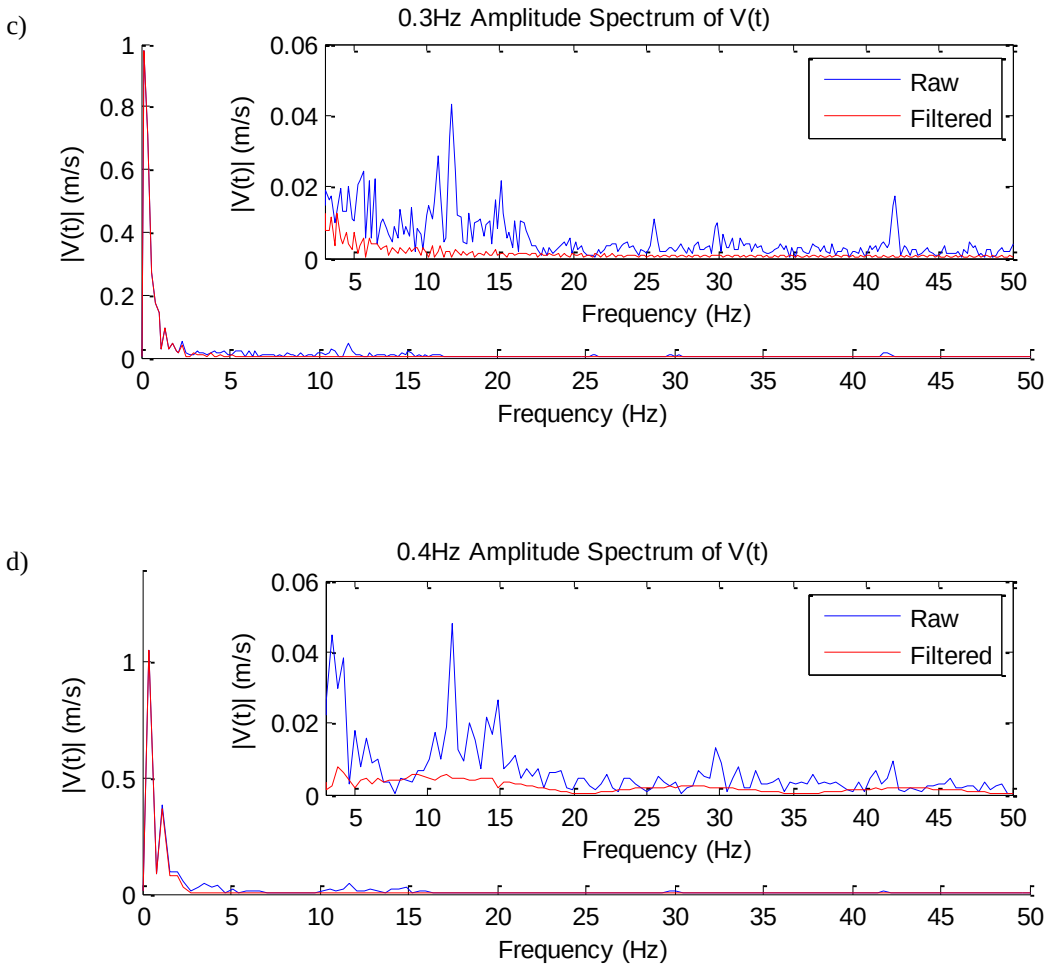

Figure 19 – Comparisons of raw velocity data reveal high-frequency fluctuations caused by vibrations in the camera-microscope assembly. Low-pass filtering is employed to smooth out these high-frequency fluctuations while maintaining data at the fundamental frequencies of the system. Figure 19a-d correspond to successively higher mirror actuation frequencies (0.1, 0.2, 0.3, and 0.4Hz respectively).

The smoothed x-position data is used to calculate the droplet's x-velocity over time. While this improves interpretation of the velocity over time, calculated acceleration values still fluctuate rapidly and must be smoothed as well.

The final data sets are shown graphically in Figure 20-23. In each subplot, a blue dotted line represents the ideal x-position, x-velocity, and x-acceleration of the laser

beam. These are formed by the relations in Equations 13-15. The constant C is chosen such that it matches the amplitude of the droplet motion.

$$x(t) = -C\,tan(cos(2\pi ft)) \tag{13}$$

$$V_x(t) = \frac{dx}{dt} = 2C\pi f \sin(2\pi ft)\sec^2(\cos(2\pi ft)) \tag{14}$$

$$\begin{aligned} a_x(t) = \frac{dV_x}{dt} &= 4C\pi^2 f^2 \cos(2\pi ft)\sec^2(\cos(2\pi ft)) \\ &\quad - 8C\pi^2 f^2 \sin^2(2\pi ft)\tan(\cos(2\pi ft))\sec^2(\cos(2\pi ft)) \end{aligned} \tag{15}$$

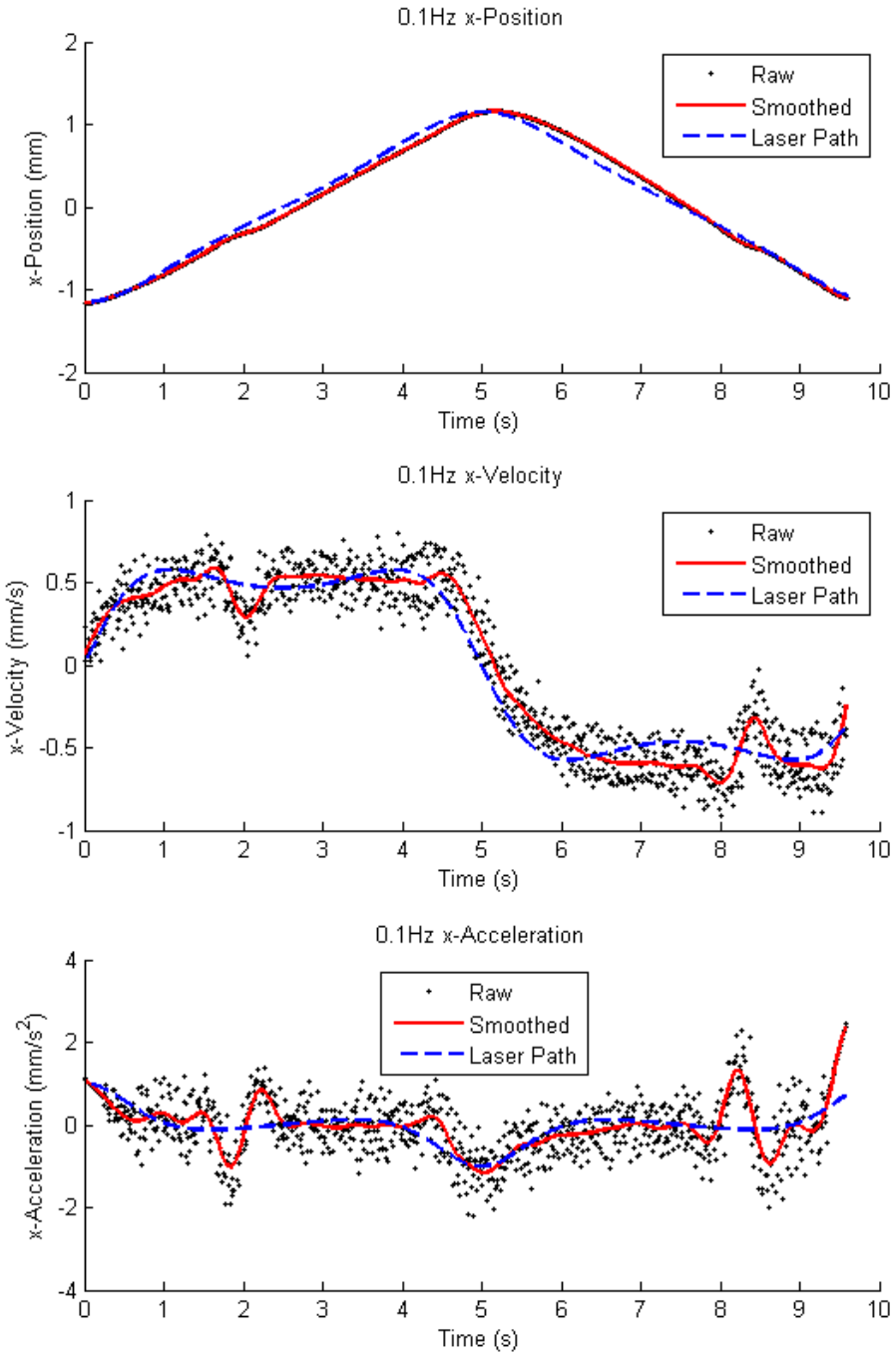

Figure 20 – Data obtained from translation of a nanoliter droplet at a mirror actuation frequency of 0.1 Hz.

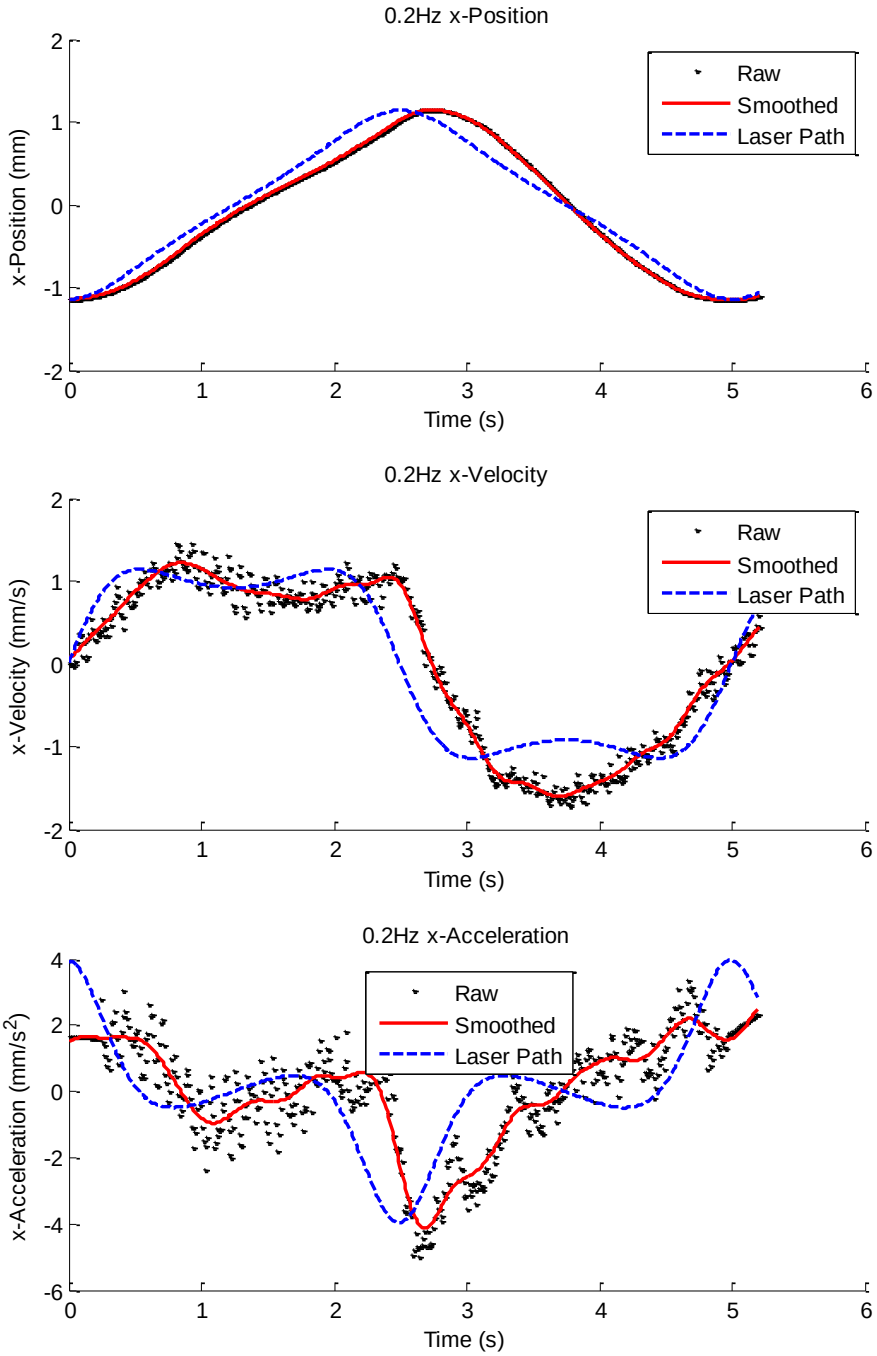

Figure 21 – Data obtained from translation of a nanoliter droplet at a mirror actuation frequency of 0.2 Hz.

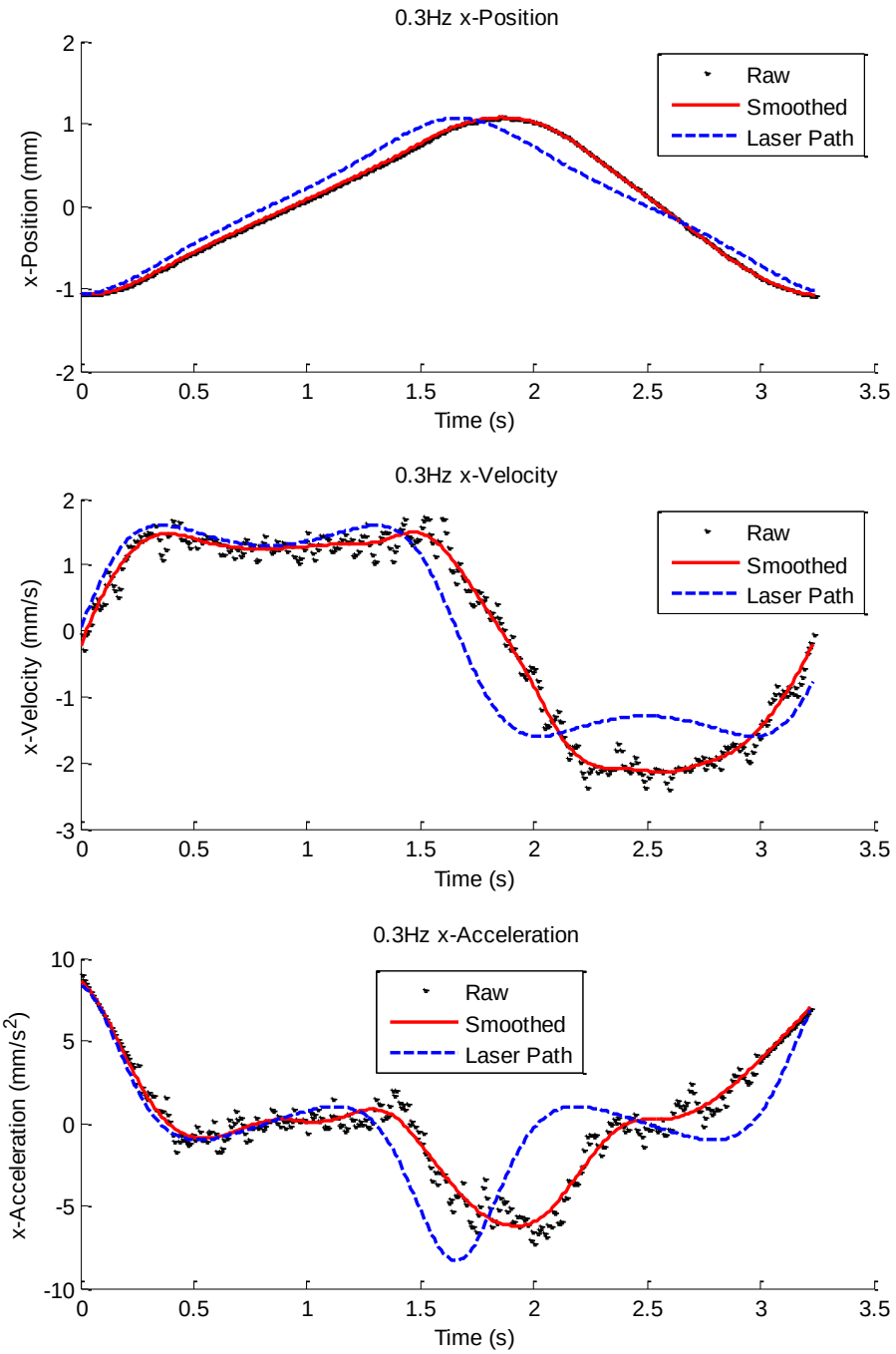

Figure 22 – Data obtained from translation of a nanoliter droplet at a mirror actuation frequency of 0.3 Hz.

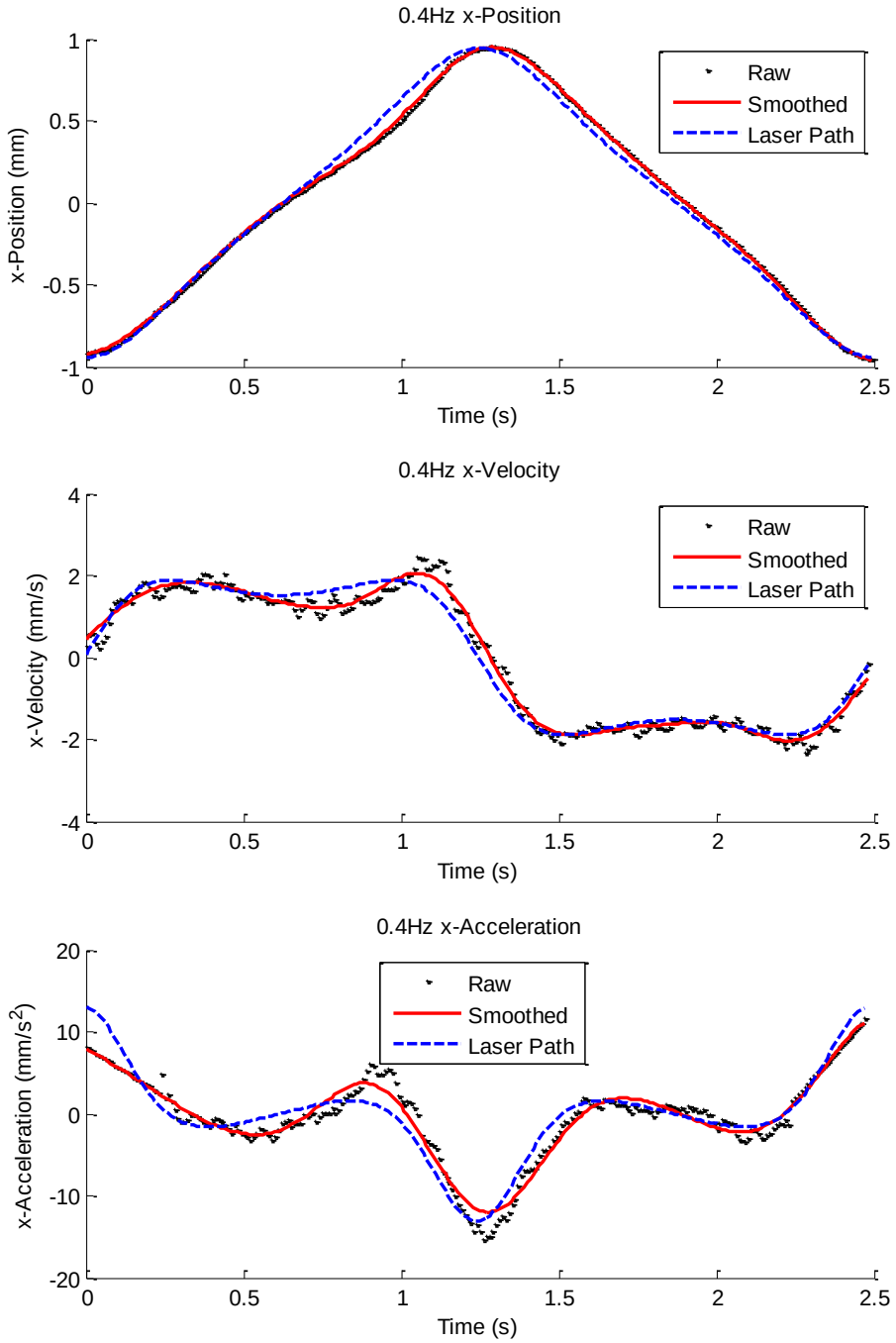

Figure 23 – Data obtained from translation of a nanoliter droplet at a mirror actuation frequency of 0.4 Hz.

3.5 Discussion of Results

By comparing the transient position of the center of the laser beam with the experimentally measured droplet position, levitation and translational control of nanoliter droplets has been shown to be possible and quite successful. Despite the reduction of data quality from vibrations in the camera-microscope assembly, meaningful results are obtained after a low-pass filtering process is employed to remove the high-frequency fluctuations in the data and preserve the relevant overall trends. The source of vibrations is not known, but could be due to vibrations in the laboratory building due to air handling systems or from within the camera which contains several moving parts (e.g. hard drive or cooling fan components).

As translational frequencies and speeds increase, there seems to be less deviation from the ideal position, velocity, and acceleration data. At lower speeds, ambient air currents have a greater chance to interact with the translating droplet over a period of motion as one period of translation is of longer duration. Despite the use of the glass enclosure, it is still possible for some air currents to interact with the droplets as the top of the enclosure is open to allow unimpeded laser beam entry. It should also be noted that in the 0.1Hz frequency test, the translating droplet encounters a small scratch on the glass substrate. This temporarily slows the droplet until the centering force becomes large enough to move the droplet back to the center of the laser beam. This slight pause in motion can be seen in the data presented in Figure 20 at 2 and 8 seconds.

3.5.1 Comparison to Traditional Means of Microfluidic Transport

The ratio of a liquid's surface tension-temperature coefficient and absolute viscosity, σ_T/μ, is used by Sammarco and Burns (1999) to predict magnitudes of thermocapillary pumping speeds. By comparing thermocapillary pumping speeds for different liquids under identical temperature differences, a reasonable estimate for the achievable thermocapillary pumping speed for silicone oil can be estimated. Fluid properties and pumping velocities at 20K and 30K temperature differences are listed in Table 2 below. Inspection of the data presented by Sammarco and Burns (1999) yields the relationship in (16) and estimated silicone oil thermocapillary pumping speed in (17).

Table 2 – Liquid property values used to estimate the thermocapillary pumping speed achievable for 5cSt silicone oil in a 100μm channel with a 20K temperature difference imposed.

Liquid	σ_T (dyn/cm/K)	μ (Poise)	σ_T/μ (cm/K/s)	V_{30K} (μm/s)	V_{20K} (μm/s)
Mineral Oil[a]	0.221	0.26	0.85	15	-
Silicone Oil	0.069	0.0459	1.50	-	V_{SO}
Toluene[a]	0.1189	0.005763	20.6	350	150

[a]Taken from Sammarco and Burns (1999)

$$\frac{V_{SO}}{V_{Tol}} \sim \frac{[\sigma_T/\mu]_{SO}}{[\sigma_T/\mu]_{Tol}} \tag{16}$$

$$V_{SO} \sim V_{Tol} \frac{[\sigma_T/\mu]_{SO}}{[\sigma_T/\mu]_{Tol}} \tag{17}$$

Translation speeds of 10μm/s are achievable by thermocapillary pumping for silicone oil based on the estimate above. To move a quantity of silicone oil 1cm at a

speed of 10um/s it would take 1000s (17minutes), an undesirably long time. Higher temperature differences could be used to increase pumping speeds, though aqueous samples would be at risk of freezing or overheating as ΔT increases.

An electric field can be used to induce electro-osmotic flow (EOF) in microchannels. In most cases, these flows are characterized by a bulk uniform slip speed with an abrupt change in the vicinity of the wall and electric double layer to satisfy the no-slip condition. This slip speed V_{EOF}, caused by the net force on the fluid within the double layer, is given by (18) where m_{EO} is a local mobility parameter and E is the magnitude of the electric field. Systems where aqueous biological samples are used would have $O(10^{-4}\text{cm}^2/\text{V/s})$ values of m_{EO}. In order to achieve moderate, O(mm/s) pumping speeds, large electric field strengths of O(kV/cm) would be necessary (Stone *et al.* 2004).

$$V_{EOF} = m_{EO}E \tag{18}$$

While demonstrating thermocapillary levitation of nanoliter-volume droplets is possible, these results also show that significant improvements in pumping speeds for LOC applications can be achieved by utilizing this method. Based on the order-of-magnitude estimate discussed previously, thermocapillary pumping speeds of O(10μm/s) are achievable for silicone oil, but speeds of O(mm/s), two orders of magnitude larger, have been achieved using this method. Higher speeds could possibly be attained, but the limiting factor in these experiments is the available test area over which a levitating droplet can accelerate to achieve these speeds. The experiments presented here represent the highest acceleration achievable. At mirror oscillation frequencies higher than 0.4 Hz,

droplets no longer remain fixed under the laser beam and wet the substrate where thermocapillary conditions are insufficient. There is also no need for applying large electric fields to achieve fluid transport.

3.6 Conclusions

Based on the success of levitating and translating these nanoliter-volume droplets, it's clear that this mechanism should be suitable for the levitation and translation of nanoliter-volume compound droplets. In order for this to be explored, a method of generating these two-phase droplets must be developed. This is examined in the following chapter.

4. COMPOUND-DROPLET GENERATION

4.1 Droplet Generator Design

The design of the compound-droplet generator is based largely on a simple, single-phase drop-on-demand system devised by Yang *et al.* (1997) and used in recent work by Terwagne *et al.* (2013). This design uses a piezoelectric diaphragm in contact with a liquid-filled chamber to initiate droplet ejection. The present compound-droplet generator, shown schematically in Figure 24, consists similarly of a piezoelectric diaphragm backing a water chamber driven by a voltage waveform to induce deformation of the membrane and corresponding pressure pulses. These pressure pulses are completely dependent on the waveform used and can be modified at will, changing amplitude, shape and/or duration to produce the desired droplet ejections.

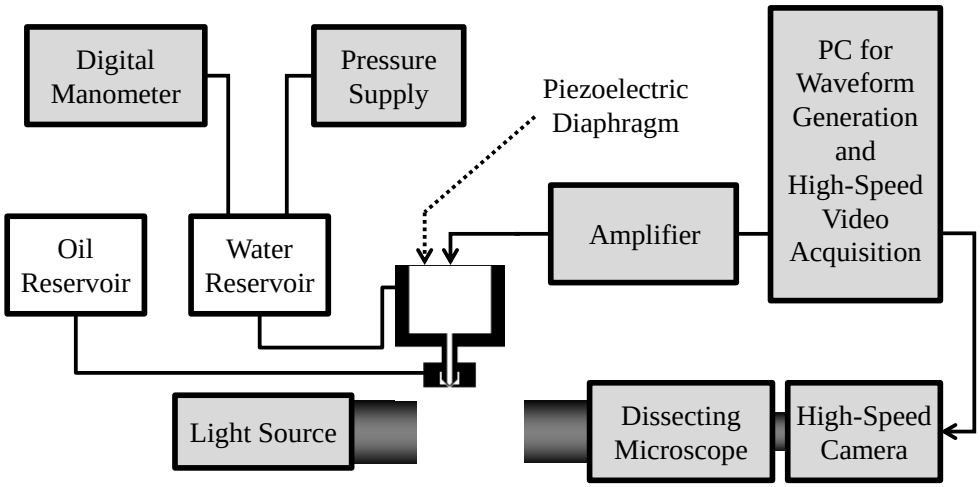

Figure 24 – Experimental setup.

The ability to generate compound-phase droplets results from the use of a specialized compound nozzle. The compound nozzle of the present droplet generator is

comprised of an inner water nozzle positioned concentrically within an outer oil nozzle, as illustrated in Figure 27, both of which are machined from stainless steel. The outer surface of the water nozzle is threaded to permit it to be attached to both the water chamber and the oil nozzle. The water nozzle has an orifice length of 500μm, diameter of 250μm, and is coated with a phosphoric-acid-modified perfluoroalkyl chain, which adheres readily to the metallic surface, rendering it hydrophobic to aid in droplet pinch off. The only surface of the inner nozzle not coated with the hydrophobic coating is the inside of the nozzle orifice to promote the mobility of the liquid-liquid interface necessary for composition variation. The oil nozzle is threaded over the inner nozzle, allowing for differences in axial position between the two, although this feature was not exploited in the results presented here. Its outer surface is coated with a commercial oleophobic coating, Rainoff MFB^{TM}, to prevent the silicone oil from wetting this surface and leaking from the oil nozzle. An exploded view of the nozzle used in these experiments, designed and rendered in SolidWorks, is given in Figure 25. Detailed engineering drawings of these parts are included in Appendix A.

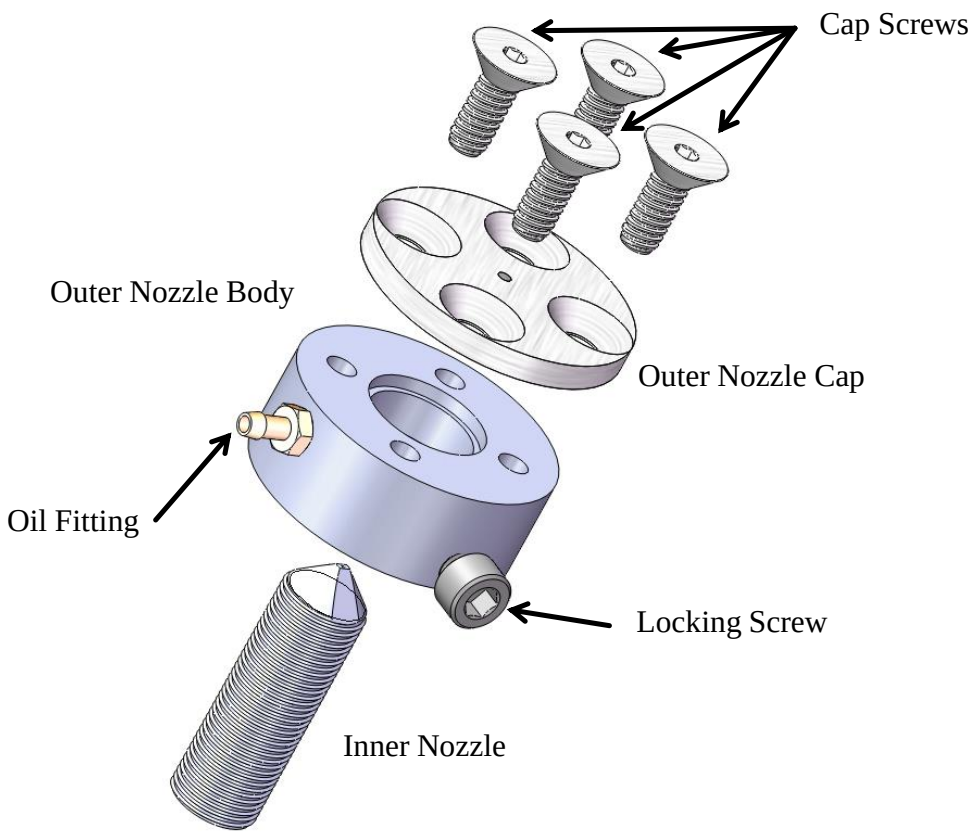

Figure 25 – An exploded view, rendered in SolidWorks, of the compound nozzle assembly. The cap screws fix the outer nozzle cap to the outer nozzle body to compose the outer nozzle. This outer nozzle is threaded over the inner nozzle, filled with oil through the oil fitting, and locked in place with the locking screw.

The water chamber, from which water flows into the inner nozzle, is refilled from a sealed reservoir, allowing for its pressure to be both controlled and varied using a Furness Controls FCO502 Pressure Supply device. This feature is crucial to the repeatable operation of the system and its ability to generate droplets of variable volume ratio. An exploded view of the body of the droplet generator is shown in Figure 26.

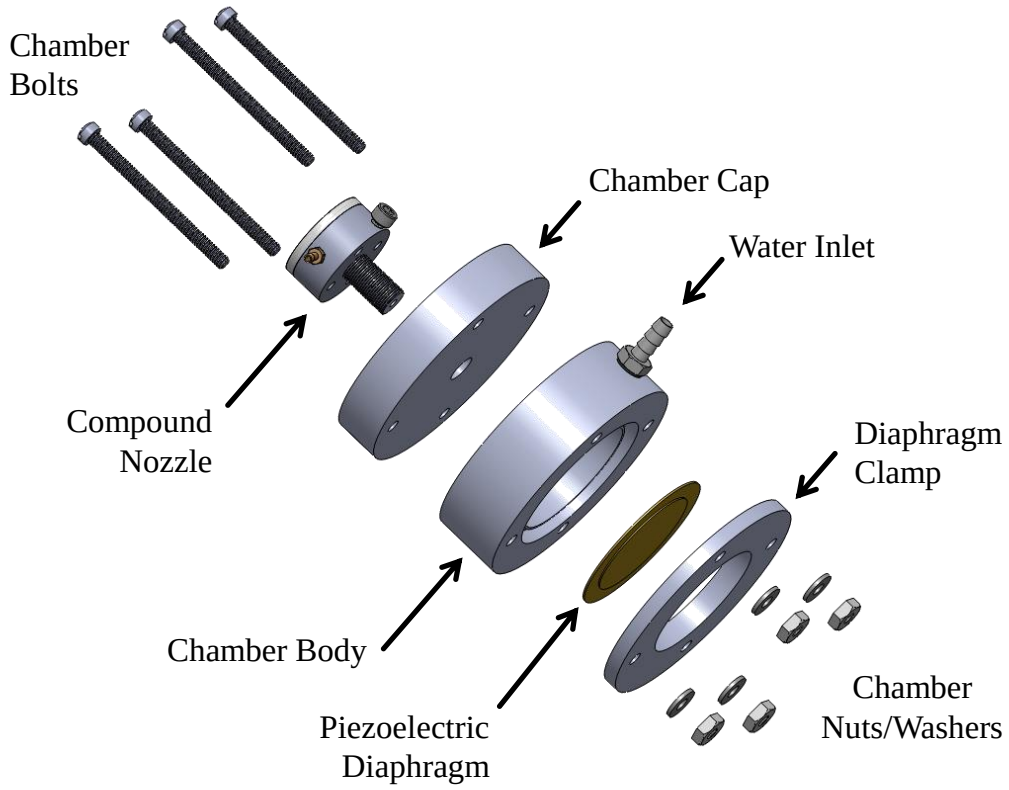

Figure 26 – An exploded view, rendered in SolidWorks, of the droplet generator assembly. The chamber bolts compress the chamber cap, chamber body, and diaphragm clamp securing the piezoelectric diaphragm against an O-ring gasket (not shown). Water fills the chamber through the water inlet and the compound droplet is threaded through the hole in the chamber cap.

Oil is gravity-fed into the surrounding outer nozzle; the pressure of the oil is not controlled precisely, but is varied by raising or lowering the oil reservoir to change the gravitational pressure head. In a production device, it is anticipated that the oil pressure would be controlled differently to permit more automatic operation on shortened time scales.

4.2 Generation Procedure

In order to create a compound droplet, the nozzle must be prepared for ejection. The steps in this process are shown in Figure 27. First, the pressure in the water is set to a value that causes water to partially fill the cylindrical cavity preceding the nozzle exit (Figure 27a). The oil reservoir is raised to increase oil hydrostatic pressure, causing the oil nozzle to fill with oil (Figure 27b). The tip of the water nozzle will have space to allow oil to flow into, the size of which is determined by the pressure set within the water chamber. Once the oil overflows the water nozzle, the oil reservoir is lowered to reduce pressure, allowing the excess oil to flow out, thereby leaving an oil-capped water column in the inner nozzle (Figure 27c). This two-phase column of liquid is what will form the liquid jet to be pinched off into a compound droplet upon actuation. The completion of the process, i.e., the encapsulation of the water droplet by the oil, occurs while the droplet is in free-flight and is driven by the surface properties of the oil/water combination. In the present embodiment, the 5cSt silicone oil quickly [in a time of O(1 ms); see Figure 29 below] surrounds the water droplet to form a compound droplet of water encased in oil.

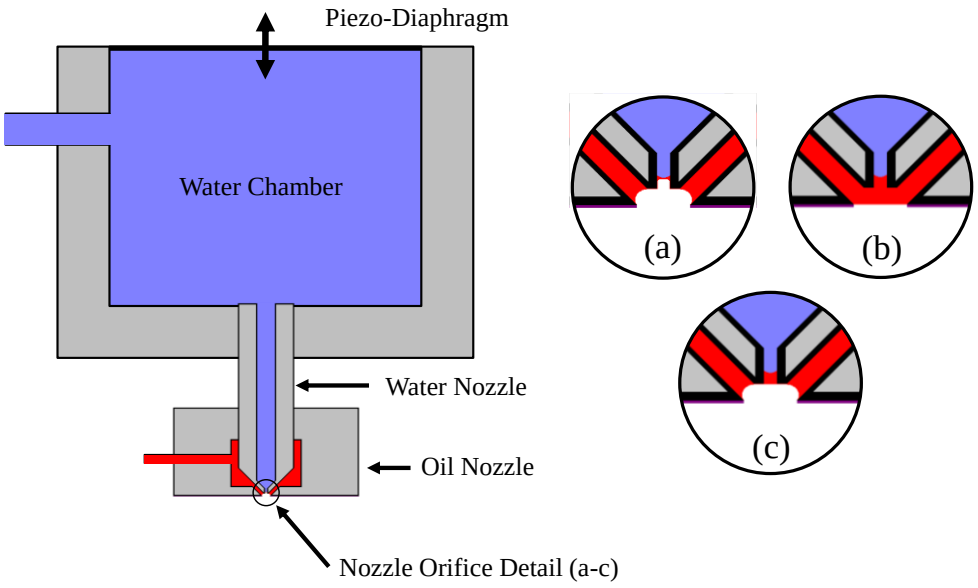

Figure 27 – The nozzle detail and steps in nozzle preparation prior to ejection are shown. (a) The pressure within the water chamber is set such that the water partially fills the inner orifice; (b) the hydrostatic pressure of the oil is increased to fill the available space within the inner nozzle; and (c) the hydrostatic pressure of the oil is decreased to remove excess oil and prepare the nozzle for compound-droplet ejection.

As mentioned previously, droplet ejection is achieved by providing pressure pulses via a voltage waveform input to the piezoelectric diaphragm. The waveform used for the results presented in this paper is the square wave shown in Figure 28. The initial voltage shift (in this case from positive to negative) provides the positive pressure pulse to eject the liquid contained within the inner nozzle to form a compound tongue of liquid. After a small amount of time, the voltage shifts rapidly again providing the negative pressure pulse that pinches off the liquid tongue from the nozzle, allowing the formation of the compound droplet. The pulse duration τ_p controlling the duration of the diaphragm deformation, is a key variable in the waveform. Longer pulse durations create a longer liquid tongue, resulting in satellite droplets or multiple droplets. A small range of pulse durations has been found to reliably generate single compound droplets. Within

this range, droplet ejection speeds are also dependent on the pulse duration, with the highest (lowest) speeds observed at the upper (lower) value of τ_p. A desire to modify the properties of the encapsulated liquid may be required (e.g. increasing viscosity), and such changes necessitate modifying the pressure pulse duration, as discussed later. The voltage waveform can also be modified to produce single compound droplets for varying chosen nozzle geometries and operating pressures. Increasing the amplitude will force liquid out more quickly during the positive pressure pulse. Trial and error has been found to be the best method to find the proper waveform parameters to yield a single compound droplet for given nozzle geometries and chamber pressures.

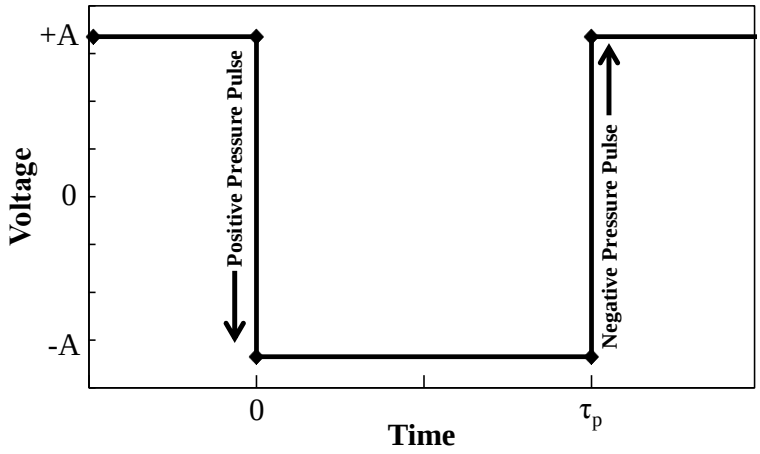

Figure 28 – Actuating voltage waveform for piezoelectric diaphragm.

Representative images of the different stages of droplet ejection are shown in Figure 29; this case is for a relatively thick encapsulating layer to illustrate the oil-water interface clearly. For these droplets, the amplitude of the waveform output from the amplifier is 67V and the pulse duration is 185μs. The times shown in these images are measured from the initial movement of the liquid within the inner nozzle. At t = 0, the

fluid is actuated and at t = 1.25 ms, the compound liquid tongue is pinched off; the oil plug riding on the front of the water is clearly visible. At t = 1.72 ms, the pinched-off liquid column with a visible oil-water interface is shown. Deformation as a result of pinch-off oscillation and oil engulfment of the inner droplet is shown at t = 2.34 ms. The final image at t = 3.91 ms shows a fully encapsulated, virtually spherical, water droplet with the oil-water interface still visible.

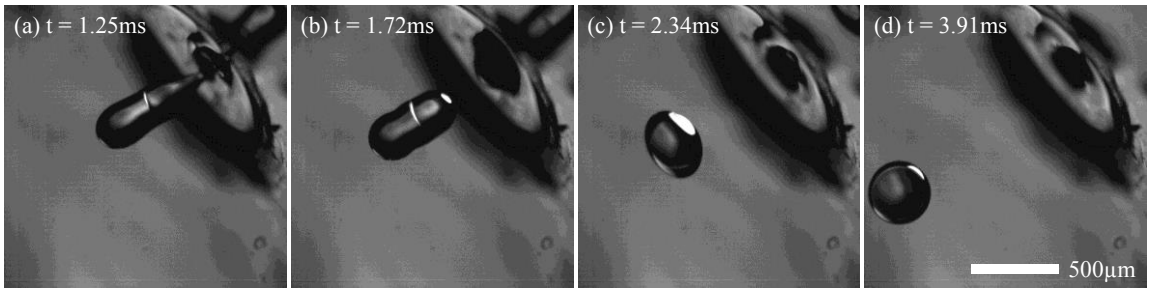

Figure 29 – Images of compound-droplet formation extracted from high-speed video.

Variations in droplet composition are achieved through changes in the water-chamber pressure for a fixed pressure pulse, although variation of the latter may also be used, if desired. All water pressures provided are those at the nozzle orifice, with the pressure regulator adjusted to compensate for hydrostatic-pressure differences between the free surface in the water reservoir and the location of the nozzle exit. As this pressure is decreased, the water retreats, permitting more oil to flow into the nozzle, leading to a corresponding increase in the amount of oil ejected. This feature allows one to vary the resulting composition of the compound droplet.

4.3 Measurement of Droplet Composition

Direct measurement of droplet composition cannot be achieved from the high-speed video alone due to the loss of information and visibility of the liquid-liquid interface within the compound droplet caused by curvature-induced lensing effects. Additionally, despite the visibility of the oil-water interface in some cases (e.g., in the final image of Figure 29), the inner-droplet volume cannot be determined from the video images due to the uncertainty of its exact position within the compound droplet. To measure both the compound-droplet volume and the inner water-droplet volume, two separate images are analyzed. Overall compound-droplet volumes are measured from the high-speed video using a droplet image assumed to be spherical. When making this assumption, care must be exercised to use an image taken after oscillations induced by droplet pinch-off have damped out. Droplets with an appreciable film thickness (e.g. the droplet shown in Figure 29) take on a spherical shape within a few milliseconds of ejection. An oscillation damping timescale for droplets composed of mostly water may be estimated as d^2/ν, where d is droplet diameter and ν is kinematic viscosity. The diameter and kinematic viscosity are of order 10^{-4} m and 10^{-6} m^2/s respectively, yielding a 10 ms damping timescale. Higher resolution videos, in which droplet trajectories visible longer than 10 ms are captured, must be examined and are sufficient to ensure a spherical shape. Weber number values ($\rho V^2 l/\sigma$) for these droplets are on the order of 10^{-2}, implying small inertial deformation thereby validating the spherical assumption for a translating, oscillation-free droplet.

Volumes of the internal water droplet are determined by depositing the compound droplets onto the surface of a bath of 350 cSt silicone oil. The lower-viscosity oil film is

miscible with the bath liquid, while the highly viscous bath liquid permits a slow descent, with a spherical shape, of the more-dense water droplet. This allows the suspended water droplet to be photographed through a planar sidewall to avoid optical distortion and its volume determined.

4.4 Results

4.4.1 Effect of Water Pressure

In order to quantify the droplet composition, we use the dimensionless film thickness, t_c, taken to be the thickness of the oil layer divided by the compound-droplet radius, and water volume fraction F_w, the aqueous droplet volume divided by the total compound-droplet volume defined as follows:

$$t_c = \frac{r_c - r_w}{r_c} \tag{19}$$

$$F_w = \frac{V_w}{V_c} = \left(\frac{r_w}{r_c}\right)^3 = (1 - t_c)^3 \tag{20}$$

In the above, r_c is the compound-droplet radius and r_w the water-droplet radius.Using these quantities, we can determine how the composition of the droplet changes with varying operating pressure. These results for fixed pulse duration of 185μs are shown in both Figure 30 and Figure 31. Data points in these figures represent averages over multiple droplet ejections, and error bars quantify a computed uncertainty estimate based on image and measurement resolutions using the method of Kline and McClintock (1953). It is clear that, as the pressure at the nozzle orifice is increased, F_w increases while t_c decreases. These trends in water fraction and film thickness are

expected since the quantity of oil available for encapsulation is dependent on the location of the oil-water interface within the inner nozzle, which moves as the pressure within the water chamber changes. High water pressures correspond to a location of the water-oil interface at or near the outer surface of the inner nozzle while lower pressures locate the interface farther from the outer surface. Higher pressures than those reported will result in additional increases in the water fraction, including single-phase water droplets, but also yield undesirable effects such as the formation of satellite droplets and forced leaking from the inner nozzle. Lower pressures suppress water-droplet ejection, yielding single-phase oil droplets. An additional effect of decreased oil-layer thickness is manifested through the longer duration of the pinch-off oscillations due to the reduced viscous damping.

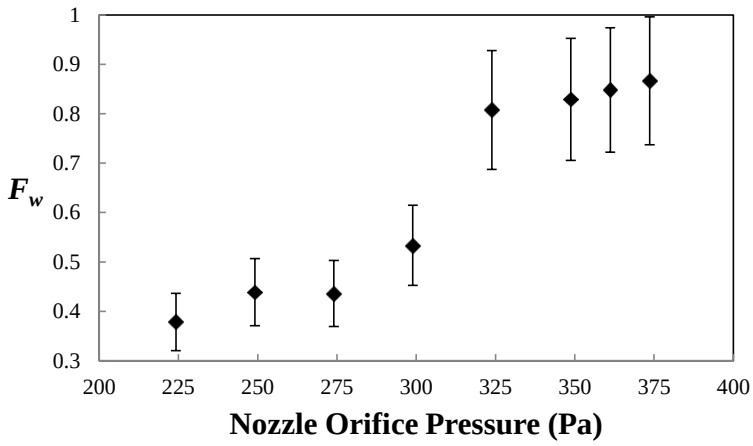

Figure 30 – Water fraction as a function of water chamber pressure. The average compound-droplet volume is 23.4nl.

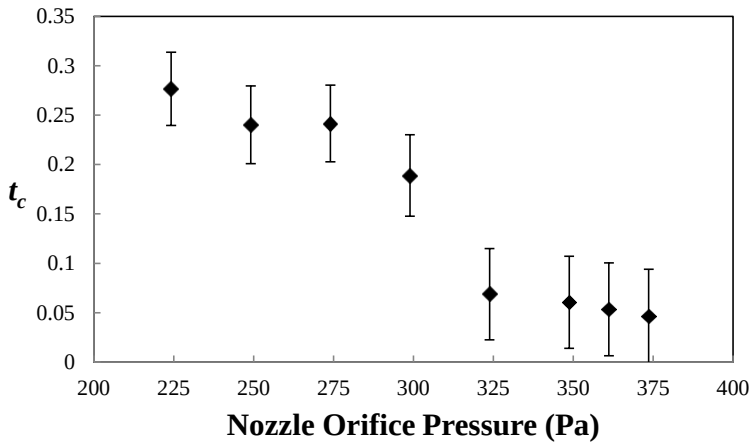

Figure 31 – Scaled film thickness as a function of water chamber pressure. The average compound-droplet radius is 170μm.

The compound-droplet and water-droplet volumes are compared in Figure 32 below. From this plot, the source of the composition variations can be seen. The inner water-droplet volume increases monotonically with water pressure, as expected. Compound-droplet total volume changes minimally throughout the range of pressures tested, averaging 23.4 nl, which is roughly the same volume as the cylindrical volume (24.5nl) of the inner nozzle orifice. Assuming that an unchanging waveform yields a minimally varying volume of liquid ejected with variations in composition due solely to the position of the liquid-liquid interface within the inner nozzle, this makes sense. At the upper limit of operating pressures, one expects the water to fill the channel, leading to a "compound" droplet the size of the water droplet alone. As the operating pressure approaches a minimum, the water droplet is nearly sucked back into the nozzle during the negative pressure pulse. Slight necking in the ejected fluid column in the vicinity of the liquid-liquid interface is observed in this case and represents the lower-pressure limit of compound-droplet formation.

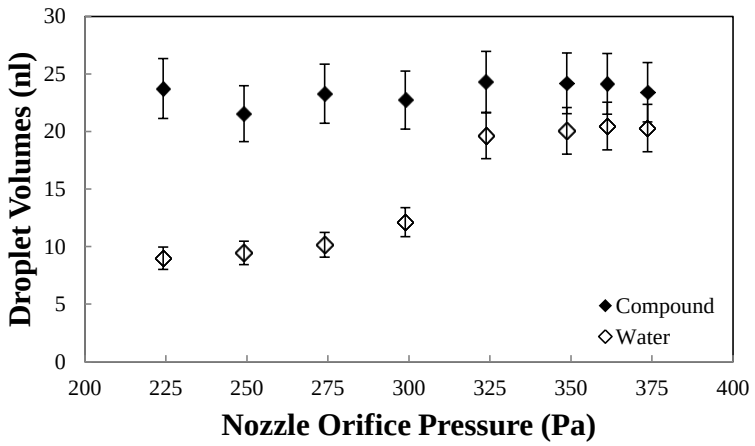

Figure 32 – Droplet volumes as a function of water chamber pressure.

The trends observed in droplet composition with pressure are a function of the location, shape, and properties of the liquid-liquid interface and metallic surface within the inner nozzle, but not ejection dynamics, as overall compound-droplet volumes remain roughly the same for the pressure pulse used in these experiments. Contributions to composition variations from interfacial shape (i.e. curvature) changes can be directly estimated by relating the operating pressure to the curvature of the liquid-liquid interface. Reductions (increases) in water (oil) volume as a result of curvature changes alone are an order of magnitude less than the variations observed and so curvature is assumed to contribute minimally. This suggests that the axial location of the liquid-liquid interface is the driving variable and this is fixed by the operating pressure. A speculation is required regarding the sharp variation in results noted in the neighbourhood of 300-325 Pa of water pressure in Figure 30 – Figure 32. Minor surface irregularities within the inner nozzle orifice could be causing pinning of this interface at one location or another, thereby giving rise to this jump, but internal observation of such features are not possible due to a lack of optical access.

4.4.2 Effect of Property Variation

In order to more fully characterize the droplet-generator operation using different liquids, the inner-liquid viscosity and interfacial tension between the encapsulant and inner droplet are varied by employing mixtures of water and glycerine for the inner liquid. These mixtures are characterized by the weight-percent of glycerine. Viscosities are measured using a Canon-Fenske viscometer and interfacial tensions between the mixture and silicone oil are determined using a pendant drop method described by Andreas, Hauser and Tucker (1938). The pendant droplets of water-glycerine mixtures are submerged in a 5cSt silicone oil bath and imaged through a flat glass side panel to obtain surface-curvature images to be used in calculating the interfacial tension. An example of such an image is shown in Figure 33 and measured values for the interfacial tension between 5cSt Silicone oil and various water-glycerine mixtures are given in Table 3 along with their kinematic viscosities.

Table 3 – Water-glycerine mixtures and 5cSt silicone oil relevant fluid properties at 22.5°C.

Glycerine Wt. %	ν^a (cSt)	σ^b (mN/m)
0	0.95	39.0
10	1.33	38.1
20	1.66	37.3
30	2.20	36.7
40	3.38	34.9
50	6.10	33.2

[a]Water-glycerine kinematic viscosity
[b]Water-glycerine and 5cSt silicone oil interfacial tension

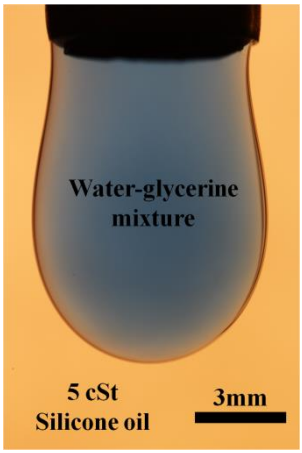

Figure 33 – Image of a pendant droplet of water-glycerine mixture in a 5cSt silicone oil bath used for measuring interfacial tension.

Modifying the inner-liquid properties significantly changes the composition limits of generated compound droplets. There are two main changes to system parameters that arise from altering the inner-fluid properties. First, a waveform modification must be made to account for the increased inner-liquid viscosity. During droplet ejection, viscous forces have a significant retarding effect on the formation of the jet at the orifice; it therefore becomes necessary to increase the positive pressure pulse duration to counter these increased viscous forces. As mentioned previously, a range of pulse durations will successfully achieve a single droplet ejection. Pulse durations are tested and chosen for the inner liquid (with no oil) to achieve a droplet-ejection speed of 0.5 m/s, roughly that observed for the pure-water case to match ejection dynamics. Ejection speed as a function of pulse duration is shown in Figure 34. For the 30% glycerine mixture a pulse duration of 210µs is used (as compared with 185µs for pure water). Minor changes to the pulse duration within the range that produces a single, satellite-free droplet have no effect on the composition of an ejected droplet as composition variation is almost entirely dependent on the location of the liquid-liquid interface within the inner nozzle.

In addition, the decreased interfacial tension between the water-glycerine mixtures and oil has a significant effect on composition limits. As this tension decreases, the range of operating pressures within the nozzle must be decreased to prevent leaking from the droplet generator. The pressure range for operation with a mixture of 30% glycerine in water is 0-150 Pa, a significant reduction from the range of 225-375 Pa employed for water as the inner liquid. The mobility of the liquid-liquid interface within the inner nozzle is impaired under these conditions allowing only droplets in the upper range of volume fractions (e.g. above 0.8 for the 30% glycerine mixture) to be produced. Error bars represent the propagated uncertainty in calculated quantities from measurements using the method of Kline and McClintock (1953). The methods are elaborated on in Appendix B.

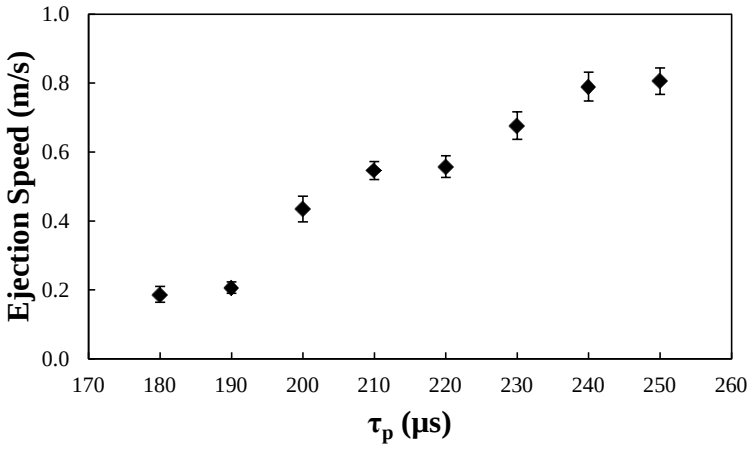

Figure 34 – Compound-droplet ejection speeds as a function of pressure pulse duration for 30% glycerine-water mixtures.

4.5 Uncertainty Analysis

Uncertainty quantification is achieved by applying the method of Kline and McClintock (1953) through the use of a propagated uncertainty estimate shown in (21) and (22).

$$\Delta q = \sqrt{\sum_{i=1}^{n} \left(\frac{\partial q}{\partial x_i} \Delta x_i \right)^2} \tag{21}$$

$$q = q(x_1, x_2, \ldots, x_n) \tag{22}$$

Here the uncertainty in a calculated quantity q (22), where q is a function of n variables $x_1, x_2, \ldots, x_n$, is Δq. Details for this analysis are contained in Appendix B.

4.6 Conclusions

We have successfully developed a technique to generate compound droplets-on-demand of varying compositions of silicone oil and distilled water. Changing the water-reservoir pressure affects the location of the oil-water interface within the water nozzle, causing changes in the volume of silicone oil pushed out of the nozzle ahead of the water. Fluid property variations were also studied to determine how system operation changes with inner liquids of increased viscosity and decreased liquid-liquid interfacial tension. Increases in viscosity are countered easily by lengthening the pressure-pulse duration to match ejection velocities of the pure water case although the interfacial-tension reductions drastically restricted the composition range for which compound droplets could be generated. Preliminary experiments suggest that, for LOC applications utilizing infrared laser heating to drive droplet levitation, ejection velocities must be significantly

reduced to allow reliable capturing of the compound droplet by the beam. This challenge is overcome by simply changing the pulse duration as described previously to decrease the ejection velocity to a point at which droplet capture is possible.

Having achieved nanoliter-droplet levitation and compound-droplet generation, the "droplet capture" problem and devised solution is presented in the following chapter.

5. DROPLET CAPTURE FOR LEVITATION

5.1 The Droplet Capture Problem

To initiate levitation experiments, a pre-formed droplet of liquid encountering a temperature gradient is required. Liquid droplets of sizes below the liquid's capillary length ($l_c = \sqrt{\sigma/\rho g}$) are generally formed by some forcing mechanism to overcome capillary forces and allow a portion of the bulk liquid to break off into a droplet. When such a droplet is under thermocapillary conditions (i.e. a temperature gradient is imposed on the droplet surface resulting in a corresponding surface tension gradient and induced surface flow), a droplet can levitate. It has been shown by Nagy and Neitzel (2008) that a droplet levitated under a laser beam of Gaussian intensity profile, but positioned off-center under the beam, can induce an asymmetric flow in the surrounding gas and a produce a net force in the direction towards the center of the beam. It is in this way that droplets can remain centered under the laser beam and translational control of droplets can be achieved when the laser beam is moved. If a droplet is deposited directly under the laser beam at the substrate, it can be captured by this centering force.

Traditional droplet generation methods produce droplets with significant velocities (0.1-1m/s) as a byproduct of the forcing mechanism used to overcome capillary forces. The high speed of such droplets after they are produced becomes problematic as the time a high-speed droplet encounters this capturing force under the laser beam is insufficient to enable droplet capture. Furthermore, if a droplet's speed is high enough when impacting the substrate, the droplet might wet the substrate before the necessary gas flow is established to prevent it. Therefore, it is necessary that a solution to this so-

called “droplet capture” problem be found so levitation experiments can be conducted on droplets much smaller than liquid’s capillary length produced by a droplet generator.

5.2 Droplet Impact Experiments

In order for a droplet to be captured, it must encounter the substrate without wetting. A multitude of studies have extensively evaluated droplet impacts on solid surfaces (Worthington 1876; Worthington 1876; Chandra and Avedisian 1991; Rioboo, Tropea and Marengo 2001) with varying roughness (Range and Feuillebois 1998), wetting characteristics (Richard and Quere 2000), and impact angles (Sikalo, Tropea and Ganic 2005). Few studies have dealt with normal impacts of droplets on smooth surfaces for which the droplet doesn’t wet the impact surface at least temporarily. The only known case is where Leidenfrost and impact conditions (i.e. substrate temperature and We) are sufficient to allow gentle film boiling of the liquid droplet in the vicinity of the substrate to prevent wetting (Tran *et al.* 2012). To date, none have done so under thermocapillary conditions such as those studied here. When thermocapillary conditions are not present, the thin gas layer that exists between a droplet and impacting surface (here called the substrate) is forced outwards, away from the impacting droplet, as it approaches. This gas layer takes a small, but finite amount of time to be displaced by the droplet’s surface but is never present long enough to prevent the impacting droplet from wetting. Some mechanism must be provided (in the case of Leidenfrost droplets, the rapid phase change due to the presence of the superheated surface) to replenish the gas layer and prevent wetting. Droplets impacting at sharp angles can glance without touching a solid surface due to the gas being temporarily forced into the lubricating layer between droplet and substrate by the relative motion of the liquid droplet (Neitzel *et al.*

2000). For thermocapillary droplets, the gas layer is sustained by the droplet's surface flow under the influence of surface tension gradients in the presence of a temperature gradient. The experiments reported on here are designed to explore droplet impacts under thermocapillary conditions to verify that droplets generated for LOC applications can impact a substrate (and subsequently be caught) without wetting.

5.2.1 Experimental Setup

The method of nanoliter droplet generation described in Chapter 3 demonstrates that droplets falling toward a cooled substrate under a laser beam can encounter the substrate without wetting if vertical momentum is sufficiently small. A series of experiments was conducted to determine relevant parameters that might predict whether a droplet traveling toward a substrate, with conditions necessary to levitate a static droplet of the same mass, might not wet that surface.

Two sizes of droplets are tested: the first are those which are of the same size as the liquid's capillary length; the second are those much smaller than the capillary length. In both cases, the test area had the same configuration. The only modification is the presence of the type of droplet generating mechanism suitable to produce droplets of the desired size. The general test area is configured as shown in Figure 35 below, much the same as in the nanoliter-volume levitation experiments. The apparatus consists of a smooth, glass plate cooled via a Peltier module and heat sink, a stationary infrared laser used as the heat source, and some way of depositing a droplet with minimal horizontal velocity.

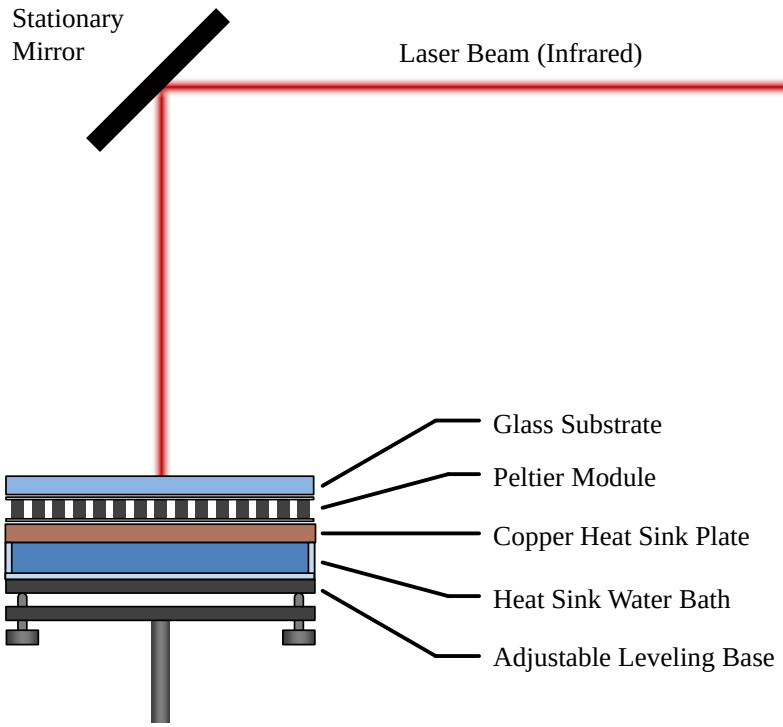

Figure 35 – The configuration of the droplet capture test area. The substrate is a smooth glass plate cooled by a Peltier module and heat sink.

For the capillary-length-sized droplets (roughly 1.5 mm in diameter for the 5 cSt silicone oil used here), a simple drip method of droplet generation is used as shown in Figure 36. Small amounts of silicone oil are deposited along a very thin wire positioned over the center of the laser-substrate contact point. The oil collects at the tip of the wire as a pendant drop until the droplet's weight overcomes surface tension forces and drips off. The resulting drop of oil, whose diameter is roughly the size of the liquid's capillary length of the 5cSt silicone used in these experiments (~1.5mm), falls toward the substrate. Vertical speeds can be varied simply by increasing the height at which the wire is positioned over the substrate allowing gravity to accelerate the droplet to different speeds over the changing fall distances. Droplet impact speeds and sizes are determined from post-processing of high speed video of each experimental run.

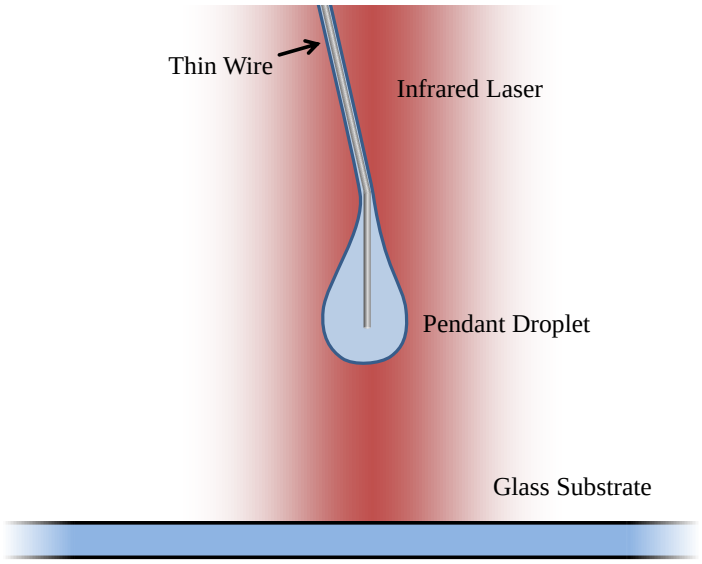

Figure 36 – To generate capillary-length-sized droplets, a simple drip method is used. Oil is deposited and allowed to flow down a thin wire where it collects, forms a pendant droplet that drips off toward the substrate after its weight overcomes the suspending surface tension forces. Droplets formed by this method are roughly 1.5mm in diameter, the capillary length of 5 cSt silicone oil.

To generate droplets smaller than the capillary length, a piezoelectric droplet generator is used with a nozzle whose orifice diameter is roughly the same size as the desired droplet size. For these experiments, a pipette of orifice diameter 0.5 mm is used to generate droplets of sizes that average roughly 0.6mm in diameter. A voltage waveform creates the necessary push-pull pressure pulse through deformation of the piezoelectric diaphragm to generate a single droplet in exactly the same manner as utilized in the compound-droplet generation experiments. As such, it is not elaborated on here. The ejection speed is controlled by modifying the positive pressure pulse duration such that a droplet is ejected with little or no horizontal velocity. Similarly to the pendant droplet generation case, the vertical distance between the pipette tip and substrate is increased to vary a droplet's impact speed. This generation method is shown in Figure 37.

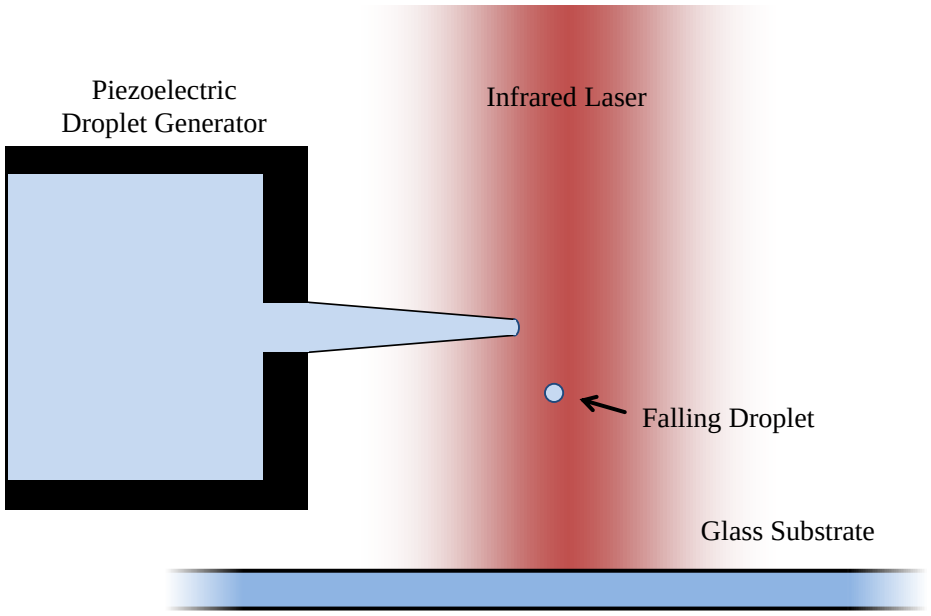

Figure 37 – To generate droplets smaller than the capillary length, a piezoelectric droplet generator is used employing push-pull pressure pulses to create a tongue of liquid and pinch it off into a droplet. Droplets generated using this method are roughly 0.6mm in diameter.

5.2.2 Droplet Deposition Examples

The series of images in Figure 38 represents the types of impacts created with the pendant-droplet generation method. Figure 38(a) shows a spherical droplet prior to impact, (b) shows the droplet shortly after impact, (c) shows the droplet with maximum spread, (d) as it is recoiling from the surface, and (e) after it has bounced back into the air. Figure 39 depicts the smaller droplets generated by piezoelectric forcing where image (a) is prior to actuation, (b) during actuation as the liquid exiting the nozzle forms a liquid tongue immediately prior to pinch-off, (c) after pinch-off during gravitational acceleration towards the substrate, (d) during impact while the droplet is at maximum spread, and (e) after bouncing off the substrate. The small droplet seen in image (d) is a satellite droplet created during pinch-off that doesn't adversely affect the experiment.

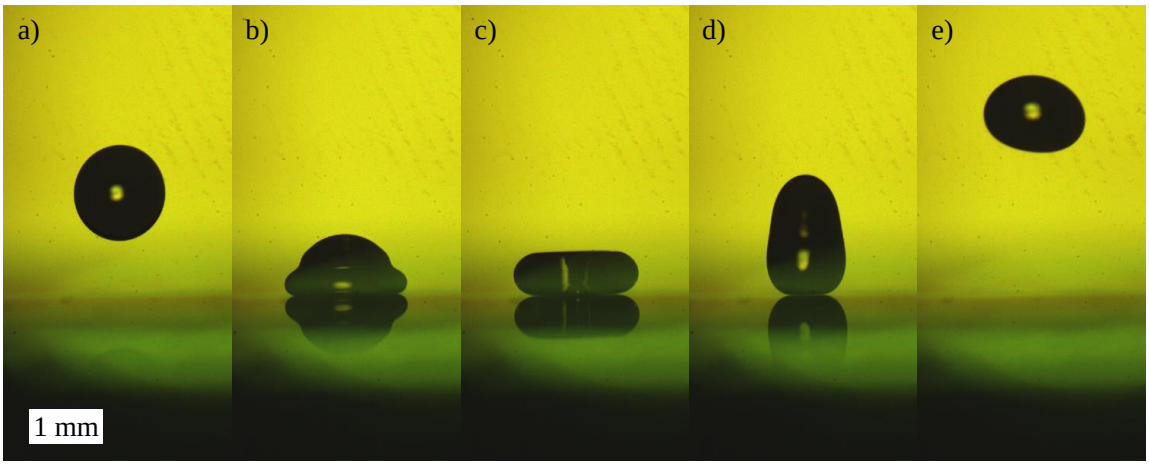

Figure 38 – Capillary-length-sized droplets are tested with increasing impact speed. Here, a 1.25mm-diameter droplet of silicone oil impacts a smooth glass surface at 0.31m/s. Image times are reported with respect to initial apparent contact with the substrate. (a) -2.4ms; (b) 1.5ms; (c) 3.9ms; (d) 6.8ms; (e) 30.7ms

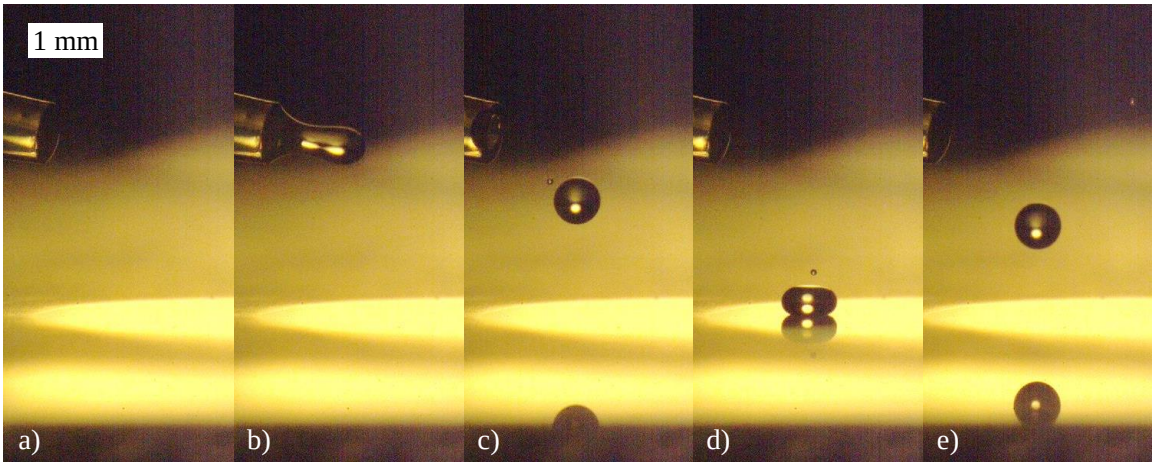

Figure 39 – Droplets of diameters smaller than the capillary length are generated using a piezoelectric droplet generator. In this series of images, a 0.63mm-diameter droplet of silicone oil is generated from the nozzle at the left and impacts a smooth glass surface at 0.19m/s. Image times are reported with respect to initial apparent contact with the substrate. (a) -20.5ms; (b) -17.6ms; (c) -7.8ms; (d) 1.2ms; (e) 16.8ms

Studies of droplets impacting superhydrophobic surfaces (Richard and Quere 2000; Richard, Clanet and Quere 2002; Clanet *et al.* 2004; Bartolo, Josserand and Bonn 2005; Bartolo *et al.* 2006; Jung and Bhushan 2008; Tsai *et al.* 2009; Reyssat *et al.* 2010;

Kwon and Lee 2012) exhibit similar rebounding where contact angles remain large. Under the impact conditions studied here (i.e. thermocapillary conditions for which a temperature gradient is imposed on the surface of the droplet) the droplets never touch the substrate and have an effective contact angle of 180 degrees. One might assume the images shown above depict droplet impacts under superhydrophobic conditions, but this is not the case. Droplets which impact the substrate with sufficient speed that the thermocapillary conditions cannot prevent droplet-substrate wetting look like the image provided in Figure 40. In this figure, an image is shown of a spherical droplet of silicone oil before impact (a) and after impact (b). This demonstrates the extreme wettability and low contact angle at the contact line and provides compelling evidence for the necessity of a gas film separating the droplet from the substrate maintained by thermocapillary conditions to prevent wetting and allow for capture.

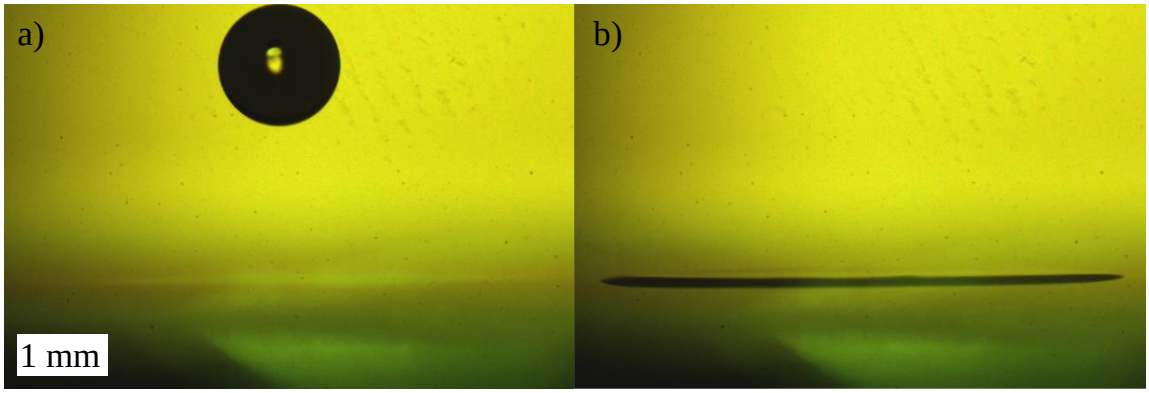

Figure 40 – Image (a) depicts a spherical droplet of 5 cSt silicone oil falling towards the substrate 4.2ms prior to impacting the substrate; (b) depicts the same oil, previously contained in the droplet, 80ms after impact having spread into a thin layer.

5.2.3 Experimental Results

The data presented in Figure 41 are the outcomes of impact experiments over a range of Weber and Reynolds numbers. Weber numbers are varied by altering both impact velocities and droplet sizes. The Weber number is the dimensionless number used to compare droplet inertial forces to surface tension forces in droplet impact experiments.

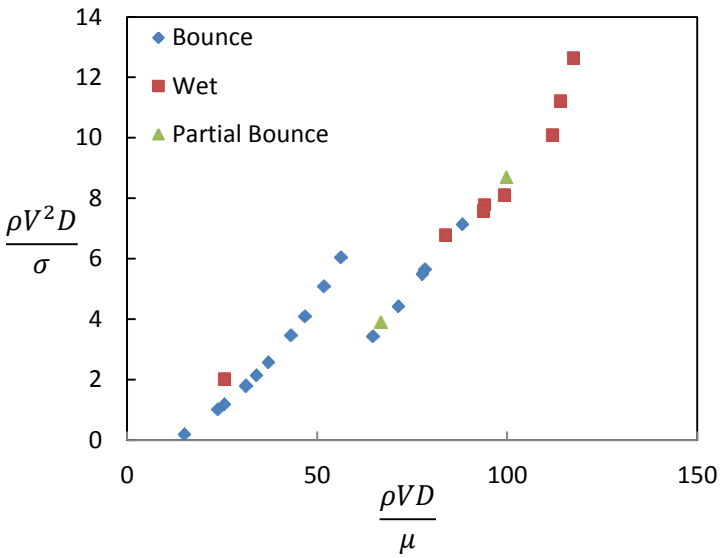

Figure 41 – Droplet impact outcomes at various Weber and Reynolds numbers. Examples of the three types of impact outcomes are shown in Figure 42.

This plot maps the outcomes of impact incidents over various Weber number values and suggests a relationship between the Weber number and the outcome of an impact. At values of We around 6 and lower, droplets tend to impact and rebound without touching the substrate. At higher values, droplets wet the substrate and either partially bounce (Figure 42b) or continue to spread over the substrate.

As inertia begins to dominate capillary forces, waves form on the surface of the droplet as shown by Richard *et al.* (2002) for We values around 4 or larger in their

experiments involving water droplets impacting superhydrophobic surfaces. These similar surface waves for droplet impacts under thermocapillary conditions could interfere with the surface flows required to sustain the lubricating gas layer between the droplet and substrate, or might displace the gas in the lubricating region and bridge the gap between the droplet and substrate immediately causing wetting.

Examples of the three types of outcomes presented in Figure 41 are given in Figure 42 below. In Figure 42(a), the droplet encounters the surface and completely bounces away, having never made contact. Figure 42(b) shows a droplet that wets the surface late in the bouncing process whereby a large portion of the droplet volume continues upward in a fluid tongue that breaks off into a smaller droplet. Finally, Figure 42(c) shows a droplet that wets early in the impact process and continues to spread into a thin oil layer.

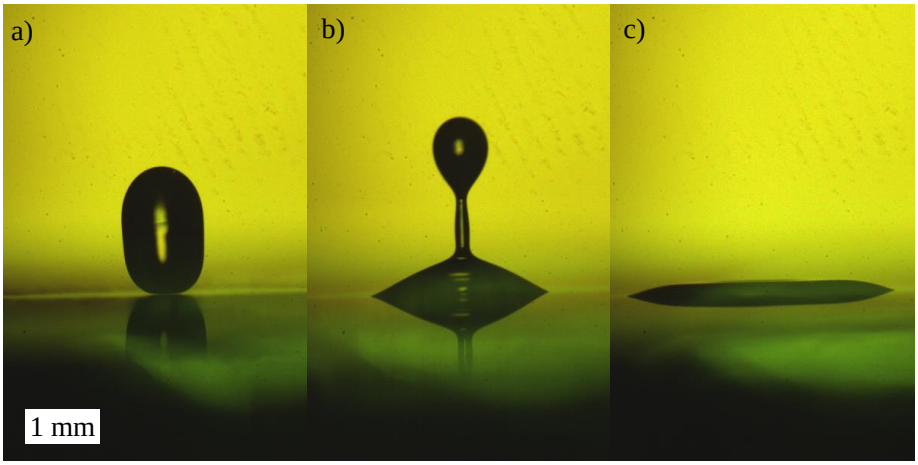

Figure 42 – The three types of impact outcomes under thermocapillary conditions are depicted: (a) bouncing 8ms after impact, (b) partial bouncing 10.5ms after impact, and (c) wetting 7.8ms after impact.

5.2.4 Contact Time and Inertial-Capillary (Rayleigh-Time) Scaling

Droplet impacts of liquids on superhydrophobic surfaces have been well studied recently as interest in research on naturally occurring superhydrophobic surfaces (e.g. the lotus leaf studies of Chen *et al.* (2011)) has increased and high-speed videography techniques yield the ability to film these impacts with very high temporal resolutions. The time between initial impact and rebound of these droplets (the contact time, t_c) on superhydrophobic surfaces scales with the Rayleigh time given in Equation 23 below. This timescale describes the oscillation period of a droplet under its lowest-order mode of oscillation.

$$\tau_R = \frac{\pi}{\sqrt{2}}\sqrt{\frac{\rho D^3}{\sigma}} \tag{23}$$

For droplet impacts in which a clean rebound occurs, the contact time can be directly measured and compared to this inertial-capillary, Rayleigh timescale. These results are presented in Figure 43 below. The best-fit linear regression has a slope of 2.72 and suggests a linear relationship between the contact time and the inertial-capillary timescale plotted on the x-axis. The dotted line in the figure corresponds to the Rayleigh time with a slope of $\pi/\sqrt{2}$.

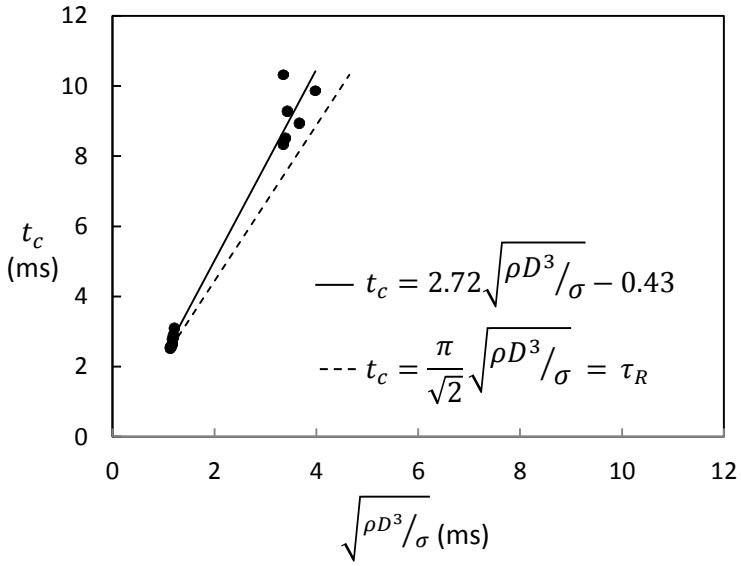

Figure 43 – Plot of the relationship between the experimentally measured contact time t_c of droplets impacting under thermocapillary conditions and the inertial-capillary timescale. A best fit line is compared to a Rayleigh-time line for the various droplet sizes under study.

The lower limit of the impact time, as predicted by Rayleigh and studied by Bird *et al.* (2013), is the Rayleigh time. Droplet impacts under thermocapillary conditions, which eliminate the need for the substrate-liquid-gas contact line to move as the droplet transitions from initial impact to maximum surface deformation and back to fully recoil from the surface, are studied here for the first time and provide further evidence that this timescale matches droplet impacts under these conditions. Figure 44 below shows the ratio of the experimentally measured contact time to the Rayleigh time over a range of Weber numbers. The horizontal dotted line is located at a value of unity where the contact time equals the Rayleigh time. For these axisymmetric impacts (as opposed to the impacts on patterned surfaces investigated by Bird *et al.* (2013)), no droplet impacts should reside under this line. Indeed none do as the Rayleigh time is the theoretical

lower bound for the contact time of droplets impacting and cleanly bouncing from a surface.

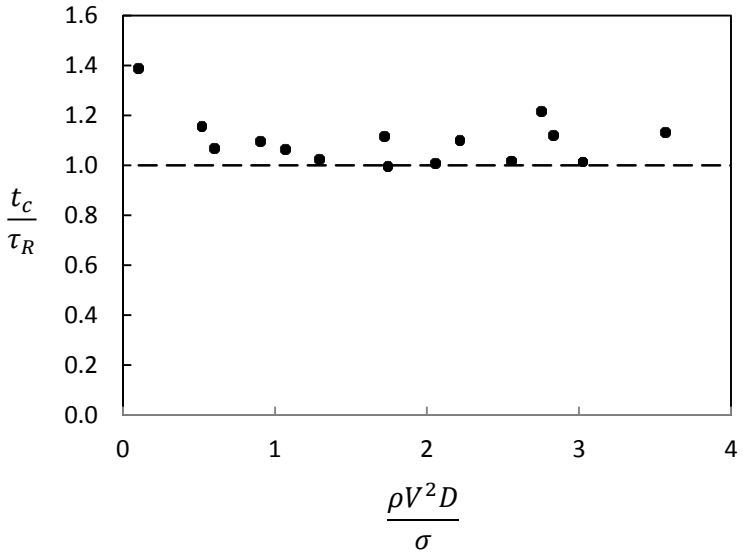

Figure 44 – The ratio of contact time to the Rayleigh time is plotted against Weber number for the droplet impacts where a clean rebound was achieved and wetting prevented.

5.2.5 Droplet Impact Conclusions

Based on these experimental results, conclusions can be drawn as to the ability for compound droplets generated by the method in Chapter 4 to safely impact and bounce under thermocapillary conditions. Ejection velocities of compound droplets created by a droplet generator are within the range of 0.1-1m/s. Droplet diameters are no more than 400μm on average, yielding Weber numbers in the range of ~0.2-20 depending on the droplet impact velocity. To achieve non-wetting bouncing, the experimental results suggest limiting droplet impact velocities to no more than ~0.6m/s to keep values of We under 6. This is achievable as shown in the compound-droplet generation studies.

5.3 Droplet Capture Methods

At the most basic level, the droplet capture problem is one in which a droplet traveling at some velocity impacts a substrate, bounces without wetting, and is "caught" by a force that places it under the laser beam with no velocity. Several types of forces can act on such a droplet: gravitational, aerodynamic, and a propelling force from asymmetric heating. Regardless of the mechanism causing the force, it should reduce both the momentum of the droplet to zero and leave it centered under the laser beam, which is a stable location, under appropriate conditions.

After multiple bounces, the vertical kinetic energy of a droplet is eventually dissipated and decays to a negligible value. All that remains to consider is the horizontal component of the droplet's momentum (velocity). The simplest methods of droplet capture are passive methods in which a droplet is captured in a way that doesn't require active variation and control of the capturing force. Relying on the naturally stable symmetry in the beam intensity profile and forces derived from asymmetric heating is the simplest passive method but has been shown to be insufficient for droplets ejected from a droplet generator that travel at speeds and with momentum in excess of that which could be decreased by forces provided by asymmetric heating alone. This has been explored experimentally and through the scaling analysis provided in the Introduction. Active methods for droplet capture could include precision air currents to decelerate the droplet into position under the laser beam, but such a method is difficult to reliably implement due the small droplet size. A finely tuned control loop feedback mechanism (e.g. a proportional-integral-derivative controller) to control the substrate angle such that a droplet that moves off-center of the laser beam is directed towards the center by angling

the surface and directing a gravitationally-induced motion in that direction could also be used to control droplet position. Any of these active methods are complex, and a simpler method is desired and devised.

An extremely simple solution is one in which the substrate shape itself induces motion, assisted by gravity towards the center of the laser beam to catch a droplet. This solution is elaborated on in the following section.

5.4 Droplet Capture via Substrate Shape

The passive method chosen for these experiments is the use of substrate geometry that induces gravitational forces to position the droplet under the laser beam. To this end, a modified substrate is proposed with a concave-upward surface to gravitationally force the droplet toward the laser beam positioned at its lowest point. The proposed design is shown in Figure 45.

Levitation experiments must be executed on a flat, smooth surface to demonstrate suitability to LOC applications. To move a levitated droplet from the curved area to a flat area, a smooth transition is required while still providing an angle such that the droplet will fall back to the bottom of the bowl if it bounces into this area. The tilted, lower-right image in Figure 45 demonstrates how this is possible by using a tangential intersection of the angled, flat substrate and the bowl.

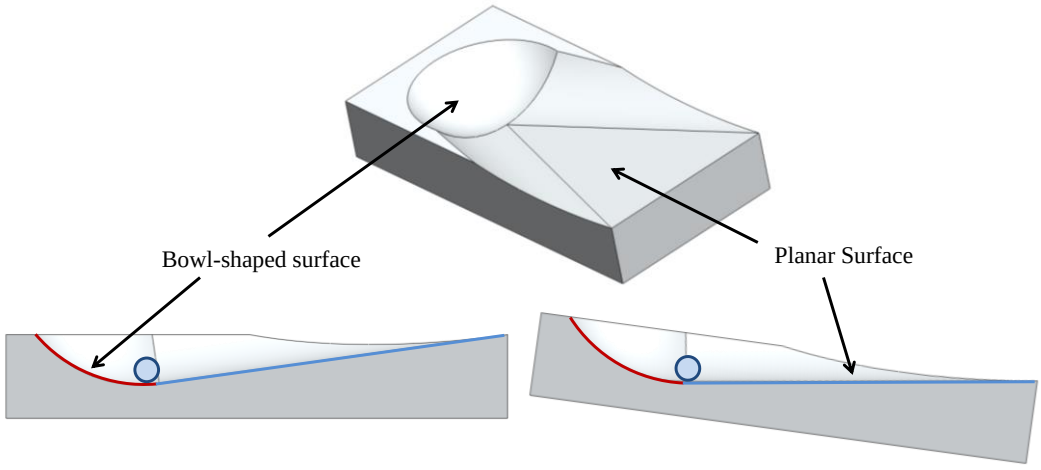

Figure 45 – The top image is an isometric, three-dimensional SolidWorks rendering of the droplet capture substrate utilizing a planar surface tangentially intersecting a curved, bowl-shaped surface. The image at the bottom left is a section view of the substrate orientation for droplet capture while the image on the bottom right is the section view of the orientation which allows the droplet to transition from the curved capturing surface to the flat test surface. The arrows directed outward from the descriptive text point to the same spot on the side-view and the isometric view.

Thermocapillary levitation has been tested exclusively on smooth glass substrates up to this point. A material change from glass to a more-easily-machined material such as aluminum shouldn't inhibit levitation so long as the surface is polished smooth enough. The metal also yields benefits via a higher thermal conductivity (reduced thermal gradients caused by the cooling module) and lower rate of substrate heating by the laser beam due to reduced radiative absorption in the infrared spectrum.

5.4.1 Droplet Capture Demonstration

As hypothesized, the proposed substrate geometry has allowed for reliable droplet capturing when droplet speeds are low enough to avoid immediately wetting prior to the first bounce. An example of a levitating, single-phase droplet resting in the bottom of the bowl portion of the aluminum substrate is provided in Figure 46. As the substrate is

tilted such that the flat portion is level, the droplet can be moved out to this region for translation studies.

Figure 46 – A single-phase, microliter-volume droplet of silicone oil is levitating, trapped in the bottom of the bowl portion of the polished aluminum substrate. This droplet has a diameter of 1.68 mm.

5.5 Comments on Steady Bouncing Droplets

Thermocapillary levitation experiments require a balance between substrate temperature (generally kept around 10°C) and laser intensity to create a vertical temperature gradient (roughly a 20°C difference between the substrate temperature and temperature at the top of the drop) such that liquid volatility doesn't become problematic. During preliminary experiments, a range of laser intensities was tested. As one would imagine, at extremely low laser intensities a sufficient temperature gradient to support levitation cannot be sustained and levitation fails. At extremely high laser intensities, droplets undergo rapid vaporization whereby the droplet size decreases and is eventually completely vaporized. Laser intensities for all experiments in this work were conducted within a small range at which levitation is achieved without encountering the adverse

effects just described. At the upper limit of laser intensities where levitation is achieved, droplets have been observed to steadily oscillate vertically and even bounce off the substrate as the laser intensity is increased further. This phenomenon was unexpected and could provide an avenue for measuring a liquid's surface-tension-temperature coefficient. This is explored further in the following.

5.5.1 Second-Order System Analogy

Theoretical models of oscillating liquid droplets have their origins in the work of Rayleigh (1879) in which he derives the timescale for the period of a droplet oscillating in its first mode. When viewed as a mass-spring-damper system, a simple model can be derived to relate relevant fluid properties to the oscillatory behaviour of the analogous system. This model formulation follows many of the conventions as presented by O'Rourke and Amsden (1987) in their TAB (Taylor Analogy Breakup) Model for aerodynamic breakup of droplets in engine sprays. In this model, we neglect aerodynamic forces as ideally levitating droplets exist in quiescent ambient conditions and describe our system as a damped, unforced, harmonic oscillator. The governing equation of such a system is given as

$$m\ddot{x} + d\dot{x} + kx = 0. \tag{24}$$

This equation describes both the typical mass-spring-damper system as well as a spherical and deformed droplet graphically presented in Figure 47. In each case, the displacement of the center of mass is x. For a droplet of density ρ and mass m, this displacement describes the motion of the droplet equator. The damping action,

characterized by the damping coefficient d in the mass-spring-damper system, is provided by the viscosity of the liquid μ for the oscillating droplet. The springing action given by the constant k in the mass-spring-damper system is provided in the droplet by the liquid's surface tension σ,.

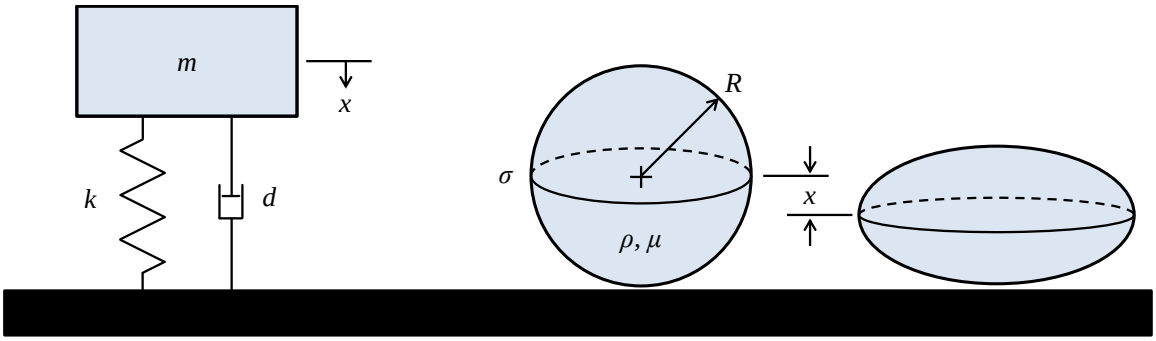

Figure 47 – Graphical comparison between a mass-spring-damper system and an oscillating droplet of a viscous liquid with radius *R*. The droplet's surface tension and viscosity are analogous to the spring constant and damping coefficient, respectively while the variable *x* represents the displacement of the center of mass of each.

The motion of an oscillating droplet in this case is restricted to its first-mode oscillations. Equation 25 can be rewritten in terms of the droplet's fluid properties with the additional coefficients C_k and C_d determined using dimensional analysis and consulting previous work by Rayleigh (1879) and Lamb (1932), respectively.

$$\ddot{x} + \frac{d}{m}\dot{x} + \frac{k}{m}x = 0 \tag{25}$$

$$\frac{d}{m} = C_d \frac{\mu}{\rho R^2}, \quad C_d = 5 \tag{26}$$

$$\frac{k}{m} = C_k \frac{\sigma}{\rho R^3}, \quad C_k = 8 \tag{27}$$

$$\ddot{x} + \left(C_d \frac{\mu}{\rho R^2}\right)\dot{x} + \left(C_k \frac{\sigma}{\rho R^3}\right)x = 0 \tag{28}$$

For such an oscillating system, the coefficient of x is the square of the undamped natural angular frequency ω_n (Eq. 29), and the period of an oscillation T can be solved for in terms of the droplet volume V and C_k as shown in Equation 30. When C_k takes a value of 8, the period of oscillation can be written as the Rayleigh time mentioned previously in the droplet impact experimental data analysis, taking the form of Equation 31.

$$\frac{k}{m} = {\omega_n}^2 = \left(\frac{2\pi}{T}\right)^2 = C_k \frac{\sigma}{\rho R^3} \tag{29}$$

$$T = \sqrt{\frac{3\pi\rho\left(\frac{4}{3}\pi R^3\right)}{C_k\sigma}} = \sqrt{\frac{3\pi\rho V}{C_k\sigma}} \tag{30}$$

$$T = \tau_R = \sqrt{\frac{3\pi\rho V}{8\sigma}} \tag{31}$$

The coefficient of $\dot{x}$ characterizes the damping of the system. For a viscous droplet, this is given by Equation 26 above. However, for the steadily oscillating droplets observed under thermocapillary conditions, the oscillations do not decay as would be expected from a viscous system. Given that the only modification of this steadily oscillating droplet from one that undergoes a decaying oscillation is the presence of the imposed temperature gradient, one can assume this is the cause of the persisting

oscillations. The nature of decaying oscillations is the viscous dissipation and damping of the energy contained in the oscillations. The presence of the temperature gradient coupled with the liquid's property of thermocapillarity creates a shear stress induced along the surface of the droplet driving internal flows that add to the oscillatory energy of the system. Underdamped, forced, second-order systems can undergo vibrations at a resonance frequency when a perturbation is provided. Ambient air currents or a small vibration in the test bench can perturb the droplet and the vibration grows at resonance. This resonance frequency ω_r is given by Equation 32 where the damping ratio ζ is given Equation 33.

$$\omega_r = \omega_n\sqrt{1-2\zeta^2} \tag{32}$$

$$\zeta = \sqrt{\frac{d^2}{4km}} \tag{33}$$

5.5.2 Experimental Observations

Multiple droplets of various sizes are examined by acquiring high speed video to measure the resonant frequency of the steady bouncing. Software is used to track the position of the top of the droplet which can then be related to the center position through a geometric symmetry assumption. The vertical, center location (above the bottom of the droplet) for a steadily-oscillating droplet of silicone oil with a diameter of 1.68mm is provided in Figure 48.

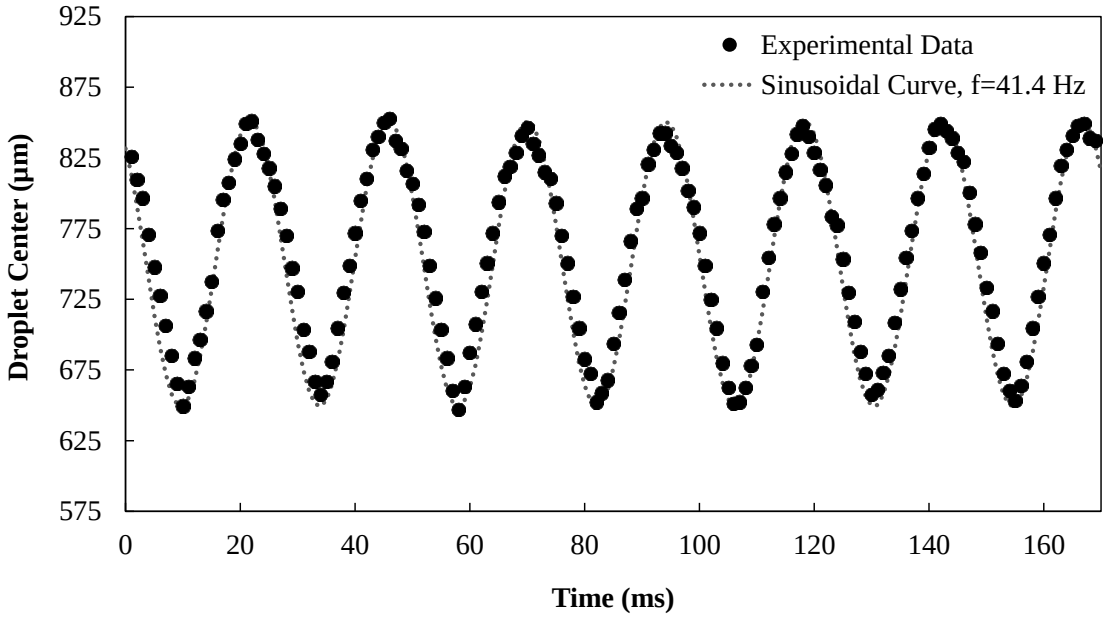

Figure 48 – Experimental data of a steadily-oscillating levitated silicone oil droplet. The data points correspond to the distance from the bottom to center of the droplet. The droplet in this example is 1.68mm in diameter.

In this example, the period of a single oscillation is 24.2ms while the Rayleigh time, the expected period of a single oscillation of a freely oscillating liquid droplet, is roughly half that at 11.6ms. A summary of similar results is presented in Table 4. To verify the Rayleigh time estimate of the freely oscillating droplet's period, such droplets of silicone oil are also observed using high speed video. Two droplets of different sizes created using the methods outlined in Section 5.2.1 above are examined shortly after initial creation while first-mode oscillations are present to measure oscillation times for comparison to the Rayleigh time. In both cases, the Rayleigh time provides a good estimate (within a few percent) of the freely oscillating droplet's period and the deviations from this timescale must be caused by the thermocapillary conditions and internal flow present during levitation.

The internal flow present during levitation consists of an upwelling return flow through the center of the droplet resulting from the downward thermocapillary surface flow. This flow resists the downward motion of the droplet and, if vigorous enough, will assist the droplet in its upward motion yielding oscillatory behaviour.

Table 4 – Observed steady oscillations of various sized droplets with diameter D, volume V, average period of oscillations T, and theoretical Rayleigh time τ_R. Oscillations are observed and averaged over n periods as shown in Figure 48.

D (mm)	V (µl)	n	T (ms)	τ_R (ms)	$\frac{T}{\tau_R}$
1.27	1.07	11	19.2	7.67	2.50
1.35	1.28	10	19.5	8.37	2.33
1.59	2.10	10	23.2	10.7	2.17
1.68[a]	2.47	6	24.2	11.6	2.08

[a]Droplet oscillations presented in Figure 48.

Based on the second-order system analogy, and experimental observations that the steady oscillations occur at a frequency (hypothetically in a resonance state) lower than the undamped frequency related to the Rayleigh time, this phenomenon could yield a better method of measuring a droplet's surface-tension-temperature relationship than current methods. A modified second-order model is provided in Equation 34 where an additional term is included to account for thermocapillarity. We choose a coefficient with dimensions of time^{-1}, consistent with the damping coefficient, whose numerator dimensionally represents the surface tension gradient, a driving shear stress, and is balanced by the absolute viscosity, a property that gives rise to a retarding shear stress. The coefficient C_t has yet to be determined, but the use of this model could yield a way of relating droplet bouncing to average surface-tension-temperature coefficient values

within the temperature range used to induce bouncing. Currently, measurements are made by heating or cooling a liquid to a specific temperature where a surface tension measurement can be made. This relationship could also be determined by analysing the changes in oscillation frequency as the temperature of the substrate-droplet system is changed. The coefficient of $\dot{x}$ in Equation 34 can be related to the damping ratio and natural frequency as shown in Equation 35.

$$\ddot{x} + \left(C_d \frac{\mu}{\rho R^2} + C_t \frac{\sigma_T \frac{\Delta T}{R}}{\mu} \right) \dot{x} + \left(C_k \frac{\sigma}{\rho R^3} \right) x = 0 \tag{34}$$

$$C_d \frac{\mu}{\rho R^2} + C_t \frac{\sigma_T \frac{\Delta T}{R}}{\mu} = 2\zeta \omega_n \tag{35}$$

5.5.3 Speculations

From the experimental observations presented above, it's doubtful that the simple, second-order-system model is sufficient for fully modeling the droplet behaviour. The increased period of oscillation seems to be a result of the internal thermocapillary flow deforming the droplet's surface much the same way as an external force would drive displacement of the spring in the mass-spring-damper system. Numerical modelling of a levitated droplet undergoing such oscillations could yield further information as well as verify the use of this phenomenon in measuring a liquid's surface tension-temperature relationship.

5.6 Conclusions

These experiments provide sufficient evidence for the ability to capture ejected droplets for thermocapillary levitation utilizing a specialized substrate shape. If droplet impact velocities are kept low enough such that surface waves do not impede the gas flow replenishing the lubricating layer between droplet and substrate, capture should be possible. Furthermore, the presence of steady droplet oscillations while thermocapillary conditions are present is an interesting phenomenon worth exploring in the future.

6. TWO-PHASE NONWETTING AND COMPOUND-DROPLET LEVITATION

The primary difference between levitation experiments involving single-phase droplets and those with multi-phase (compound) droplets is the presence of the liquid–liquid interface in the interior of the droplet. As mentioned previously, the internal thermocapillary convection will certainly be altered by the presence of this interface. Experiments involving levitation of compound droplets, merging of levitated droplets, and translation of levitated compound droplets are presented here.

In order to investigate the effect of the oil-water interface without testing compound-droplet levitation, an experiment that up to this point has not been performed, a few experiments are conducted to qualitatively describe this effect.

6.1 Permanent Nonwetting for Two-Phase Systems

Previously, permanent nonwetting experiments have been conducted on single-phase pendant droplets hung from a heated post. When brought into apparent contact against a cooled plate to induce thermocapillary convection, wetting is suppressed as gas is driven into the lubricating region between the squeezed droplet and plate. An image of such a test is shown in Figure 49 as performed by Dell'Aversana *et al.* (1997).

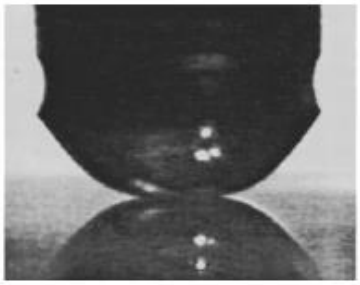

Figure 49 – A drop of 5 cSt silicone oil pressed against a cooled glass surface (Dell'Aversana *et al.* 1997).

A similar experiment is devised in which a droplet of water is deposited within a pendant droplet of oil. The ability to suppress wetting and drive internal thermocapillary convective currents is expected as the compound droplet is lowered towards and pressed against a smooth, cooled glass plate. Experiments are conducted with two configurations of the inner droplet: a case where the water droplet is wetting the underside of the post to which the compound droplet is attached and a case for which the water is freely suspended entirely within the oil and doesn't touch the post. In the former, suppression of wetting is expected although in the latter it is not yet clear how the presence of the more-dense, inner droplet near the bottom of the outer droplet will affect wetting suppression. The oil surface flows from the heated top post to cooler bottom adjacent to the glass and returns up the center precisely where the water droplet will rest when thermocapillary conditions aren't present. These experiments are described in the following and attempt to elucidate whether permanent nonwetting, and by extension compound-droplet levitation, is possible.

6.1.1 Experimental Setup

A heated copper post with a pinning diameter of 3mm is used to hang pendant compound droplets to be pressed against a cooled glass plate (as sketched in Figure 50). The copper post is heated by a length of Nichrome wire coiled around the cylindrical post surface under a layer of insulating material. When electrical current is passed through the high-resistance wire, the electrical energy is converted to heat and conducted through the post. The post is able to translate along and rotate about its symmetry axis. Axial translation allows the pendant droplets to be pressed to the cooled glass surface. The rotation allows internal flow asymmetries to be examined. The experiments presented here utilize distilled water as the inner liquid and 5cSt silicone oil as the outer liquid, the same liquids used for compound-droplet experiments.

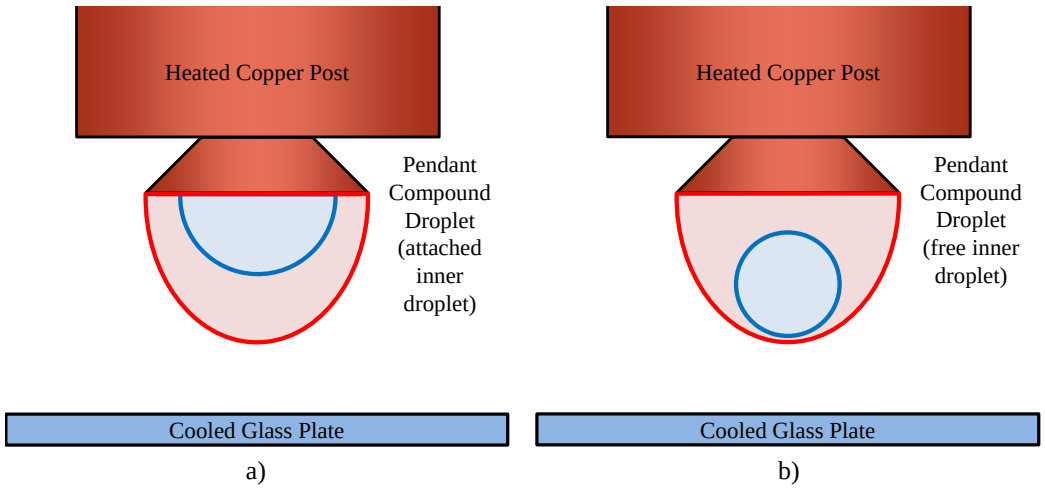

Figure 50 – Two configurations of pendant droplet experiments are performed. The first (a) has the inner droplet wetting the underside of the post (attached) and the second (b) has the inner droplet free to move within the surrounding liquid. The second of the two configurations provides the better representation of the inner flow structures present for a levitating compound droplet. In both cases, pendant droplets are of microliter volumes (5mm pedestal on the left and 3 mm pedestal on the right).

In the first configuration, sketched in Figure 50a, the inner droplet is wetting the underside of the copper post. This configuration is meant to mimic the lower hemisphere of a symmetric compound droplet. In the second configuration shown in Figure 50b, the inner droplet is free to move and be influenced by flow currents within the surrounding oil and yields a closer representation of a levitated compound droplet.

6.1.2 Experimental Results

The first of this set of experiments utilizes an attached (i.e., like the sketch in Figure 50a) inner droplet. This configuration is the easiest to create simply by depositing the water droplet centered on the underside of the post. Silicone oil can then be deposited over the water droplet. It was hypothesized that what would be observed is axially symmetric internal flow similar to what is observed for single-phase experiments. This is shown to be false. The flow image on the left in Figure 51 shows a plane of symmetry of the internal flow normal to the image and coincident with the axis of the cylindrical post. Glass spheres are deposited in the water as a flow visualization aid. The spheres in focus in Figure 51 are towards the front side of the water droplet and seem to flow from top to bottom (what would be expected if the flow was axisymmetric about the droplet axis as sketched on the right in Figure 51). But the tracer particles towards the back of the droplet exhibit flow in the opposite (downward) direction. The resulting symmetry is of a mirror-type about a plane coincident with the droplet axis and normal to the viewing plane. The lack of concentration of tracer particles down the center of the droplet (the plane of symmetry) also suggests that the flow pattern exhibits this mirror symmetry. This unexpected result prompts an obvious question as to whether this type of symmetry

is exhibited for cases where the inner droplet is free to move about the surrounding liquid.

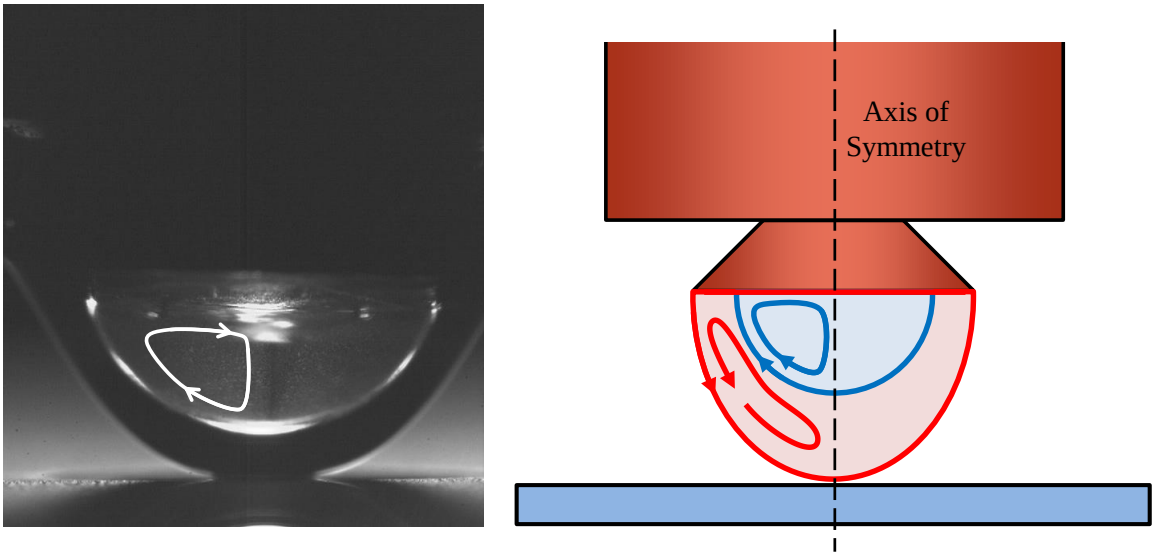

Figure 51 – On the left, a compound droplet is brought into the vicinity of a cooled glass plate where the inner droplet of water is wetting the underside of the copper post. The outer liquid, silicone oil, undergoes thermocapillary convection. Glass spheres are used as tracer particles in the water. The flow exhibits mirror symmetry about the plane coincident with the axis of the droplet and normal to the viewing plane, counter to the expected axisymmetric flow shown in the graphic on the right.

The second set of experiments utilizes the unattached inner droplet to explore both the ability to suppress wetting with a two-phase system as well as explore the internal flow to determine whether the previously described symmetry persists. The series of images shown in Figure 52 show the second configuration where a free inner droplet is present within the silicone oil. Image (a) shows the starting position of the inner droplet when the compound droplet is pressed against the cooled glass plate. Every successive image shows the position of the droplet after the post to which the compound droplet is attached is slowly rotated a quarter of a turn. The inner droplet in image (b)

can be seen on the right side of the compound droplet, in the front in image (c), on the left in image (d), and finally towards the back in image (e) similar to (a).

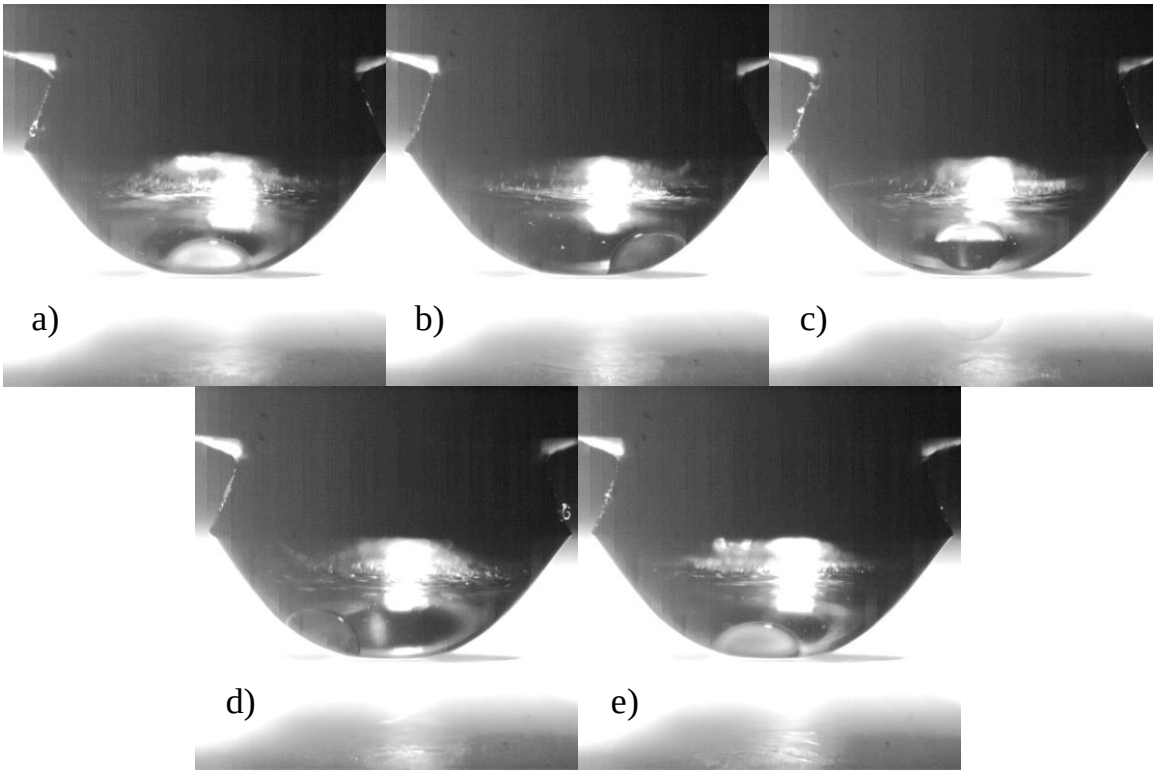

Figure 52 – These five images show a compound droplet pressed against a cooled glass plate with a relatively small inner droplet. Images (a-e) respectively show the starting position with the inner droplet at the back of the drop and the successive position of the inner droplet after the heated rod is rotated a quarter turn each time about its cylindrical axis. The diameter of the copper pedestal (where the oil is pinned) is 5mm.

One interesting observation is the behavior of the inner droplet. If the outer surface of the compound droplet (the oil-air interface) can be thought of as a treadmill in motion towards the bottom of the droplet, the inner droplet seems to roll up along the liquid side of this interface. Similar results are shown when the inner droplet is much larger. A representative image is shown on the left in Figure 53.

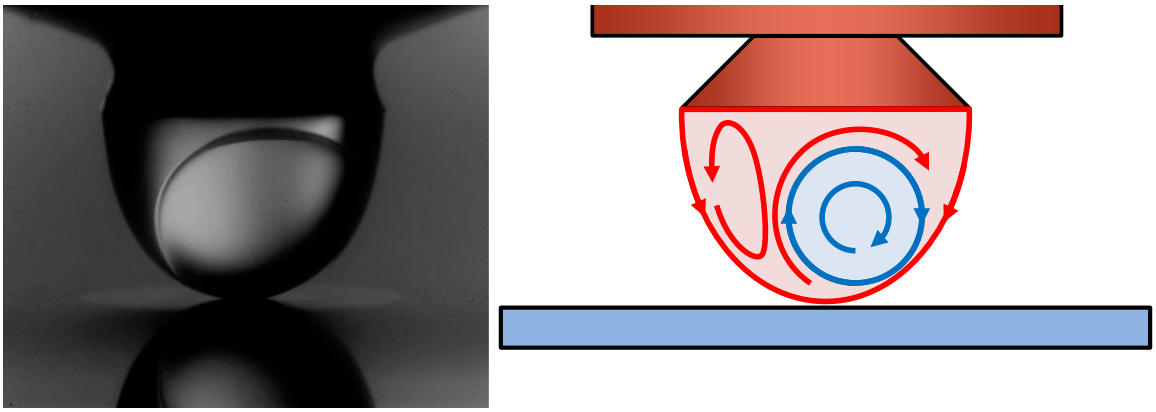

Figure 53 – On the left, a compound droplet is pressed against a cooled glass plate with a large, free inner droplet. The position of the inner droplet is clearly visible on the right side of the silicone oil droplet. On the right, the flow patterns exhibited are shown graphically. The diameter of the copper pedestal (where the oil is pinned) is 3 mm.

After considering the previous experiments of Dell'Aversana *et al.* (1997) regarding the shape of the lubricating film that exists between the droplet and substrate, the movement of the droplet from the center to one side can be explained. A dimple forms at the lowest point of the droplet as it is brought into the vicinity of the cooled plate. The shape of this dimple has been measured and is shown in Figure 54. Under the action of gravity, a droplet residing on the center of this dimple would naturally fall to one side down this "hill" as the droplet is pressed against the plate. In nanoliter-scale droplets, this hill would be smaller than for the larger, microliter-scale droplets presented above, but the same behavior is still expected. As the internal flow develops, it can't assume the normal axisymmetric flow pattern observed for single-phase droplets due to the presence of the bump caused by the dimpled interface. The flow shown graphically on the right in Figure 53 develops instead.

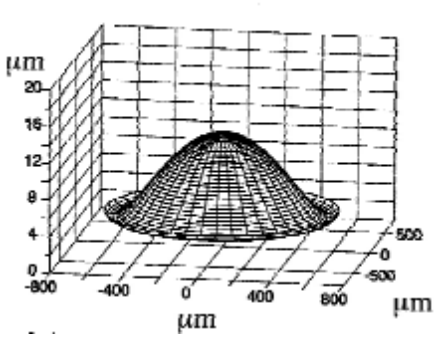

Figure 54 – The liquid-gas interface shape as measured by Dell'Aversana *et al.* (1997) in the vicinity of apparent contact between a droplet of silicone oil and a smooth glass plate. This dimple causes a droplet of water located inside the compound droplet to move to one side as it falls down the dimple's "hill" under the action of gravity.

Interestingly, the asymmetric behavior of a two-phase, nonwetting system has been shown previously, but not commented on. The following images in Figure 55 are taken from the proof-of-concept work by Nagy and Neitzel (2008).

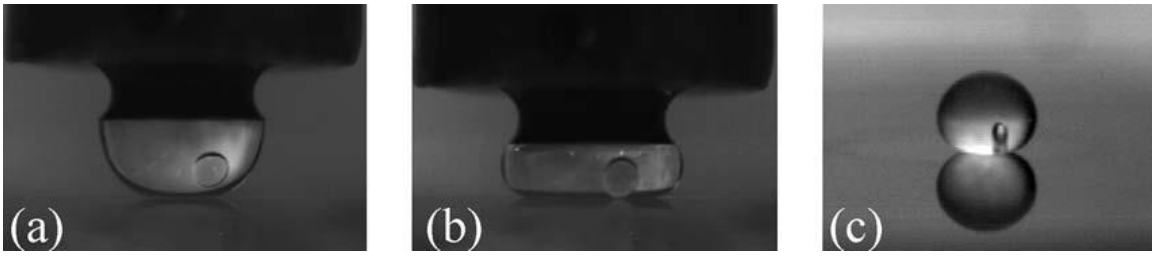

Figure 55 – (a) A water droplet inside a nonwetting silicone-oil droplet attached to a heated pedestal. (b) The same two-phase system pressed against a cooled substrate. (c) A smaller water droplet trapped inside a silicone oil droplet (Nagy and Neitzel 2008).

6.1.3 Two-Phase Permanent Nonwetting Conclusions

Based on the results of these experiments, it appears that compound-droplet levitation is indeed possible. Previous concerns regarding the presence of the higher-density water droplet located at the bottom of the silicone oil droplet where it would

obstruct the return thermocapillary flow through the center of the droplet have been mitigated by these experiments and most notably the demonstration that permanent nonwetting is possible even for an inner droplet as large as the one presented in Figure 53. The following experiments are designed to explore the levitation, merging, and translation of compound droplets.

6.2 Compound-Droplet Levitation

In order to efficiently explore compound-droplet levitation, a slight modification to the droplet generation mechanism is introduced. Previously, compound droplets have been generated in a drop-on-demand fashion where the generator nozzle is prepared for ejection by going through a series of steps prior to ejection. For the experiments presented here, the hydrostatic pressure of the oil was increased slightly allowing for a constant flow of oil into the compound nozzle and the generator is run continuously producing a single droplet every 0.3 – 1.5 seconds. Droplet capturing requires adjustment of droplet speed, trajectory, and impact placement on the capturing substrate for stable levitation. Droplet generator position as well as waveform parameters are adjusted to accommodate these requirements and allow for droplets to be more easily captured. Due to these changes in operating parameters, it is not guaranteed that the composition of ejected and levitated droplets will follow the results as presented in Chapter 4. This poses a similar problem as was encountered in the compound-droplet generation work as optical viewing of the oil-water interface is not always possible due to the curvature of the oil-air interface. Furthermore, the position of the inner droplet is not precisely known in order to utilize ray-tracing arguments for inner-droplet-volume calculations. Therefore, a new method for determining composition of levitated droplets

is needed. This method takes advantage of droplet shape changes during the merging of two droplets, and is therefore not described here, but after the merging process is described.

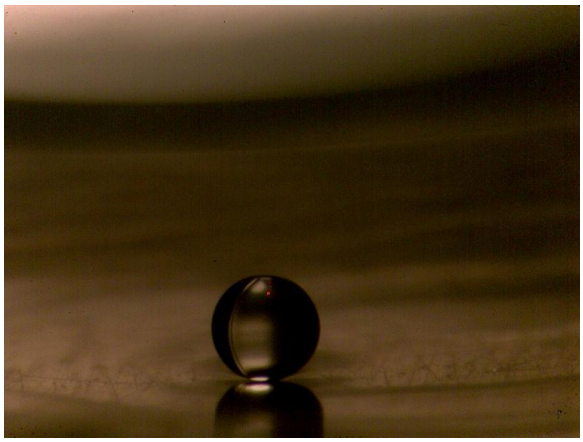

Figure 56 – A levitating, compound droplet with a volume of 12.4 nl. Composition is unknown due to altered generator parameters and unknown position of inner droplet.

Levitation of compound droplets is indeed possible, as shown in Figure 56 depicting a 12.4 nl compound droplet, but the composition is not known. Variations in composition, to explore how composition affects levitation ability (if at all), are conducted along with the merging experiments as explained in the following.

6.3 Merging Compound Droplets

Merging compound droplets for chemical testing is an important capability of LOC systems and processes. Where compound droplets are merged, both the encapsulant and inner phases must successfully merge. The experiments described here are designed to demonstrate the merging of compound droplets and test the composition limits for which merging and sustained levitation of the resulting droplet is possible.

6.3.1 Experimental Setup

The merging of compound droplets is achieved using the same bowl–shaped, capturing substrate utilized in the compound-droplet-levitation experiments. When multiple compound droplets are ejected into the capturing area, they naturally fall toward the bottom of the bowl. In this area, they are levitated and trapped by the infrared laser beam where they naturally migrate toward the center, highest intensity region of the infrared laser beam and end up adjacent to one another. This process prepares them for merging.

6.3.2 The Merging Process

Levitated droplets naturally migrate to the center of the laser beam due to asymmetric heating. When two droplets attempt to occupy the center of the capturing beam, they naturally press against each other in an attempt to occupy the center point with highest intensity. After a short period of time, the air film that temporarily separates the droplets is squeezed out from between them under this force provided by asymmetric heating, and their outer silicone oil phases merge to create a single compound droplet with two separate inner droplets of water. These two water droplets may interact or not depending on the composition of the constituent droplets, but these droplets must interact and merge to complete the process to be useful for intended applications (i.e. LOC architectures where chemical testing is desired). Therefore, several outcomes of the merging process are possible, which are dependent on the composition of the droplets merged, and are presented in Figure 57 and described below.

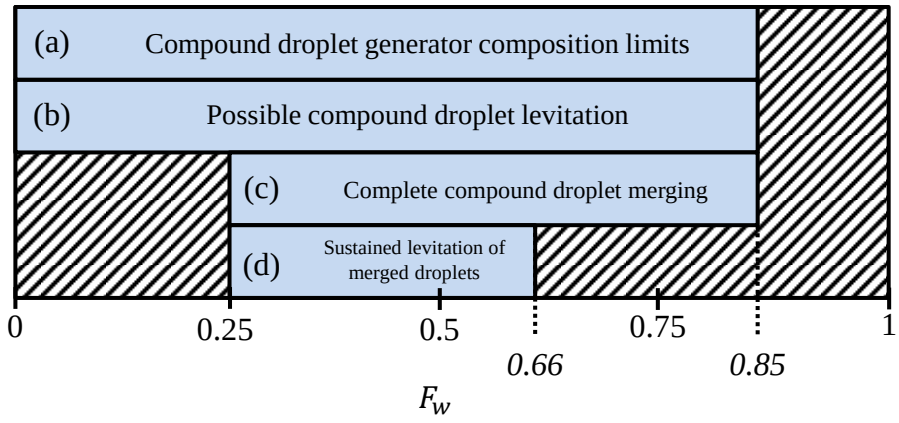

Figure 57 – Composition limits for various stages in droplet merging experiments. Each stage is describes as follows: (a) composition limits of the compound-droplet generator; (b) compositions where compound-droplet levitation is possible; (c) compositions where complete merging is possible; (d) the successful experimental range of sustained levitation after merging is achieved.

The entire range of compound-droplet compositions is from a water fraction of nearly 0 (a mostly oil droplet with very little water present) to nearly 1 (a water droplet with a very thin film of oil). Region (a) in Figure 57 covers the portion of this range of droplet compositions that can be produced by the compound-droplet generator presented in Chapter 4.

Region (b) describes the range over which compound droplets can be levitated for the purposes of the LOC application. The upper limit of region (b), where $F_w = 0.85$, is the highest water fraction for which droplets have been levitated. Droplets of decreasing water fraction can also be levitated. A water fraction of 0, the lower bound of this region, corresponds to the case of single-phase droplet levitation explored in Chapter 3. In all cases where merging is attempted, levitated droplets interact resulting in coalescing of their respective constituent silicone oil phases. Complete merging is defined as the

merging of both outer and inner phases yielding a merged compound droplet composed of a single encapsulated inner water droplet.

Region (c) is the water fraction range over which complete merging occurs. The upper limit is the same as for successful compound-droplet levitation. At the lower limit of droplet compositions, where droplets are composed of mostly oil, a simple geometric analysis shows that water droplets are not guaranteed to interact at all. The diameters of these droplets are less than the radius of the combined droplet and may never touch. Water droplets small enough can even be fully entrained by the convective currents within the oil phase essentially serving as a flow visualization aid. As inner droplet size increases, the likelihood of interaction increases due to their increased size but is still capable of being prevented by the return flow of oil upwards through the center of the droplet which would keep the water droplets apart. For compositions less than 0.25, droplets are not likely to complete the merging process. At water fractions of 0.25, the same geometric analysis shows that the water droplets will interact. At this point, the diameter of the two water droplets present after encapsulant coalescence is equal to the radius of the compound droplet. Thus, the droplet surface at the gas-oil interface begins to press the water droplets against each other, and after a short time the water droplets will merge and complete the merging process.

Region (d) corresponds to the range of water fractions over which sustained levitation of completely merged compound droplets is achieved. At the upper composition limit of droplet levitation, where droplets are composed of mostly water with a thin oil layer, a completely merged compound droplet does not survive for an appreciable time after merging of the water droplets.

The steps in the merging process for such droplets are shown in Figure 58 along with timestamps for each image. The outer phases of two compound droplets (Figure 58a) merge to form a droplet with spheroidal shape (Figure 58b). One would expect droplets of this size with a diameter much smaller than the capillary lengths of the constituent liquids to take a spherical shape. The size of the inner droplets, which haven't yet merged, coupled with the relatively small amount of oil, unable to form a spherical shell around both droplets, results in this shape of the encapsulant surface. The force on the inner droplets caused by the deformation of the oil-gas interface presses the two inner droplets against one another. The interstitial film of oil is drained by this squeezing action until the water droplets touch and merge. For the droplet merging shown in Figure 58, this part of the merging process lasts 559ms. A release of surface energy occurs as the water droplets merge propelling the droplet upwards (Figure 58c) much the same as the self-propelled bouncing droplets studied by Boreyko and Chen (2009). As the droplet comes back to rest on the substrate, the oil is driven by thermocapillary stress to the bottom of the compound droplet under the more-dense water droplet Figure 58d. The normal return-flow of oil (as in single-phase levitation or levitation of compound droplets with smaller water fractions) is impeded by the minimal thickness of the oil layer and the oil accumulates at the bottom of the droplet. The orientation of this top-heavy compound droplet is unstable and it inevitably falls to one side as in Figure 58e. Once the droplet comes to rest on its side, there is insufficient surface motion to drive gas between the bottom of the droplet and substrate, and the merged droplet can no longer sustain levitation. For this droplet, the time from merging of the water droplets to levitation failure is 54ms. The total life of the compound droplet

(from initial merging of the outer oil phases of separate compound droplets to levitation failure) is 613 ms. This upper composition range will result in failed merging.

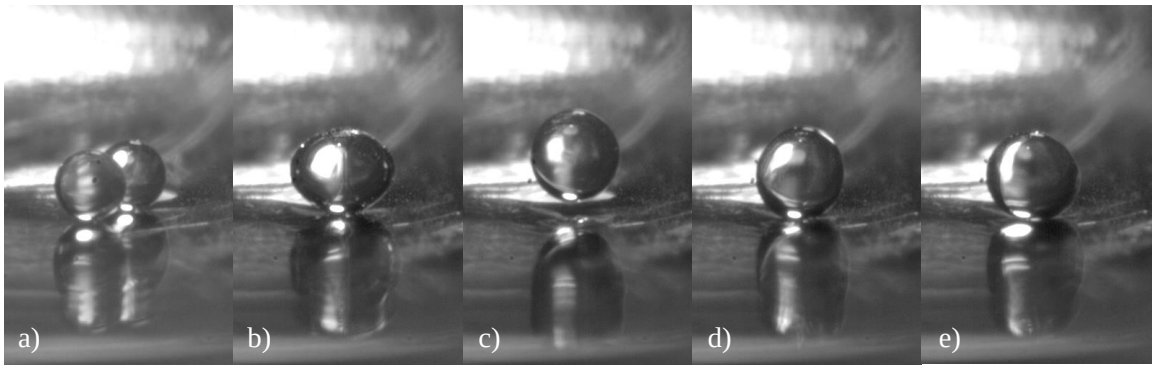

Figure 58 – The steps in the merging of two compound droplets are depicted. Descriptions and timestamps (relative to the first image) for each are as follows: (a) two droplets shown just before outer-phase merging (0ms); (b) compound droplet with two water (inner) droplets with a spheroidal shape (90ms); (c) compound droplet after merging of inner droplets showing vertical bounce due to a release of surface energy from the water-oil interface (564ms); (d) compound droplet as it comes back to rest on the substrate (584ms); (e) compound droplet after rolling to one side and just before levitation breakdown (614ms). The composition of this droplet is F_w = 0.66 with a final volume of 22.6 nl.

6.3.3 Composition Measurement for Levitated Droplets

As mentioned previously, the method for measuring the composition of a levitated droplet utilizes the merging process to gain information examining a levitating droplet alone would not be able to provide. Two measurements are required to characterize the droplet composition: inner droplet volume and total droplet volume.

The total droplet volume can be measured in one of two ways. The first is to directly measure the volumes of the constituent droplets prior to merging and add them together. Assuming negligible phase change of any liquid phase (a good assumption over the short timescales examined), the final volume of the merged compound droplet is

equal to the sum of the constituent droplet volumes. The second way to measure total droplet volume is to examine the droplet after merging of the oil films but prior to merging of the water droplets. The oil-air interface takes the shape of a spheroid, a shape which can be obtained by rotating an ellipse about its major axis, as described in Figure 59 below. After measuring the major and minor axes of the revolved ellipse, the volume of the spheroidal droplet can be calculated by using Equation 36, where V_e is the spheroidal volume, A is the length of the major axis, and B is the length of the minor axis. In many cases, total droplet volume can be measured in one way but not the other due to droplets not being in focus at various stages of the process (e.g. if one droplet enters focus from behind as it merges with the second or if the oil interface merging occurs out of focus but the constituent droplets were able to be viewed and measured). These two methods of total droplet volume calculation can be compared for cases where both methods are able to be used and yield similar results.

$$V_e = \frac{\pi A^2 B}{6} \tag{36}$$

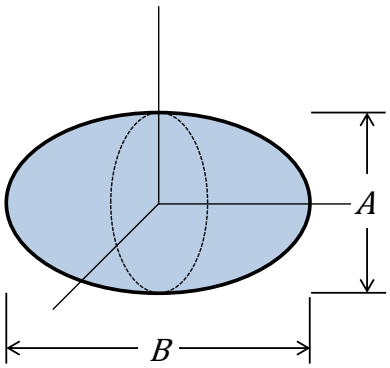

Figure 59 – Illustration showing an ellipse with minor and major axes of lengths *A* and *B*, respectively. Rotating this ellipse about its major axis creates a spheroid, the shape of compound droplet after initial merging of the oil phases.

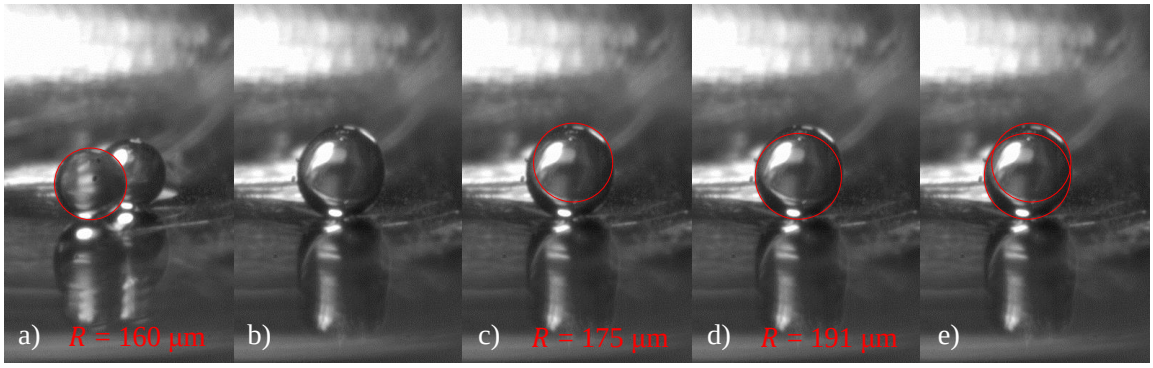

Figure 60 – A series of images describing the process for measuring composition during the merging process are provided along with interface curvature where appropriate. Images (b-e) are identical with circles superimposed to show curvature differences exploited for composition measurement. These images are: (a) two compound droplets prior to merging, *R* = 160 μm; (b) compound droplet just after water droplet merging; (c) superimposed circle for measurement of the curvature of the water droplet, *R* = 175 μm; (d) superimposed circle for measurement of local oil curvature, *R* = 191 μm; (e) both circles superimposed for direct comparison. The composition of this droplet is F_w = 0.66 with a final volume of 22.6 nl.

The inner droplet volume is determined just after complete merging of the droplet occurs. After the inner droplets merge, they spontaneously bounce as described earlier and shown in Figure 58c. As this occurs, most of the oil flows from the top of the droplet to the bottom and the shape (i.e. curvature) of the spherical internal water droplet can be

briefly examined and measured on the upper side of the droplet. Images elaborating on this method are given in Figure 60.

Figure 60a depicts the constituent compound droplets prior to merging. Figure 60b - Figure 60e show circles superimposed on the droplets being measured to show curvature differences exploited for composition determination.

By using image analysis software, the entire circular, cross-sectional shape of the spherical water droplet can be extrapolated by picking three points that lie along its curved surface (Figure 60c). This circular area can then be used to determine the radius and volume of the water droplet. Once both the inner (from Figure 60c) and compound-droplet volumes (by doubling the single droplet volume measurement from Figure 60a) are known, the water fraction of the merged compound droplet can be calculated by dividing the former by the latter. This is also the water fraction of the constituent droplets assuming they have identical composition.

6.3.4 Merging Results

It is important to determine the upper composition threshold at which complete merging will occur while still sustaining levitation. The lower threshold is of lesser interest as minimizing the oil-layer thickness (thus operating near the upper composition limit) is desirable from a process standpoint for minimizing consumption of encapsulating liquid. A series of experiments where droplets of varying compositions are ejected, captured, levitated, and merged is conducted and the results reported in Figure 61.

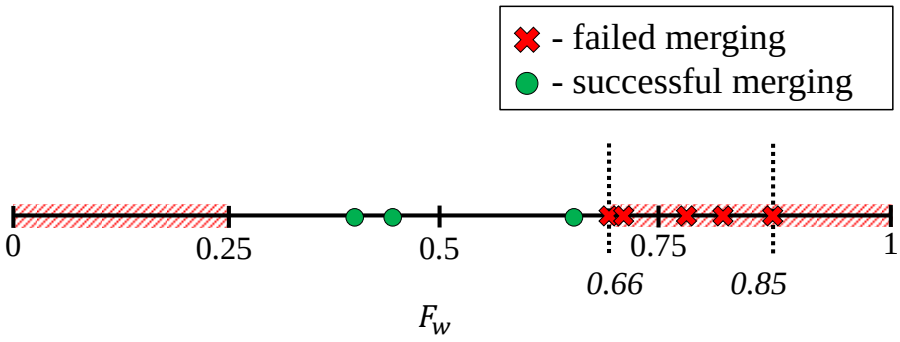

Figure 61 – Experimental results for merging of compound droplets of various compositions. Water fraction ranges shaded in red are those for which complete merging (i.e. merging of outer and inner phases while sustaining levitation) is not successful.

In Figure 61, the red hatched regions at water fractions below 0.25 and above 0.66 are areas where compound-droplet levitation and merging are attempted but fail to yield sustained levitation. The region $0.25 < F_w < 0.66$ is region (d) from Figure 57. A representative image of sustained levitation of a compound droplet formed by merging two compound droplets is shown in Figure 62. This particular droplet sustains levitation at least 1.3 seconds after the water droplets of the two original compound droplets merge. The measurement of sustained levitation of such a droplet is not limited by levitation failure, but by the duration of the video captured after complete merging occurs (in this case roughly 1.3 seconds).

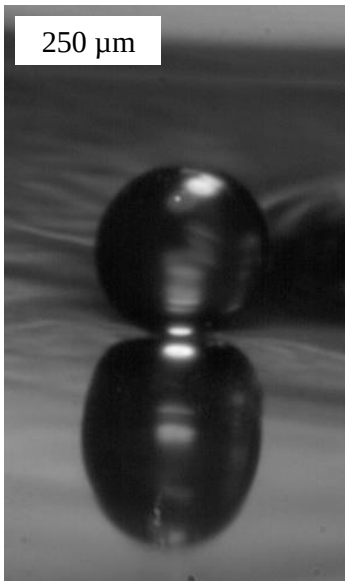

Figure 62 – Image of a 15.5 nl levitated droplet created from the merging of two smaller droplets roughly 1.3 seconds after completion of the merging process.

6.3.5 Summary

Merging and levitation of compound droplets is achieved over the composition range of the compound-droplet generator. Sustained merging, where the merged compound droplet survives the complete merging process and persists after, is shown for a subset of these compositions. The position of the water droplet within the compound droplet at various stages of the merging process, coupled with the thin oil layer, results in levitation failure at the upper end of the composition spectrum.

6.4 Levitating Compound-Droplet Translation

Translation of merged compound droplets is a desired feature of LOC applications utilizing thermocapillary levitation of samples. Unfortunately, translation demonstrations comparing translational speeds to single-phase droplet have not been achieved using the designed capturing substrate, but translation has been achieved.

Small quantities of oil are deposited on the capturing surface to assist in droplet capture. Although not adversely affecting merging experiments, this oil layer completely retards the ability for droplets to translate while the laser is actuated. Droplets can, however, be moved slowly from the bowl-shaped capturing surface to the flat test area designed for translation. Droplets are moved by changing the angle and position of the substrate while the laser is held stationary. The droplet remains under the center of the IR laser beam while the substrate is moved beneath. Thus, droplet translation relative to the substrate is possible despite not being able to test achievable speeds under normal LOC circumstances.

6.5 Conclusions

Extensions of thermocapillary nonwetting and levitation are explored and have been shown to be possible for two-phase systems. Compound-droplet generation and capturing via a specialized substrate shape allows for levitation and merging experiments to be performed. Levitation and merging experiments are conducted over the compositions range of the compound-droplet generator to determine the composition limits where merging and sustained levitation of compound droplets is possible. Translation is achieved, and experiments are attempted to compare speeds to single-phase droplet experiments. These experiments are unsuccessful due to the presence of the oil layer used for droplet capture which significantly retards droplet translation ability. Adding substrate vibration to create walking droplets might aid in motion towards a clean area of substrate where translation can be achieved.

7. CONCLUSION

Utilizing variations in surface tension caused by thermal gradients (thermocapillarity), a number of experiments have explored the applicability of droplet surface motion and levitation techniques to LOC applications. Prior to this research, thermocapillarity has been used as a means of inducing noncoalescence and nonwetting in liquid-liquid and liquid-solid interactions, respectively. The proof-of-concept work of Nagy and Neitzel (2008) that demonstrated the application of thermocapillary nonwetting to free droplets to induce levitation, serves as a foundation for the research presented here. This levitation mechanism shows promise in its application to LOC processes. A number of underlying problems are explored and solved to show the capability of this phenomenon to support and improve current LOC processes. Problems addressed include the following:

1. Capability of levitating and translating droplets of nanoliter volumes;
2. Difficulty of aqueous sample levitation due to volatility and surface contamination;
3. Feasibility of thermocapillary levitation of two-phase (compound) droplets;
4. Minimization of encapsulant thickness while still supporting levitation;
5. Capturing of compound droplets after ejection from droplet generator;
6. Persistence of levitation through the merging process of two compound droplets; and
7. Translation ability of compound droplets.

7.1 Nanoliter Droplet Levitation and Translation

Levitation studies performed to date have focused on microliter-volume droplets. These droplets are easy to generate via gravitational stretching methods (e.g. dripping or pipette dispensing) and are readily levitated via thermocapillarity. Additionally, gravitational forces, large enough to overcome capillary forces for microliter droplets of silicone oil of diameters larger than the capillary length, alter the droplet shape and increase the apparent contact area over which the increased pressure within the lubricating region is able to act. For smaller droplets, this area is smaller as the relative magnitude of gravitational forces is reduced compared with capillary forces.

Levitation studies conducted on nanoliter-volume droplets and reported on in this dissertation have shown that this reduction in contact area does not impede the ability for these droplets to levitate under thermocapillary conditions. The decreased inertia of the droplets due to their smaller size and lack of substrate contact also allows for translation at speeds much greater than those achieved by typical microfluidic transport mechanisms.

7.2 Compound Droplet Generation

The need to levitate aqueous samples leads to the design of a compound droplet generator capable of producing oil-encapsulated water droplets. The oil encapsulant allows for the use of its thermocapillarity, low volatility, and low surface tension to prevent surface contamination in order to support the levitation of aqueous samples without such favorable levitation properties.

The droplet generator design employs a specialized nozzle to deliver small quantities of oil to the inner water nozzle to provide for the encapsulation of water. Control and variation of the inner droplet generator water pressure allows for successful composition changes that are desirable to minimize the thickness of the oil layer for LOC applications. Droplet generation parameters are also able to be altered to promote droplet capturing.

7.3 Droplet Capture

Nanoliter-volume compound droplet generation requires a forcing actuation from a compound nozzle for formation. Unlike larger, microliter droplet formation which can passively use gravity for breakup, the forcing action of the pressure pulses create droplets traveling at speeds not suitable for capturing under the laser beam used for levitation.

Droplet impact studies are conducted to determine whether the thermocapillary conditions present for levitation can prevent wetting of an impacting droplet. For the thermocapillary conditions used for levitation, droplets can impact a substrate at a normal trajectory without wetting. These impacting droplets are not able to be captured passively by utilizing the Gaussian intensity distribution within the laser, so another method is devised to assist in droplet capture.

A substrate designed specifically for capturing droplets ejected from a droplet generator is fabricated and successfully used. The substrate consists of a bowl-shaped capturing area tangentially intersecting a planar surface to be used for translation experiments.

7.4 Capture, Levitation, and Merging of Compound Droplets

Prior to the present studies, the effect on levitation capability of a second phase with concomitant liquid-liquid interface within a droplet was unknown. Two-phase, pendant droplet studies qualitatively explore the addition of a second phase. Alteration of internal flow currents is caused by the liquid-liquid interface, but sufficient surface motion exists to force air between the droplet and substrate to prevent wetting.

Compound droplets are generated, captured via the specialized substrate and levitated for use in merging experiments. During the merging process, the curvature of the inner water droplet can be viewed for a short time. Composition measurements are made utilizing this information and the composition limit (i.e. the smallest oil layer thickness that still supports levitation and merging) of these levitating droplets is studied.

7.5 Future Work

A key component of using compound droplets for LOC applications is the ability to translate them. This work is left largely unfinished but should be completed in the future. Refining the droplet capture process to eliminate the need to deposit an oil layer for dissipating a portion of the kinetic energy of an impacting droplet is necessary for further advances here. The presence of the oil layer significantly retards droplet translation speed as the laser is moved and the droplet attempts to follow.

Droplet levitation experiments with inclined surfaces and static droplets might be utilized to determine maximum translational forces able to be imposed by the laser beam intensity profile. Surface roughness was observed to have a retarding effect on

translation speed. To date, experiments have utilized smooth surfaces to demonstrate and test the limits of translation speed. Exploring the relationship between surface roughness and translation speed might be a necessary step before commercialization of a test platform utilizing thermocapillary levitation. Surfaces with large obstacles, with heights the same order of magnitude as the lubricating film or larger, can also be used to explore a droplets mobility when encountering these constructs. Vibrating substrates might also be utilized to enhance a droplet's ability to navigate such obstacles.

Temperature mapping of the surface of a levitating droplet would also be useful when attempting to determine the surface tension distribution over the liquid-gas interface. Optical magnification utilizing lenses transparent in the IR spectrum would allow for IR measurement of droplet temperatures. Scattering of infrared radiation is also an issue but could be alleviated by taking IR measurements outside the range of wavelengths generated by the beam heating source.

The research presented in these studies is almost entirely experimental. Significant additions to thermocapillary convection and levitation research could be made by utilizing computational models to explore the impact that variations in fluid properties, or other parameters not able to be experimentally varied here, might have on flow patterns and levitation ability. A complete model considering droplet shape, liquid properties, surrounding gas properties, laser beam intensity profile, and radiative heat transfer properties of the droplet surface would significantly add to the understanding of flow current in both the liquid and gas phases of the system.

The presence of the liquid-liquid interface within levitating compound droplets significantly alters the internal flow patterns exhibited in the single-phase case resulting in a departure from axisymmetry. Computational studies would yield a great deal of insight into these flow patterns where experimental observations are not possible. Tracer particles for flow visualization can be used to qualitatively assess flow patterns, but quantification is not possible due to the curvature of the droplet surface, their small size, and lack of knowledge of specific position of the inner droplet within the surrounding liquid.

The bouncing droplets presented in Chapter 5 deserve further studies to determine whether the oscillatory system behavior can be exploited for determination of the surface tension-temperature relationship. A numerical simulation and duplication of this experimental observation might shed light on such a relationship.

These are a few areas where future research would be beneficial for this application and the general body of knowledge with respect to thermocapillary droplet levitation. As with any research, the results and observations of these studies have revealed a number of new questions and phenomena worthy of future study.

APPENDIX A: COMPOUND NOZZLE DESIGNS

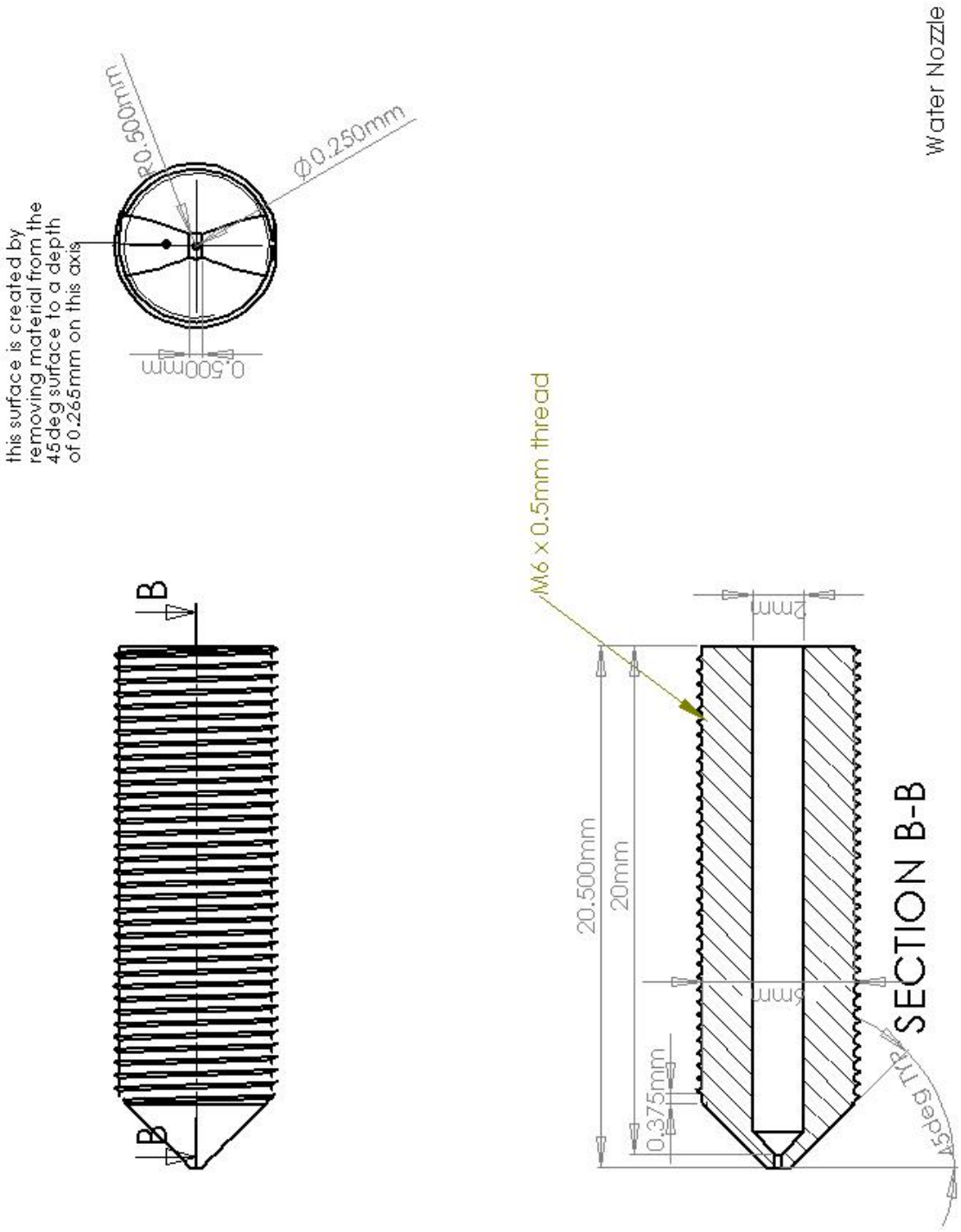

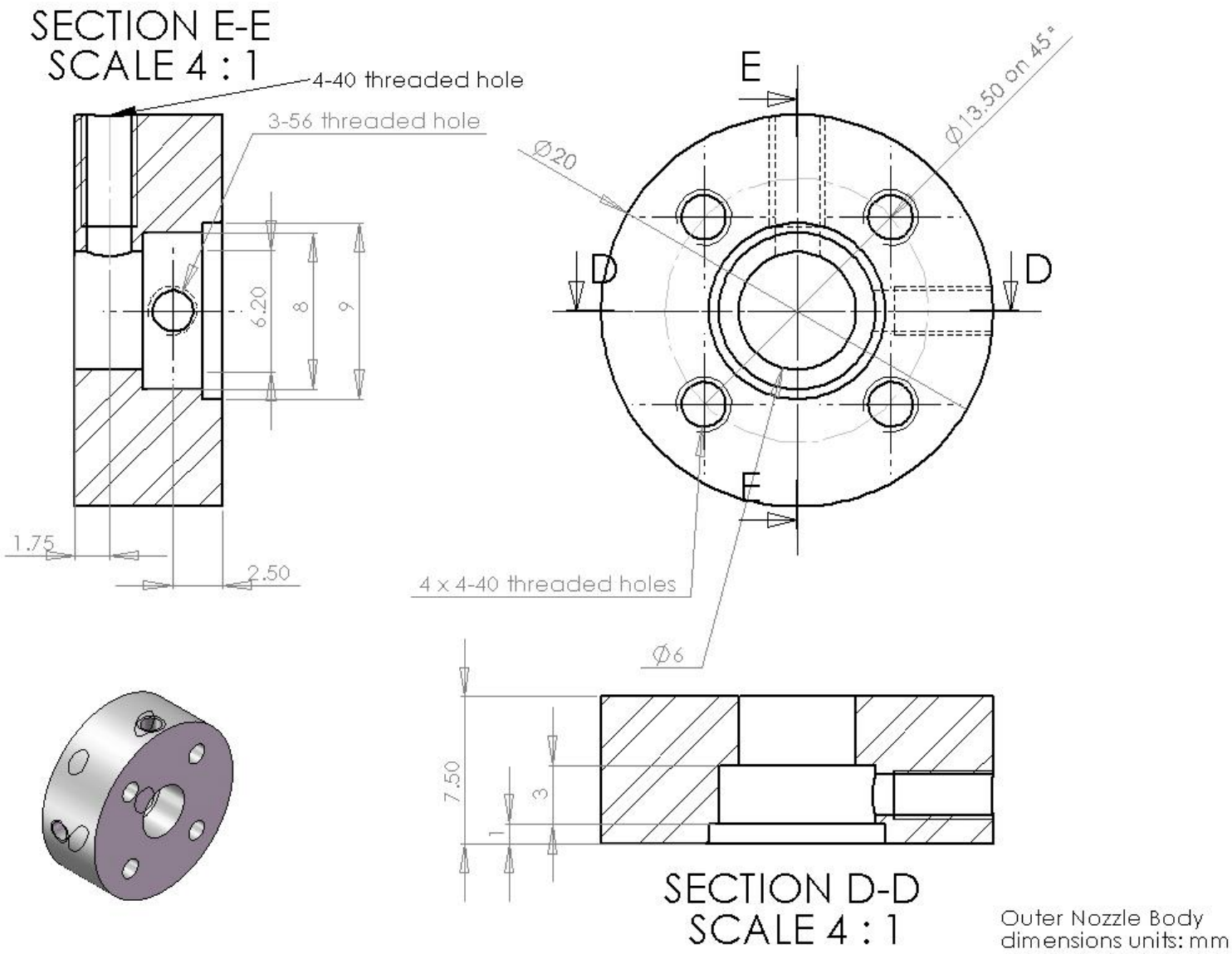
SECTION E-E
SCALE 4 : 1
4-40 threaded hole
3-56 threaded hole
6.20
8
9
1.75
2.50
E
D
D
F
Ø20
Ø13.50 on 45°
4 x 4-40 threaded holes
Ø6
7.50
3
1
SECTION D-D
SCALE 4 : 1
Outer Nozzle Body
dimensions units: mm

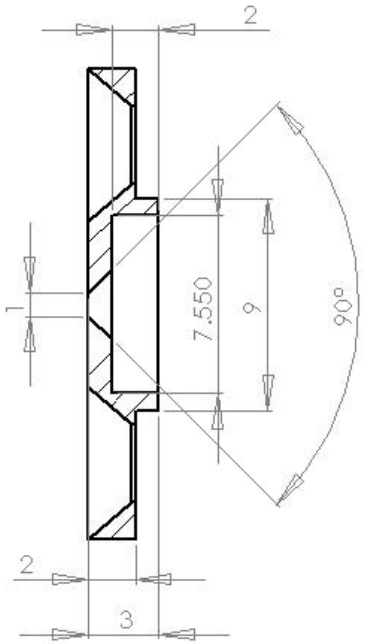

SECTION A-A
SCALE 4 : 1

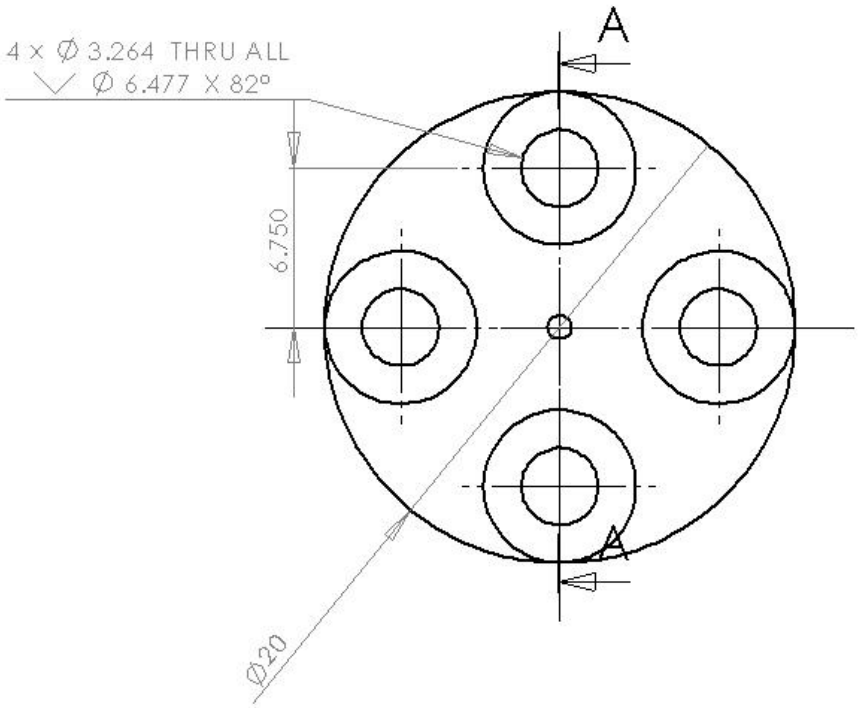

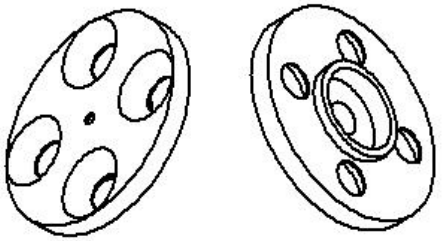

Outer Nozzle Top Cap
dimension units: mm

APPENDIX B: ERROR ANALYSIS

Uncertainty quantification is achieved by applying the method of Kline and McClintock (1953) through the use of a propagated uncertainty estimate shown in (37) and (38).

$$\Delta q = \sqrt{\sum_{i=1}^{n} \left(\frac{\partial q}{\partial x_i} \Delta x_i \right)^2} \tag{37}$$

$$q = q(x_1, x_2, \dots, x_n) \tag{38}$$

Here the uncertainty in a calculated quantity q (38), where q is a function of n variables $x_1, x_2, \dots, x_n$, is Δq. Details for this analysis are as follows.

Images are extracted from high speed video to make dimensional measurements. The image analysis software used is capable of providing a cross-sectional area measurement of an image in pixels^2 based on a superimposed circle. As mentioned previously, all images used for dimensional measurements are of droplets assumed to be spherical. For every droplet, two images are analyzed to measure droplet composition, an image of the compound droplet and an image of the inner water droplet suspended in the viscous silicone oil bath. Each of these images has three contributions to measurement uncertainty: the uncertainty in the area measurement in pixels^2, the uncertainty in the length measurement of the length scale, and the uncertainty in the number of pixels associated with the length scale. These are estimated by visually determining a maximum and minimum for each parameter based on the blur within the image. A measurement of the minimum and maximum cross-sectional area for a compound droplet

can be gained directly. The uncertainty associated with the cross-sectional area for a droplet would then be $\Delta A = {}^{1}/_{2(A_{max}-A_{min})}$ where A_{max} and A_{min} correspond to the maximum and minimum cross-sectional areas, respectively. A similar estimate is obtained for the pixel length of a known length scale to obtain $l_c[pix]$. The uncertainty of the known length scale $l_c[\mu m]$ is conservatively estimated as the width of the tick marks on the high resolution (1/32 inch) ruler used. Once these quantities are known, they can be used in conjunction with the error formulations that follow to quantify the uncertainty.

B.1 Uncertainty in Water Fraction

The uncertainty in the calculated water fraction ΔF_w is given by (39) where V_w and ΔV_w are the inner water droplet volume and its associated uncertainty and V_c and ΔV_c are the compound droplet volume and its associated uncertainty. Equations 39, 42, and 43 are derived from the application of (37) to (40) and (41).

$$\Delta F_w = \sqrt{\left(\frac{F_w}{V_w}\Delta V_w\right)^2 + \left(\frac{F_w}{V_c}\Delta V_c\right)^2} \tag{39}$$

$$V_w = \frac{4}{3}\pi {r_w}^3 = \frac{4}{3}\pi\left[\frac{\left(A_w[pix^2]\left(\frac{l_w[\mu m]}{l_w[pix]}\right)^2\right)}{\pi}\right]^{3/2} \tag{40}$$

$$V_c = \frac{4}{3}\pi {r_c}^3 = \frac{4}{3}\pi\left[\frac{\left(A_c[pix^2]\left(\frac{l_c[\mu m]}{l_c[pix]}\right)^2\right)}{\pi}\right]^{3/2} \tag{41}$$

$$\Delta V_w = \sqrt{\left[\frac{3}{2}\left(V_w \frac{\Delta A_w[pix^2]}{A_w[pix^2]}\right)\right]^2 + \left[3\left(V_w \frac{\Delta l_w[\mu m]}{l_w[\mu m]}\right)\right]^2 + \left[-3\left(V_w \frac{\Delta l_w[pix]}{l_w[pix]}\right)\right]^2} \quad (42)$$

$$\Delta V_c = \sqrt{\left[\frac{3}{2}\left(V_c \frac{\Delta A_c[pix^2]}{A_c[pix^2]}\right)\right]^2 + \left[3\left(V_c \frac{\Delta l_c[\mu m]}{l_c[\mu m]}\right)\right]^2 + \left[-3\left(V_c \frac{\Delta l_c[pix]}{l_c[pix]}\right)\right]^2} \quad (43)$$

Error bars in Figure 30 visually represent the propagated uncertainty in the water fraction and are sized as $\pm\Delta F_w$.

B.2 Uncertainty in Dimensionless Film Thickness

The dimensionless film thickness can be expressed as a function of the water fraction as shown in (20). Once the uncertainty associated with the water fraction is found from (39) above, it can be used to directly calculate the uncertainty in the film thickness using (44).

$$\Delta t_c = \sqrt{\left(\frac{\partial\left(1 - {F_w}^3\right)}{\partial F_w}\Delta F_w\right)^2} = \sqrt{\left(-3{F_w}^2\Delta F_w\right)^2} \quad (44)$$

Error bars in Figure 31 visually represent the propagated uncertainty in the water fraction and are sized as $\pm\Delta t_c$.

B.3 Uncertainty in Ejection Speed

The ejection speed is measured by comparing the location of an ejected droplet in two images of a high speed video of the ejection process. By dividing the distance traveled s_d by the time differential between the two images, $t_2 - t_1$, the ejection speed is calculated in (45). This calculation assumes that the speed is constant in the vicinity of

the nozzle, appropriate for the small time differentials used in this analysis. The calculation for the uncertainty Δv_e in (46) again utilizes (37) where Δs_d is a conservative estimate of the uncertainty caused by the blurred droplet surface, $\Delta l_v[\mu m]$ is the uncertainty in the length of the known length scale $l_v[\mu m]$, and $\Delta l_v[pix]$ is the uncertainty in the number of pixels corresponding to the length scale $l_v[pix]$.

$$v_e = \frac{s_d}{t_2 - t_1}\frac{l_v[\mu m]}{l_v[pix]} \tag{45}$$

$$\Delta v_e = \sqrt{\left(\frac{v_e}{s_d}\Delta s_d\right)^2 + \left(\frac{v_e}{l_v[\mu m]}\Delta l_v[\mu m]\right)^2 + \left(\frac{v_e}{l_v[pix]}\Delta l_v[pix]\right)^2} \tag{46}$$

REFERENCES

ANDREAS, J. M., HAUSER, E. A. AND TUCKER, W. B. 1938. Boundary tension by pendant drops. *Journal of Physical Chemistry*. **42** (8), 1001-1019.

BARTOLO, D., BOUAMRIRENE, F., VERNEUIL, E., BUGUIN, A., SILBERZAN, P. AND MOULINET, S. 2006. Bouncing or sticky droplets: Impalement transitions on superhydrophobic micropatterned surfaces. *Europhysics Letters*. **74** (2), 299-305.

BARTOLO, D., JOSSERAND, C. AND BONN, D. 2005. Retraction dynamics of aqueous drops upon impact on non-wetting surfaces. *Journal of Fluid Mechanics*. **545**, 329-338.

BARTON, K. D. AND SUBRAMANIAN, R. S. 1989. The Migration of Liquid-Drops in a Vertical Temperature-Gradient. *Journal of Colloid and Interface Science*. **133** (1), 211-222.

BASARAN, O. A. 2002. Small-scale free surface flows with breakup: Drop formation and emerging applications. *Aiche Journal*. **48** (9), 1842-1848.

BIRD, J. C., DHIMAN, R., KWON, H. M. AND VARANASI, K. K. 2013. Reducing the contact time of a bouncing drop. *Nature*. **503** (7476), 385-+.

BOREYKO, J. B. AND CHEN, C. H. 2009. Self-Propelled Dropwise Condensate on Superhydrophobic Surfaces. *Physical Review Letters*. **103** (18).

BRADLEY, S. G. AND STOW, C. D. 1978. Collisions between Liquid-Drops. *Philosophical Transactions of the Royal Society of London Series a-Mathematical Physical and Engineering Sciences*. **287** (1349), 635-678.

BURNS, M. A., JOHNSON, B. N., BRAHMASANDRA, S. N., HANDIQUE, K., WEBSTER, J. R., KRISHNAN, M., SAMMARCO, T. S., MAN, P. M., JONES, D., HELDSINGER, D., MASTRANGELO, C. H. AND BURKE, D. T. 1998. An integrated nanoliter DNA analysis device. *Science*. **282** (5388), 484-487.

CHANDRA, S. AND AVEDISIAN, C. T. 1991. On the Collision of a Droplet with a Solid-Surface. *Proceedings of the Royal Society of London Series a-Mathematical Physical and Engineering Sciences*. **432** (1884), 13-41.

CHE, Z. Z., WONG, T. N., NGUYEN, N. T. AND CHAI, J. C. 2012. Formation and breakup of compound pendant drops at the tip of a capillary and its effect on upstream velocity fluctuations. *International Journal of Heat and Mass Transfer*. **55** (4), 1022-1029.

CHEN, J. N. AND STEBE, K. J. 1997. Surfactant-induced retardation of the thermocapillary migration of a droplet. *Journal of Fluid Mechanics*. **340**, 35-59.

CHEN, L. Q., XIAO, Z. Y., CHAN, P. C. H., LEE, Y. K. AND LI, Z. G. 2011. A comparative study of droplet impact dynamics on a dual-scaled superhydrophobic surface and lotus leaf. *Applied Surface Science*. **257** (21), 8857-8863.

CHRISTOPHER, G. F. AND ANNA, S. L. 2007. Microfluidic methods for generating continuous droplet streams. *Journal of Physics D-Applied Physics*. **40** (19), R319-R336.

CLANET, C., BEGUIN, C., RICHARD, D. AND QUERE, D. 2004. Maximal deformation of an impacting drop. *Journal of Fluid Mechanics*. **517**, 199-208.

DARHUBER, A. A., DAVIS, J. M., TROIAN, S. M. AND REISNER, W. W. 2003. Thermocapillary actuation of liquid flow on chemically patterned surfaces. *Physics of Fluids*. **15** (5), 1295-1304.

DARHUBER, A. A., VALENTINO, J. P., TROIAN, S. M. AND WAGNER, S. 2003. Thermocapillary actuation of droplets on chemically patterned surfaces by programmable microheater arrays. *Journal of Microelectromechanical Systems*. **12** (6), 873-879.

DELL'AVERSANA, P. AND NEITZEL, G. P. 2004. Behavior of noncoalescing and nonwetting drops in stable and marginally stable states. *Experiments in Fluids*. **36** (2), 299-308.

DELL'AVERSANA, P., TONTODONATO, V. AND CAROTENUTO, L. 1997. Suppression of coalescence and of wetting: The shape of the interstitial film. *Physics of Fluids*. **9** (9), 2475-2485.

DELLAVERSANA, P., BANAVAR, J. R. AND KOPLIK, J. 1996. Suppression of coalescence by shear and temperature gradients. *Physics of Fluids*. **8** (1), 15-28.

GRIGORIEV, R. O., SCHATZ, M. F. AND SHARMA, V. 2006. Chaotic mixing in microdroplets. *Lab on a Chip*. **6** (10), 1369-1372.

GRIGORIEV, R. O., SCHATZ, M. F. AND SHARMA, V. 2006. Optically controlled mixing in microdroplets. *Lab on a Chip*. **6** (1369), 1.2.

HILL, M. J. M. 1894. On a Spherical Vortex. *Proceedings of the Royal Society of London*. **55** (331-335), 219-224.

JIANG, Y. J., UMEMURA, A. AND LAW, C. K. 1992. An Experimental Investigation on the Collision Behavior of Hydrocarbon Droplets. *Journal of Fluid Mechanics*. **234**, 171-190.

JUNG, Y. C. AND BHUSHAN, B. 2008. Dynamic effects of bouncing water droplets on superhydrophobic surfaces. *Langmuir*. **24** (12), 6262-6269.

KLINE, S. J. AND MCCLINTOCK, F. 1953. Describing uncertainties in single-sample experiments. *Mechanical Engineering*. **75** (1), 3-8.

KWON, D. H. AND LEE, S. J. 2012. Impact and wetting behaviors of impinging microdroplets on superhydrophobic textured surfaces. *Applied Physics Letters*. **100** (17).

LAMB, H. 1932. *Hydrodynamics*. Cambridge university press.

LE, H. P. 1998. Progress and trends in ink-jet printing technology. *Journal of Imaging Science and Technology*. **42** (1), 49-62.

LEIDENFROST, J. G. 1966. On the fixation of water in diverse fire. *International Journal of Heat and Mass Transfer*. **9** (11), 1153-1166.

LOSCERTALES, I. G., BARRERO, A., GUERRERO, I., CORTIJO, R., MARQUEZ, M. AND GANAN-CALVO, A. M. 2002. Micro/nano encapsulation via electrified coaxial liquid jets. *Science*. **295** (5560), 1695-1698.

NAGY, P. T. 2006. *Investigation of nonwetting system failure and system integration*. Ph.D. 3248739, Georgia Institute of Technology.

NAGY, P. T. AND NEITZEL, G. P. 2008. Optical levitation and transport of microdroplets: Proof of concept. *Physics of Fluids*. **20** (10), 1-4.

NEITZEL, G. P. AND DELL'AVERSANA, P. 2002. Noncoalescence and nonwetting behavior of liquids. *Annual Review of Fluid Mechanics*. **34**, 267-289.

NEITZEL, G. P., DELL'AVERSANA, P., TONTODONATO, V. AND VETRANO, M. R. 2000. Principles, Limits and Microgravity Applications of Self-Lubricated Liquids. *First International Symposium Microgravity Research and Aplications in Physical Sciences and Biotechnology*, Sorrento, Italy.

O'Rourke, P. J. and Amsden, A. A. (1987). The TAB method for numerical calculation of spray droplet breakup, SAE Technical Paper.

OKUSHIMA, S., NISISAKO, T., TORII, T. AND HIGUCHI, T. 2004. Controlled production of monodisperse double emulsions by two-step droplet breakup in microfluidic devices. *Langmuir*. **20** (23), 9905-9908.

PFANN, W. G. AND THURSTON, R. N. 1961. Semiconducting Stress Transducers Utilizing Transverse and Shear Piezoresistance Effects. *Journal of Applied Physics*. **32** (10), 2008-2019.

PLANCHETTE, C., LORENCEAU, E. AND BRENN, G. 2010. Liquid encapsulation by binary collisions of immiscible liquid drops. *Colloids and Surfaces a-Physicochemical and Engineering Aspects*. **365** (1-3), 89-94.

QIAN, J. AND LAW, C. K. 1997. Regimes of coalescence and separation in droplet collision. *Journal of Fluid Mechanics*. **331**, 59-80.

QUÉRÉ, D. AND AUSSILLOUS, P. 2002. Non-stick droplets. *Chemical Engineering & Technology*. **25** (9), 925-928.

RANGE, K. AND FEUILLEBOIS, F. 1998. Influence of surface roughness on liquid drop impact. *Journal of Colloid and Interface Science*. **203** (1), 16-30.

RAYLEIGH, L. 1879. On the Capillary Phenomena of Jets. *Proceedings of the Royal Society of London*. **29** (196-199), 71-97.

RAYLEIGH, L. 1879. On the capillary phenomena of jets. *Proc. R. Soc. London*,

REYNOLDS, O. 1881. On drops floating on the surface of water. *Chemical News*. **44**, 221-222.

REYSSAT, M., RICHARD, D., CLANET, C. AND QUERE, D. 2010. Dynamical superhydrophobicity. *Faraday Discussions*. **146**, 19-33.

RICE, C. L. AND WHITEHEAD, R. 1965. Electrokinetic Flow in a Narrow Cylindrical Capillary. *Journal of Physical Chemistry*. **69** (11), 4017-4024.

RICHARD, D., CLANET, C. AND QUERE, D. 2002. Surface phenomena - Contact time of a bouncing drop. *Nature*. **417** (6891), 811-811.

RICHARD, D. AND QUERE, D. 2000. Bouncing water drops. *Europhysics Letters*. **50** (6), 769-775.

RIOBOO, R., TROPEA, C. AND MARENGO, M. 2001. Outcomes from a drop impact on solid surfaces. *Atomization and Sprays*. **11** (2), 155-165.

SAMMARCO, T. S. AND BURNS, M. A. 1999. Thermocapillary pumping of discrete drops in microfabricated analysis devices. *Aiche Journal*. **45** (2), 350-366.

SIKALO, S., TROPEA, C. AND GANIC, E. N. 2005. Impact of droplets onto inclined surfaces. *Journal of Colloid and Interface Science*. **286** (2), 661-669.

SMITH, M. K. 1995. Thermocapillary Migration of a 2-Dimensional Liquid Droplet on a Solid-Surface. *Journal of Fluid Mechanics*. **294**, 209-230.

SONG, H., TICE, J. D. AND ISMAGILOV, R. F. 2003. A microfluidic system for controlling reaction networks in time. *Angewandte Chemie-International Edition*. **42** (7), 768-772.

STONE, H. A., STROOCK, A. D. AND AJDARI, A. 2004. Engineering flows in small devices: Microfluidics toward a lab-on-a-chip. *Annual Review of Fluid Mechanics*. **36**, 381-411.

TERRY, S. C. 1975. *A gas chromatography system fabricated on a silicon wafer using integrated circuit technology*. Pd.D. Stanford University.

TERWAGNE, D., GILET, T., VANDEWALLE, N. AND DORBOLO, S. 2010. Double emulsion in a compound droplet. *Colloids and Surfaces a-Physicochemical and Engineering Aspects*. **365** (1-3), 178-180.

TERWAGNE, D., LUDEWIG, F., VANDEWALLE, N. AND DORBOLO, S. 2013. The role of the droplet deformations in the bouncing droplet dynamics. *Physics of Fluids*. **25** (12).

THOMPSON, R., DEWITT, K. AND LABUS, T. 1980. Marangoni bubble motion phenomenon in zero gravity. *Chemical Engineering Communications*. **5** (5-6), 299-314.

TRAN, T., STAAT, H. J. J., PROSPERETTI, A., SUN, C. AND LOHSE, D. 2012. Drop Impact on Superheated Surfaces. *Physical Review Letters*. **108** (3).

TSAI, P. C., PACHECO, S., PIRAT, C., LEFFERTS, L. AND LOHSE, D. 2009. Drop Impact upon Micro- and Nanostructured Superhydrophobic Surfaces. *Langmuir*. **25** (20), 12293-12298.

TUFTE, O. N., LONG, D. AND CHAPMAN, P. W. 1962. Silicon Diffused-Element Piezoresistive Diaphragms. *Journal of Applied Physics*. **33** (11), 3322-3327.

UMBANHOWAR, P. B., PRASAD, V. AND WEITZ, D. A. 2000. Monodisperse emulsion generation via drop break off in a coflowing stream. *Langmuir*. **16** (2), 347-351.

UTADA, A. S., LORENCEAU, E., LINK, D. R., KAPLAN, P. D., STONE, H. A. AND WEITZ, D. A. 2005. Monodisperse double emulsions generated from a microcapillary device. *Science*. **308** (5721), 537-541.

WEILERT, M. A., WHITAKER, D. L., MARIS, H. J. AND SEIDEL, G. M. 1996. Magnetic levitation and noncoalescence of liquid helium. *Physical Review Letters*. **77** (23), 4840-4843.

WHITESIDES, G. M. 2006. The origins and the future of microfluidics. *Nature*. **442** (7101), 368-373.

WHITESIDES, G. M. AND STROOCK, A. D. 2001. Flexible methods for microfluidics. *Physics Today*. **54** (6), 42-48.

WORTHINGTON, A. M. 1876. On the Forms Assumed by Drops of Liquids Falling Vertically on a Horizontal Plate. *Proceedings of the Royal Society of London*. **25** (ArticleType: research-article / Full publication date: 1876 - 1877 / Copyright © 1876 The Royal Society), 261-272.

WORTHINGTON, A. M. 1876. A Second Paper on the Forms Assumed by Drops of Liquids Falling Vertically on a Horizontal Plate. [Abstract]. *Proceedings of the Royal*

Society of London. **25** (ArticleType: research-article / Full publication date: 1876 - 1877 / Copyright © 1876 The Royal Society), 498-503.

YANG, J. C., CHIEN, W., KING, M. AND GROSSHANDLER, W. L. 1997. A simple piezoelectric droplet generator. *Experiments in Fluids*. **23** (5), 445-447.

YOUNG, N. O., GOLDSTEIN, J. S. AND BLOCK, M. J. 1959. The Motion of Bubbles in a Vertical Temperature Gradient. *Journal of Fluid Mechanics*. **6** (3), 350-356.